SEDIMENTATION AND CONTAMINANT CRITERIA FOR WATERSHED PLANNING AND MANAGEMENT

Completion Report

OWRR Project No. B-014-COLO;

by

Hsieh W. Shen

Department of Civil Engineering

Colorado State University

submitted to

Office of Water Resources Research

U. S. Department of Interior

Washington, D. C. 20240

June, 1972

The work upon which this report is based was supported in part by funds provided by the United States Department of the Interior, Office of Water Resources Research, as authorized by the Water Resources Research Act of 1964, and pursuant to Grant Agreement No. 14-01-0001-1435.

ENVIRONMENTAL RESOURCES CENTER
Colorado State University
Fort Collins, Colorado

Norman A. Evans, Director

CER71-72HWS48

TABLE OF CONTENTS

TABLE OF CONTENTS - (Continued)

TABLE OF CONTENTS - (Continued)

LIST OF FIGURES

LIST OF FIGURES (Continued)

LIST OF FIGURES (Continued)

LIST OF TABLES

ABSTRACT

SEDIMENTATION AND CONTAMINANT CRITERIA FOR
WATERSHED PLANNING AND MANAGEMENT

When precipitation reaches its watershed, part of the water will infiltrate and percolate through the soil as ground water and a large portion of water will form surface runoff. This report is to describe a study on the effect of vegetation on the flow rates, sediment yield, and dispersion of contaminantes (such as herbicides, pesticides, and radioisotopes) attached to particles during surface runoffs in watersheds.

A model to estimate the resistance of flow due to various combinations of tall vegetation (such as trees) on the order of flow depths is given here. An empirical curve by regression to estimate the flow resistance with large rigid roughness (short vegetation such as grasses) in the order of normal boundary roughness is developed. The possibility of applying this curve to flexible roughness has also been explored. An analytical method to investigate the effect of vibrating flexible roughness elements in flow rate is also presented. The relative effect of various combinations of tall vegetation on the reduction of sediment yields based on the reduction of flow rates is studied. This should be rather useful in determining the relative effect on sediment yields by clear cutting and other selective cutting of forest lumber. The effect of rainfall on these sheet flows is investigated and a simplified method to estimate the rainfall effect on flow resistance is also developed. The dispersion of contaminated bed particles for different time and space can be found from graphical solutions as illustrated here. An empirical curve

to estimate the sediment bed material load for various flow conditions is found.

Shen, Hsieh W.
SEDIMENTATION AND CONTAMINANT CRITERIA FOR WATERSHED PLANNING AND MANAGEMENT
Completion Report to the Office of Water Resources Research, Department of the Interior, Washington, D.C.
KEYWORDS: *watershed management/*watershed protection/*water resources management/*sediment yield/*erosion control/*forest cutting management

Chapter 1

INTRODUCTION

When precipitation reaches the watershed, part of the water will infiltrate and percolate through the soil as ground water. A large portion will form surface runoff. This surface runoff will erode top soil and disperse contaminated particles attached to the soil. The erodibility of soil under different climates, soil moisture, organic-matter content, etc., is being actively investigated by the U.S. Agricultural Research Services in Arizona, Indiana, Iowa, Minnesota, Missouri, South Dakota and Wisconsin. Their research will complement the proposed study, which is, to study the effect of vegetation on the flow rates, sediment yield, and dispersion of contaminates (such as herbicides, pesticides, and radioisotopes) attached to particles during surface runoff in watersheds. To be specific, the objectives of this study are listed in the following section (Section I).

I. OBJECTIVES

A.

Study the effect of vegetation on resistance to flow. Different sizes and spacings of obstacles (rigid cylinders and semi-flexible plastic fibers to simulate vegetation) will be placed in large tilting water flumes to study the effect of simulated vegetation on resistance to flow. The size of the obstacle will be of the same order of magnitude as flow depth.

B.

Study the effect of vegetation on sediment yield. Sediment transport rate under different simulated vegetation and hydraulic conditions, as described above will be investigated.

C.

Study the effect of rainfall on sheet flow. (This was not listed in the original proposal, but it is an important part of the soil sheet erosion process.)

D.

Study the dispersion of contaminants attached to the top soil in watersheds under different flow conditions.

E.

Based on knowledge acquired in this study, some economical considerations for watershed planning and management will be recommended.

II. ORGANIZATION OF THE REPORT

This research project includes several relatively independent investigations performed through the joint efforts of the principal investigator and several other researchers. Each chapter in this report deals with a particular subject with Chapters 6 and 7 briefly describing all these studies. Chapters 2 and 3 deal with the effect of vegetation on resistance to flow and is partially based on the Ph.D. thesis by S. Petryk. It is prepared with the capable assistance of Ruh-Ming Li. Chapter 4 on the effect of rainfall on sheet flow, is a summary of a M.S. thesis by Ruh-Ming Li. Chapter 5 on the dispersion of contaminants (such as herbicides, pesticides and radioisotopes) attached to the top soil, is a joint effort with P. Todorovic and Hin Fatt Cheong. Chapter 7 gives a list of published publications sponsored by this grant and also a list of publications under preparation. Copies of the published publications have been sent to the sponsoring agency and copies of the publications under preparation will be forwarded to the sponsoring agency if and when they are published. Each chapter uses different notations.

Chapter 2

EFFECT OF VEGETATION ON RESISTANCE TO FLOW

I. INTRODUCTION

The effect of vegetation on flow resistance has been discussed in various books dealing with watershed management (for instance, see Colman, 1953) and forest management (for instance, see Molchanov, 1960). Unfortunately, no method is available to estimate quantitatively the effect of vegetation on resistance to flow.

From a hydraulic engineers view point, the effect of vegetation on flow retardation can be divided into three parts: i) tall vegetation (such as trees) on the order of flow depths, ii) short vegetation (such as grasses) on the order of normal boundary roughness, and iii) vegetation in the order of 20 to 80 percent flow depth. The main effort in this study is toward tall vegetation on the order of flow depth. A preliminary study on short vegetation is presented in Appendix A and a theoretical analysis on the vibration of cylinders in a fluid stream is included in Appendix B of this chapter.

II. SINGLE CYLINDER (TALL VEGETATION) IN OPEN CHANNEL FLOW

A. Flow Field Descriptions

The flow structure is rather complex around a single cylinder inserted in an open channel flow. As described by Roper, Schnieder and Shen (1967) and Shen, Schneider and Karaki (1969), the dominant feature of the flow near a cylinder is a large scale eddy structure or the system of vortices, which develop about the cylinder. Depending on the type of cylinder and free stream conditions, the eddy structure can be composed of any, all, or none of the following three basic

systems: the horseshoe-vortex system, the wake-vortex system, and/or the trailing-vortex system. The vortex systems are an integral part of the flow structure and strongly affect the vertical component of the velocity in the neighborhood of the cylinder. The vortex filaments, transverse to the flow in a two-dimensional undisturbed velocity field, are concentrated by the presence of a cylinder to form the horseshoe-vortex system. The mechanism by which the concentration is accomplished is the pressure field induced by the cylinder. If the pressure field is sufficiently strong, it causes a three-dimensional separation of the boundary layer which, in turn, rolls up ahead of the cylinder to form the horseshoe-vortex system. The cylinder serves as a focusing or concentrating device for the vorticity already present in the undisturbed stream. The ends of the vortex filaments, composing the horseshoe-vortex, stretch downstream toward infinity, increasing the rotational velocities in the vortex core in accordance with the kinematic laws of vortex behavior. Clearly, the geometry of the cylinder is important in determining the strength of the horseshoe vortex. The horseshoe-vortex system, however, is not steady for all flow conditions studied. Schwind (1962) noted that for some Reynolds numbers the horseshoe-vortex is shed periodically.

The vorticity concentrated in the wake-vortex system is generated by the cylinder itself, contrary to the case of the horseshoe-vortex. The wake-vortex system is formed by the rolling up of the unstable shear layers generated at the surface of the cylinder. The shear layers are detached from either side of the cylinder at the separation line. At low Reynolds number (3 to 5 $< \bar{R} <$ 40 to 50), these vortices are stable and form a standing system downstream close to the cylinder. For

Reynolds numbers of practical interest, however, the system is unstable, and the vortices are shed alternately from the cylinder and are converted downstream. The strength of the vortices in the wake system varies greatly depending on cylinder shape and fluid velocity. The regularity of shedding ranges from the very stable von Karman vortex street (80 to $90 < \bar{R} < 150$ to 300) to a practically chaotic state in the transcritical range [$(3.5 \times 10^6 < \bar{R})$, Roshko (1961)].

The wake-vortex system is related to the so-called upflow which has been observed by Posey (1949), Masch and Moore (1963), Roper (1965 and 1967), and others.

The trailing-vortex system usually occurs only on completely submerged cylinders and is similar to that which occurs at the tips of finite lifting surfaces in finite wing theory. It is composed of one or more discrete vortices attached to the top of the cylinder and extending downstream. These vortices form when finite pressure differences exist between two surfaces meeting at a corner, such as at the top of the cylinder.

Roper (1965 and 1967) gave a more detailed description of these vortex systems.

The drag coefficient of a cylinder in two-dimensional cross-flow varies significantly as the Reynolds number increases from 5×10^6. The drag coefficient is dependent on the regime of flow around the cylinder, and the Reynolds number at which these different regimes of flow occur.

One can define three regimes of flow for a cylinder at high Reynolds number. Each type of flow may be defined by the separation characteristics of the cylinder boundary layer. The subcritical flow occurs when

the boundary layer separates laminarly between 72° and 90° to form a relative wide wake (all angular readings are with respect to the forward stagnation point, unless specified otherwise). The critical flow occurs when the boundary layer separates laminarly, quickly becomes turbulent and reattaches to the cylinder to separate again at about 135°. This separation phenomena is generally referred to as a "laminar separation bubble." The supercritical region occurs when the boundary layer Reynolds number is high enough for transition to turbulence to occur before any separation takes place; the turbulent boundary layer separates at about 110°.

The drag coefficient generally decreases as the angle of separation increases. This follows from the fact that as the angle of separation increases, the size of the wake decreases.

The coefficient of drag in an idealized two-dimensional flow is about 1.2 for a cylinder Reynolds number range of 8×10^3 to 2×10^5, as reported in standard texts such as Schlichting (1968). At higher Reynolds numbers the coefficient of drag drops as one approaches the transition cylinder Reynolds number. The "transition" Reynolds number is defined as the cylinder Reynolds number at which the flow changes from subcritical to critical. Achenbach (1968) found that the coefficient of drag is .7 at the transition Reynolds number of about 2.6×10^5.

B. Differences Between Cylinder Drag in Idealized Two-Dimensional Flow and Cylinder Drag in Open Channel Flow - Previous Literature

The flow around a vertical cylinder in open channel flow has many characteristics (as briefly described below) which could significantly

change the drag magnitude from the well known idealized two-dimensional flow conditions. See Petryk (1969a) for a more detailed discussion.

1. The Effects of Open Channel Turbulence: Bearman (1968), and Sevik (1966) placed a cylinder in two-dimensional flow downstream of a turbulence grid and studied the effects of turbulence characteristics in the transition Reynolds number. They found that turbulence tends to cause turbulent transition in the separated cylinder boundary layer sooner than in a corresponding idealized two-dimensional flow case. The transition Reynolds numbers were in the order of 5 to 6 x 10^4 with increased turbulence fluctuations from the value of 2 to 3 x 10^5. Below this transition Reynolds number the effects of turbulence on cylinder drag are negligible.

2. Free Surface Effects: "Wave drag" is a common term used to describe the free surface effects on drag magnitude for cylinder Froude numbers less than or equal to about one, i.e., before aeration occurs. Hsieh (1964) attributed wave drag to explain the increase of drag coefficient over that in a two-dimensional flow. Actually Hsieh's experimental results could also be partially due to the blockage effects as discussed later. Issacs (1965) showed that the effect of the free surface on drag is small and that the wave drag is actually negative for deep flows where the water depth cylinder diameter ratio is greater than about four.

3. The Effect of a Non-Uniform Velocity Profile: Dalton and Masch (1968) studied experimentally the variation of drag coefficient with the height of a cylinder which was placed in a flow with linear velocity profile. They found that the drag coefficient varied from 0.8 to 2.4 for a typical run and the corresponding drag coefficient for a

cylinder in a two-dimensional flow is about 1.2. Petryk (1969b) pointed out that if the drag coefficient was based on the averaged integrated flow velocities across the cylinder and with the blockage effect eliminated, the deviation from the two-dimensional case would be negligible.

4. The Effect of Blockage: Allen and Vincurti (1944) considered the wall interference in a dimensional flow wind tunnel. Petryk (1969a) gave a detailed analysis of how blockage effect may be estimated.

C. Experiment Performed in this Study

A four foot wide flume at Colorado State University was used as the open channel facility for the determination of individual cylinder drag magnitudes. It is 60 feet long from the head box to the tailgate and is mounted on screw jacks for slope adjustment.

To stabilize the flow in the flume three baffles were installed at the outlet of the head box. At certain flow conditions surface waves formed as the water came through the baffles. Accordingly, a wave damper, dimensioned two feet by four feet, was placed across the flume on the water surface to dampen the waves. Measurements on individual cylinders were taken 39 feet from the head box, or about 34 feet from the end of the wave damper. The mean velocity profile was almost fully developed at this location because the depth of flow was always less than one foot and the inlet conditions were turbulent.

The cylinders used for this drag study were 1/2, 1-3/4 and 4 inches in diameter; each one was one foot long. They were made from sections of smooth transparent plexiglass pipe.

For drag measurements, one of the above cylinders was mounted on the frictionless "drag balance" as discussed by Petryk and Shen (1971) and Petryk (1969a).

The accuracy of the drag balance, for given flow conditions, was estimated from possible errors in calibrating the balance and from repeated drag measurements. The maximum calibration error was estimated to be one percent, arising from minor draft in voltage with time, and small nonlinearity in the calibration relation of force vs voltage. Eight drag measurements were taken twice to obtain an estimate of the balance repeatability. The difference in magnitude of the drag force between any two runs did not exceed 1.5 percent; therefore, repeatability of the balance is expected to be at least within two percent. Therefore, the balance measured drag force to within an accuracy of at least three percent.

The wake development was studied downstream of a cylinder in the center of the flume. Most of the measurements were carried out downstream of an instrumented 1-3/4 inch cylinder. Limited wake measurements were taken downstream of a 1/2 inch cylinder to show the effect of the free surface on the shape of the wake. The wake measurements included only mean velocity measurements taken with a standard 1/8 inch O.D. pitot tube.

The 1-3/4 inch cylinder was instrumented with pressure taps to measure the coefficient of drag and the pressure distribution around the cylinder. The pressure taps were all located at one angular position and at the following depth intervals: 1/8 inch, 1/2 inch and one inch from the bottom, and then at one inch intervals up to the top of the cylinder. The total length of the cylinder was 12 inches. It was mounted so that it could be rotated for pressure readings at different angular positions.

The pressure readings around the cylinder were measured relative to a "static pressure" tap located in the flume floow ten diameters upstream. The cylinder piezometer readings and the pitot tube readings were taken with a Pace differential transducer. The readout equipment included a Pace CD-25 carrier demodulator, an averaging circuit, and a Mosely 680 strip chart recorder. The transducer with the readout equipment was calibrated with a vertical water manometer.

The secondary flow pattern was studied by injecting dye in the near-wake region, and correlating the flow pattern with the measured average variation of pressure along the back of the cylinder.

D. Discussion of Experimental Results

1. Flow Field: Most of the detailed cylinder pressure distribution and wake measurements were carried out with U_o = 1.29 fps , D = 7-5/8 inches , and d = 1-3/4 inches where:

U_o = average velocity based on discharge divided by channel flow area

D = depth of flow

d = diameter of cylinder.

Under the above flow conditions, the secondary flow along the front and back of the cylinder is downward, and at the back of the cylinder the pressure is higher near the surface than near the bottom.

The downward secondary flow along the front of the cylinder is attributed to the nonuniform approach velocity. The downward circulation pattern at the back of the cylinder disagrees with previous investigations where a two-dimensional object was placed in a nonuniform flow field.

In shear flows, it has generally been reported that the secondary flow in the near wake region of a cylinder is in the direction of increasing velocity head. This phenomena has been argued from the fact that generally as the approach velocity to the cylinder increases, the pressure at the back of the cylinder decreases. It follows that the secondary flow should be in the direction of decreasing pressure, or in the direction of increasing velocity head. All wind tunnel investigations report this circulation pattern [see Baines (1965) and Roper (1967)]. Dalton and Masch (1968) also found that the secondary flow was in the direction of increasing velocity head. They placed a cylinder in a water tunnel with a linear velocity profile, and demonstrated that this secondary flow pattern was applicable to flow without free surface effects. Masch and Moore (1963) and Roper (1965) reported the same secondary flow pattern downstream of a cylinder in an open channel flow with a nonuniform velocity profile.

The observed downward circulation at the back of the cylinder under the flow conditions given in the beginning of this section may be explained by: i) the free surface effects, and ii) the vortex shedding pattern at the back of the cylinder. The vortices are shed irregularly and their strength is relatively low. The flow in the separated region circulates quiescently.

The pressure throughout the separated region is expected to be approximately hydrostatic because of the relatively low flow velocities in that region. The reentrainment velocity is expected to be higher near the surface than near the bottom because of the higher approach velocity near the surface. The higher reentrainment velocity, impinging on the rear portion of the cylinder, appears to be enough to cause a

pressure gradient downward. It follows that, with a downward pressure gradient, the secondary flow is also downward.

At lower velocities the vortex shedding pattern changes and the secondary flow is directed upward. The separated region swings from side to side as the strong vortices are shed alternately from the cylinder. With the strong shedding of the vortices, the separation points on the cylinder and the rear stagnation point vibrates with the vortex shedding frequency. A very good description of this separation phenomena is given by Mattingly (1962). A sketch showing a strong vortex in the upper half of the separated region is shown in Fig. 2.1. The upper vortex is shed, and then a strong vortex in the lower half is formed; it is shed, and so on.

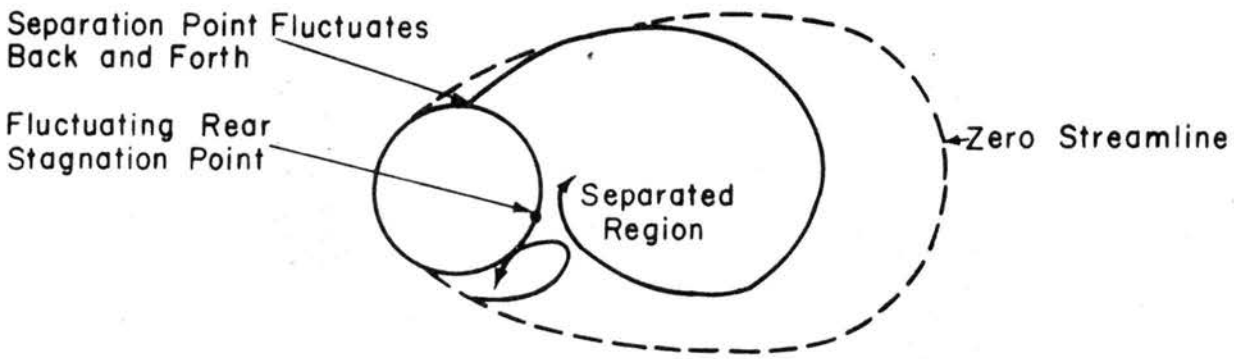

Fig. 2.1. Separation and Oscillation Behind Cylinder (top view).

Under these latter flow conditions, the higher velocity near the surface forms stronger vortices which are produced immediately behind the cylinder. Therefore, it follows that the pressure behind the cylinder will decrease with increasing distance from the floor in a fully developed channel flow. In this case, the free surface appears to have little effect and the secondary flow is upward.

Limited wake measurements were taken at the initial flow conditions and velocity measurements were taken at the following distances from the floor: .25 inches, .50 inches, and then at successive .50 inch intervals to 7.0 inches. The velocities at these depths were measured at 38 locations across the channel, at 9.5, 18.5 and 27.5 diameters downstream of the cylinder.

2. Wake Decay: The experimental values of wake width $b_{1/2}$ which is defined as one-half of the wake width at half the depth of the velocity defect, as a function of x is given by Petryk (1969a). The spread and decay rate of a wake is approximately the same as measured by Eskinazi (1959).

Under the experimental flow conditions Petryk (1969a) found that the relations which were chosen to describe a wake in an open channel are (where u_1 is the velocity defect in the wake region, u_{max} is the maximum defect velocity at the center of the wake averaged over the depth of flow, x, y and z are longitudinal, vertical and transverse directions respectively, U_o is the mean flow velocity based on channel cross area, and C_d is the drag coefficient):

$$u_1 = \frac{u_{max}}{2}\left[1 + \cos\left(\frac{\pi z}{2b_{1/2}}\right)\right] \tag{2.1}$$

$$\frac{u_{max}}{U_o} = -.90\left(\frac{x}{C_d d}\right)^{-.7} \tag{2.2}$$

$$\frac{2b_{1/2}}{C_d d} = .48\left(\frac{x}{C_d d}\right)^{.59} . \tag{2.3}$$

They were chosen on the basis of the limited experimental results presented above, and their approximate agreement with Eskinazi's data (1959).

Petryk also stated that the detailed characteristics of the mean velocity field in channel wakes are a complex function of the free surface effects, and the secondary flow patterns ahead and back of the cylinder. Because of the three-dimensional nature of the flow, it was not possible to analyze the wake characteristics as a function of the distance from the channel floor.

The shape of the wake is adequately described by averaging the velocity across the depth of flow at each point downstream of the cylinder. By averaging, it is possible to describe the shape of the wake with old established wake relations such as Eq. (2.1).

Wakes decay and spread much faster in open channels than in the idealized two-dimensional case. The wake spread and decay rate is of the same order of magnitude as found by Eskinazi. Equations (2.1), (2.2) and (2.3), which were determined from a limited amount of data, describe wake diffusion downstream of a cylinder placed in a fully open channel flow.

Petryk (1969a) presented a useful and reasonable method to estimate the effect of slope on wakes in open channel flow. He reasoned that the effect of slope is to reduce the velocity defect u_{max}, while its effect of the wake width $b_{1/2}$ is small. This result follows when one compares the physics of flow for a wake developing in a fully developed channel flow with a turbulent wake developing in a non-turbulent negative pressure gradient flow field. Hill, et. al., (1963) found that the velocity defect u_{max} will decay more rapidly with x in a negative pressure gradient wake than in a corresponding zero pressure gradient wake, and the wake width $b_{1/2}$ will spread less rapidly with x than in a corresponding zero pressure gradient wake. The effect of slope on u_{max}

in an open channel is qualitatively the same as for a wake produced in a negative pressure gradient flow. However, the effect of slope on the rate of spread of a wake ($b_{1/2}$ vs x) is not qualitatively the same. To help clarify this point, consider two channels with uniform flow conditions, one rough and one smooth, each having a similar cross section geometry, each having the same depth of flow, and each having the same discharge. The slope of the rough channel will be larger than in the smooth channel. Also, the turbulence level will be higher in the rough channel than in the smooth channel. Now, consider a wake created downstream of a cylinder in each channel. It may be reasoned that the wake in the rougher channel would spread more rapidly owing to the higher turbulence level than in the smooth channel. The effect of turbulence is opposite to the effect of pressure gradient (or slope) described by Hill, et. al. Since it is very difficult to quantitatively describe these two effect, it was decided to neglect the effect of slope on the variation of $b_{1/2}$ with x.

If the change in displacement thickness varies with downstream distance according to relationships developed by Hill, et. al. (1963), Petryk (1969a) found that u_{max} will vary according to

$$\frac{u_{max}}{U_o} = -.9 \left(\frac{x}{C_d d}\right)^{-.7} \left(\frac{1}{1 - \frac{g\Delta y}{\frac{U_o^2}{2}}}\right)^{3/2} \qquad (2.4)$$

where Δy is the change in water surface elevation between two points in the channel and g is the gravitational acceleration. The variation of $b_{1/2}$ is as given previously in Eq. (2.3). Relations (2.1), (2.3) and (2.4) completely describe the mean velocity distribution for a wake in open channel flow. Yano's (1966) basic wake equations in zero pressure gradient, are:

$$\frac{u_{max}}{U_o} = -.83 \left(\frac{x}{C_d d}\right)^{-.5} \tag{2.5}$$

$$\frac{2b_{1/2}}{C_d d} = .57 \left(\frac{x}{C_d d}\right)^{.5} \quad . \tag{2.6}$$

If Yano's equations are used in open channel flow, then relation corresponding to (2.3) and (2.4) are (2.6) and

$$\frac{u_{max}}{U_o} = -.83 \left(\frac{x}{C_d d}\right)^{-.5} \left(\frac{1}{1 - \frac{g\Delta y}{\frac{U_o^2}{2}}}\right)^{3/2} \quad . \tag{2.7}$$

3. Drag Coefficient: Figure 2.2 summarizes the results of the drag measurements obtained from the experimental work. The drag coefficient C_d is plotted as a function Froude number based on cylinder size F_d, and Froude number based on depth of flow F_D. The contour lines given in the figure separate the different drag coefficient magnitudes.

In general, the CSU results are in agreement with Hsieh's (1964) data. However, Hsieh's paper tended to emphasize the importance of the Froude number based on depth of flow, F_D, while the CSU results show the importance of both F_d and F_D.

The following conclusions are derived for drag coefficient from the results obtained by Hsieh (1964), Isaacs (1965) and in this study by Petryk (1969a).

i) At low F_D values, the effect of blockage is smaller than at higher F_D values for subcritical channel flow for values of $F_d \lessapprox 1$.

ii) The wave drag is positive in subcritical channel flow for shallow depths (where the depth-to-diameter ratio is less than or equal to about four). The maximum value of wave drag occurs for cylinder

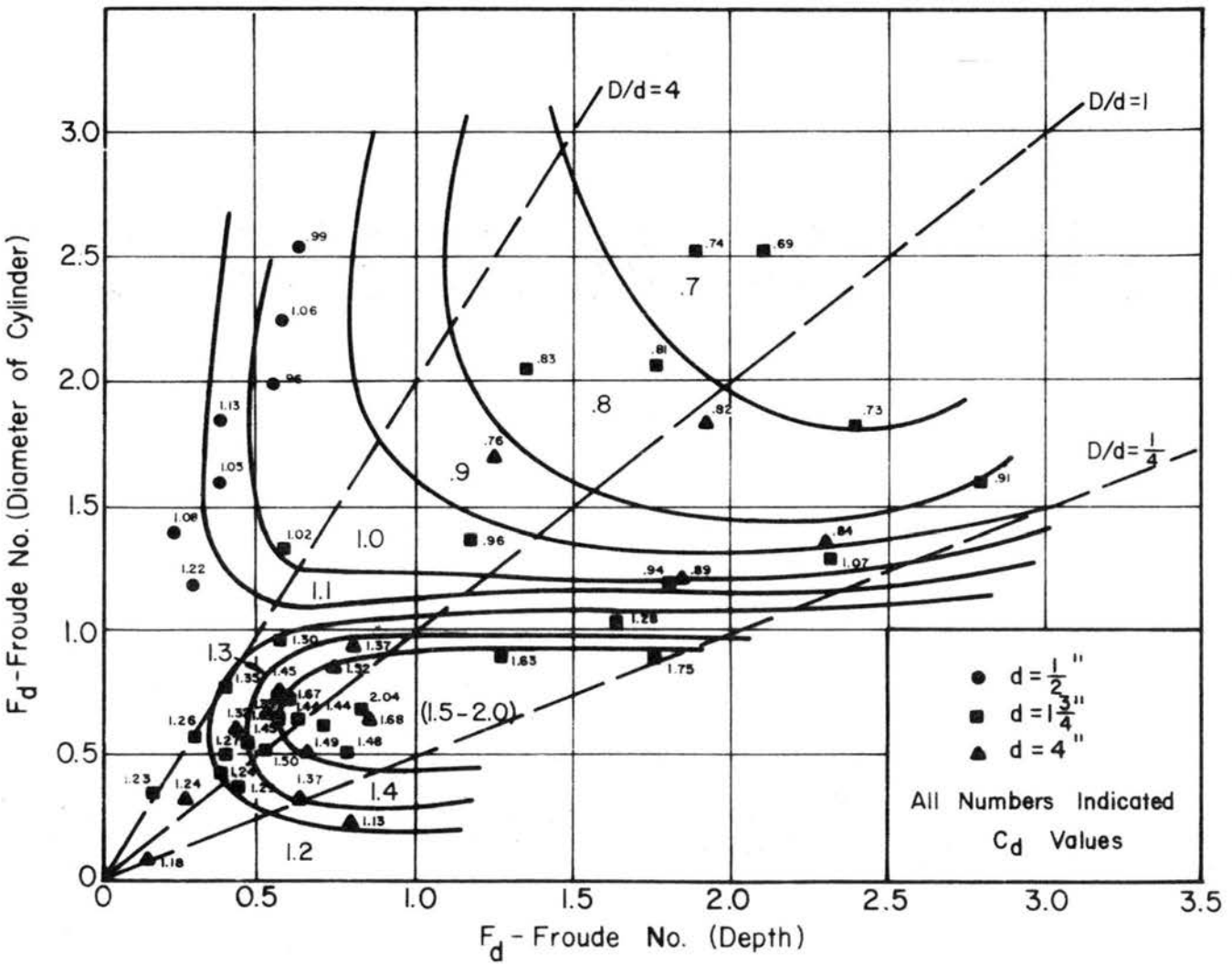

Fig. 2.2. Drag Correlation for Cylinders in Open Channel Flow

Froude numbers between .5 and .9 at channel Froude numbers greater than or equal to .5. Hsieh's data shows how the wave drag increased as the depth-to-diameter ratio decreased from four to two. This is in agreement with the CSU data in Fig. 2.2; the effect of wave drag becomes more important as one moves along the dotted lines of decreasing depth-to-diameter ratio.

iii) The effect of wave drag is very small for a depth-to-diameter ratio greater than or equal to about four for cylinder Froude numbers less than or equal to about one, as found by Isaacs. Hsieh's results which show large values of C_d, larger than 1.2, at D/d equal to four are due to blockage effects.

iv) From ii) and iii), it follows that the mechanics of flow near the surface are significantly influenced by the channel floor at shallow depths.

v) The high drag coefficient values of 1.5 to 2.0 given in Fig. 2.2, are mostly due to wave drag at these shallow depths, and partly a consequence of the free surface effects due to blockage. Two-dimensional blockage corrections, according to Allen and Vincenti (1944) would reduce these high drag coefficients by less than or equal to about eight percent.

vi) The experimental data indicates that for $F_d \lesssim 1$, the increase in drag coefficient due to wave drag may be as high as about 60% above the two-dimensional value of 1.2, when the depth-to-diameter ratio is less than about four.

In summary, from the experimental results of Hsieh, Isaacs, Dalton and Masch, and Fig. 2.2, it is concluded that if there is no aeration behind the cylinder ($F_d \lesssim 1$) the best estimate of the drag coefficient

is the two-dimensional value of 1.2, if the flow conditions are outside of the wave drag region, as shown in Fig. 2.2.

III. INDIVIDUAL CYLINDER DRAG IN AN OPEN CHANNEL WITH A MULTI-CYLINDER DISTRIBUTION

The main topics presented in this section include:

i) A review of previous experimental work applicable to the present problem.

ii) A mathematical model which predicts individual cylinder drag, and the resistance to flow in any cylinder distribution if certain restrictions are met and certain assumptions are made.

iii) Experimental data and discussion of results for (1) verifying the mathematical model and for (2) correlating the drag of two cylinders placed at different relative positions, which are outside of the restrictions for the mathematical model.

A. Review of Previous Experimental Work (Partially Reviewed by A.T. Roper)

A good deal of testing has been carried out for multi-cylinder arrangements in conjection with tube banks in heat exchanges. An interesting flow visualization study of such arrangements is presented by Wallis (1939) [they also are reproduced in Knudsen and Katz (1958)].

In qualitative tests investigators generally consider the total effect of an entire array of cylinders on the flow. The total effect is then presented in terms of a modified friction factor expression. This expression contains factors describing the array such as the numbers of cylinders, the size, the spacing, orientation, etc. A wealth of such information was presented by Kays and London (1954), Bergelow, et. al. (1950), Chilton and Genereaux (1933), Gunter and Shaw (1945), Grimson

(1937) and Jakob (1938). The results of most of these tests were summarized and discussed by Knudsen and Katz (1958).

Very little detail work seems to have been done on the detail interference of the individual cylinder flow fields in multi-cylinder arrangements. Some early aeronautical work was done on the influence of cylindrical struts in close proximity. Some of these results are available in Hoerner (1958) and Biermann and Herrnstein (1933). These results will be discussed in the section on lateral and longitudinal interference. Yano (1966) suggested a method for obtaining multi-cylinder wake behavior through superposition of momentum defect fluxes which is also discussed later.

One analytical solution for wake behavior behind a row of cylinders in a uniform flow exists. This solution was due to Gran Olsson (1936) and will be discussed in the next section. The solution was also discussed by Schlichting (1960) (pp. 604-605).

1. Wake Behind a Row of Cylinders in a Uniform Flow: Consider such a configuration with pitch Δ as shown in Fig. 2.3. This case was investigated both experimentally and theoretically by Gran Olsson (1936). At a certain downstream location, the width of the wake of a given cylinder will equal the pitch Δ. It is assumed that the Oseen approximations are valid and that the applicable form of the governing equation is

$$-U_\infty \frac{\partial u_1}{\partial x} = \frac{1}{\rho} \frac{\partial \tau}{\partial z} \qquad (2.8)$$

where U_∞ is the upstream undisturbed flow velocity, u_1 the velocity defect, ρ the fluid density and

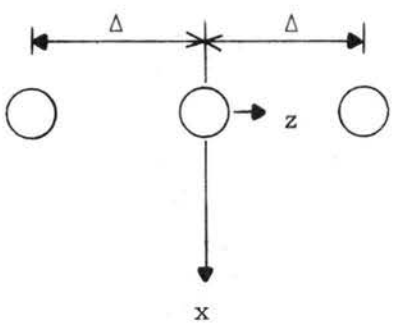

Fig. 2.3. Cylinder Definition Sketch

τ the shear stress. The mixing length hypothesis was used to determine the form of τ .

In fully developed flow the periodic dependence of u_1 upon z is assumed to be of the form,

$$u_1 = U_\infty A \left(\frac{x}{z}\right)^{-1} \cos (2\pi z/\Delta) \quad . \tag{2.9}$$

A is a free constant which Schlichting (1960) determined to be

$$A = (\Delta/\ell)^2 \, 8 \, \pi^3 \tag{2.10}$$

where ℓ is the mixing length. The magnitude of ℓ is dependent upon Δ/d (Gran Olsson obtained $\ell/\Delta = 0.103$ for $\Delta/d = 8$). Gran Olsson found the above solution to be valid for $x/\Delta > 4$.

A second approximation for shorter downstream distances was accomplished by Cordes (1937).

2. Longitudinal and Lateral Interference: There are two distinct interference mechanisms at work in this problem. One is due to the effects of longitudinal, the other due to lateral interference. Some cases must, of course, be considered a combination of both.

a) Longitudinal Interference: The behavior of the flow in the cavity is very dependent upon conditions in the first few diameters downstream of the base [Roshko (1961) and Mattingly (1962)]. Roskho (1954) investigated the effect of splitter plate interference and found that the conditions return to their undisturbed levels when nose of the plate moves more than approximately 2.5 diameters downstream from the first cylinder. The conclusion was that the major interference effects occur in the first 2.5 diameters downstream due to modification of the pressure depression. This conclusion was substantiated by Hoerner (1958) who showed that the major interference effect on C_D

caused by placing a second cylinder in the wake of the first occurs in the first 2.5 diameters downstream. The effect on both cylinders was favorable in this range (i.e., drag reduced on both).

The drag on the second cylinder is greatly reduced partially due to the result of decreased wake dynamic pressure. A second effect is the increased turbulence level of the flow approaching the second cylinder. This increased turbulence level can delay separation and effectively push the second cylinder from the subcritical regime (separation before 90°) into the lower drag critical or supercritical regime (separation beyond 90°).

The dynamic pressure effect can be expected to be negligible for $x/d > 600$ (this number was arrived at somewhat arbitrarily from Eskinazi's data on the decrease of the peak defect to 1/10 its maximum value at 5.1 diameters). The effect of turbulence decays much more rapidly and is probably negligible by 100 diameters.

b) Lateral Interference: The behavior of a pair of cylinders with various lateral spacings was investigated by Hoerner (1958). When the spacing between the cylinder sides was zero they presented a more bluff object to the flow than a single cylinder of their combined diameter, and, hence, a slightly higher drag coefficient. The wake vortex structure is that of a single body. As the lateral distance is increased beyond the point the behavior continues to be that of a combined system until the spacing between centerlines is $2d$. The behavior is apparent in the rising portion of the Strouhal frequency curve up to $\Delta/d = 1$ (i.e., centerline distances of $2d$). Beyond this point there is a rapid drop in the shedding frequency as the system is altered from a combined system to two single systems. For

Apelt and Isaacs (1968) measured the total drag force on two cylinders spaced at 1-5/8, 2, 3 and 4 diameters at different angular positions. The experimental work was carried out in a laboratory flume at a cylinder Reynolds number of about 1.2×10^4 .

Yano (1966) used wake superposition concept to predict mean velocity profiles downstream of multi-cylinder distributions. Superposition refers to the method by which the effects of the upstream wake producing objects are added to predict the final downstream flow field. Linear superposition refers to adding linearly the effects of two or more wake producing bodies.

Laird, et. al. (1959), studied the effect of a similar sized cylinder placed upstream at different radial angles. Their cylinder Reynolds numbers were mostly in the subcritical to critical regime of flow. The scatter of data for different runs at similar flow conditions was fairly large. As a result, they could only reach qualitative conclusions that the presence of a neighboring cylinder caused a reduction in the mean drag force, and a large increase in the fluctuating lift and drag forces, and that the spacing was important in these effects.

3. Wake Superposition: Yano (1966) suggested that the wakes of many cylinders can be combined by the linear superposition of the wake momentum defect fluxes. For example (u_1 is the flow velocity defect)

$$u_1^2 \text{ (2 cylinders)} = u_1^2 \text{ (First)} + u_1^2 \text{ (Second)} \quad . \quad (2.11)$$

Yano began his justification of this form from a discussion of the characteristics of the turbulent kinetic energy. He assumed the flows to be quasi-isotropic which seems doubtful except perhaps far downstream of the cylinder. Next, it was assumed that the largest turbulent eddies

larger separations the behavior is that expected of two independent systems.

For close spacings the flow visualization photos by Wallis (1938) [see also Knudsen and Katz (1958)] appear to indicate a coupling of adjacent wakes. For all cases the wake growth appears to be reduced from the no interference case. This could be a result of the favorable pressure gradient induced by a distortion of the external velocity field discussed in section (x). While the variation may not be of the x^n variety, other variations could produce the same gross behavior.

The distortion of the flow field in closely spaced cylinders produces regions of increased velocity between the cylinders. For spacings close enough to produce favorable pressure gradients equivalent to $n > + 1/3$, the wake width would be expected to decrease with x (that is collapse rather than grow). This behavior appears to be substantiated by Schlichting's description (1960), (p. 605) of von Bohl's experiments on bar spacings in wind tunnels. Von Bohl found that for large solidarity ratios (i.e., ratio of total bar area to total cross-sectional area) that the regions of high velocity (jets) close in on one another. This would appear to be a case of wake collapse.

c) Lateral and Longitudinal Interference: Bierman and Herrnstein (1933) took drag measurements on two cylinders at different spacings in a wind tunnel. The cylinders were arranged in-line and then crosswise with respect to the flow direction. The drag force on each cylinder was measured at different spacing ratios for different cylinder sizes. The cylinder Reynolds number was greater than or equal to about 7×10^4.

of each wake are created independently by a mean flow instability in each wake. Thus, since the energy is known to cascade from the large scale eddies downward to the smallest eddies and there is litter interaction of eddies of the same size, the linear superposition of both wakes is justified.

$$\bar{u}'^2 \text{ (2 wakes)} = \bar{u}'^2 \text{ (First)} + \bar{u}'^2 \text{ (Second)} \quad . \tag{2.12}$$

Based upon a statement by Townsend (1956) (p. 135) that the turbulent intensity of the wake $\bar{u}'^2$ has a characteristic similar to the momentum defect u_1^2, Yano arrived at his initial equation.

The assumption of independent development of the largest scale eddies is the cornerstone upon which the above argument is based. This independent development seems highly unlikely at least for small longitudinal and lateral cylinder spacing. The largest scale eddies are those shed from the cylinder and do not develop independently for small spacings. This assumption like that of quasi-isotropy can be true only at some distance downstream of the cylinder base.

Yano used the expressions developed by Schlichting (1960) for wake growth and defect decay in the following symbolic form

$$u_1 \equiv u_{max} f(x,z) \tag{2.13}$$

where $u_{max} = u_1(z=0)$

$$b_{1/2} \equiv C_2 \, 1/F(x) \tag{2.14}$$

where $b_{1/2}$ is the width for which $u_1/u_{max} = 1/2$ and C_2 is a constant

$$u_{max} \equiv U_\infty \, C_1 \, F(x) \tag{2.15}$$

where C_1 is a constant and

$$f = [1 - 0.293 \, (z/b_{1/2})^{3/2}]^2 \tag{2.16}$$

$$F(x) = (x/d)^{-1/2} \quad . \tag{2.17}$$

As we have seen during the development of these equations, they are valid only for the zero pressure gradient case far downstream of the cylinder. These conditions do not seem to be well satisfied for the problem at hand, particularly if we consider longitudinal rather than lateral spacings. Yano then listed the boundary conditions

$$C_1 F(0+) \equiv 1 \quad (\text{for } x = 0+)$$

$$f(x,z) = 1 \quad (\text{for } z = 0) \quad .$$

The first is merely the stagnation condition at the cylinder surface which is in a region where the solution is clearly not valid (self-similar or laterally universal profiles can develop only at some distance downstream of this point). The second condition is merely a statement that $z = 0$ corresponds to the wake centerline.

The author then proceeded to develop the recursion relations for computing the wake defect for various longitudinal arrays of cylinders with pitch Δ. A problem arises at this point because C_1 contains the drag coefficient which is clearly a function of cylinder position in the array and Δ. However, the author assumed C_1 a constant.

Despite the obvious shortcomings of the theoretical justification, Yano's results compare quite favorably to his measured data. Cylinder lateral and longitudinal pitch were not particularly small being on the order of 5.3 diameters which may have helped. Comparisons for u_m behind the several cylinders were good to spacings of 5.3d (the smallest measured). While this would at first appear contrary to the range of validity of the similarity solution, it must be recalled that this same phenomena occurs in both Schlichting and Eskinazi's data. It would appear that the similarity solution validity extends close then the $x/C_D d > 50$ suggested by Schlichting (1960) if we are willing to

overlook the deviation of the tails of the defect profile from Gaussian. This same deviation is apparent in the author's measured profiles.

Yano's predicted wake widths also agree well with measured widths for multi-cylinder longitudinal arrays. The wake width grows as $x^{1/2}$ for only the first cylinder. Each succeeding wake appears to take a longer downstream distance to attain a simple power law growth rate (for all cylinders the power approaches 1/2 however). For example, the second cylinder wake varies as $x^{1/2}$ beginning about 21 diameters downstream, the third 37 diameters, etc.

In conclusion, it would appear that the wake momentum defect method proposed by Yano (1966) holds promise as a means of predicting wake development of multi-cylinder arrangements. This conclusion is not based upon the author's theoretical justification. It is based upon comparison of measured and predicted results. Whether this conclusion holds for configurations other than that tested by Yano remains to be seen. If the superimposed wake extent and defect downstream of a multi-cylinder array can be predicted then the drag of the array can also be predicted from momentum considerations applied to the flow field.

B. Mathematical Model for Resistance to Flow in a Channel with a Multi-Cylinder Distribution

A mathematical model is derived in this study to describe the mean flow properties in an open channel with a multi-cylinder distribution. Basically the model predicts the drag on each cylinder and the normal depth of flow if certain conditions are met, and the following data is given: i) the size and distribution of cylinders, ii) the discharge, iii) the average slope of the channel, and iv) the local coefficient of drag of the cylinders in the channel.

Assumptions are necessary for a closed form solution to the problem. The cylinders are assumed to be distributed in such a manner that uniform flow in the channel exists. The slope in the channel should be uniform. Each wake decays independently of the downstream or upstream distribution of cylinders; this assumption allows one to use the superposition of wakes concept to calculate the approach velocity to each cylinder. Once the approach velocity is known then the cylinder drag is calculated according to a normal drag force equation if the local drag coefficient C_d is known.

In order to predict the approach velocity to each cylinder it is necessary to determine the wake spread and decay characteristics. For approximately zero slope relations, Eqs. (2-1), (2-2) and (2-3) may be used if the drag coefficient is known. However, if the slope is relatively large a correction for the effect of slope on the decay of wakes is necessary and Eqs. (2-1), (2-3) and (2-4) may be used.

Yano (1966) used linear superposition of momentum defects, or

$$u^2_{total} = u_1^2 + u_2^2 + u_3^2 + \ldots \qquad (2.18)$$

From Reichardt's (1943) theory of turbulence, Petryk (1969a) argued that linear superposition of velocity defects was permissible, or

$$u_{total} = u_1 + u_2 + u_3 \ldots \quad . \qquad (2.19)$$

This section describes how superposition may be used to predict the velocity profile across the channel and to predict the drag force on each cylinder. From now on, superposition will be used as a general term, unless otherwise specified. It may refer to either Yano's method or to Petryk's method.

The following analysis starts with flow characteristics behind a single cylinder, and then proceeds to a multi-cylinder arrangement.

1. Single Cylinder: The flow approaching the cylinder is assumed to be fully developed open channel flow. Experimental drag measurements verify that the two-dimensional value of 1.2 is a satisfactory value for the local drag coefficient if: i) the wave drag is small, ii) no aeration takes place behind the cylinder, and iii) the cylinder Reynolds number is low enough where the cylinder is well in the subcritical regime of flow, but greater than or equal to about 8×10^3 . The velocity distribution in the wake of the cylinder is described by (see Fig. 2.4)

$$\bar{U}(x,z) = U_\infty(x) + u_1(x,z) \tag{2.20}$$

where $u_1(x,z)$ is the velocity defect at point (x,z) , which is solved from Eqs. (2.1), (2.3) and (2.4) or Eqs. (2.1), (2.6) and (2.7), depending on whether Petryk's or Yano's method is used. $\bar{U}(x,z)$ is the resultant mean velocity at point (x,z) and $U_\infty(x)$ is regarded as the reference free stream velocity at distance x from the cylinder; $U_\infty(x)$ can be derived as follows:

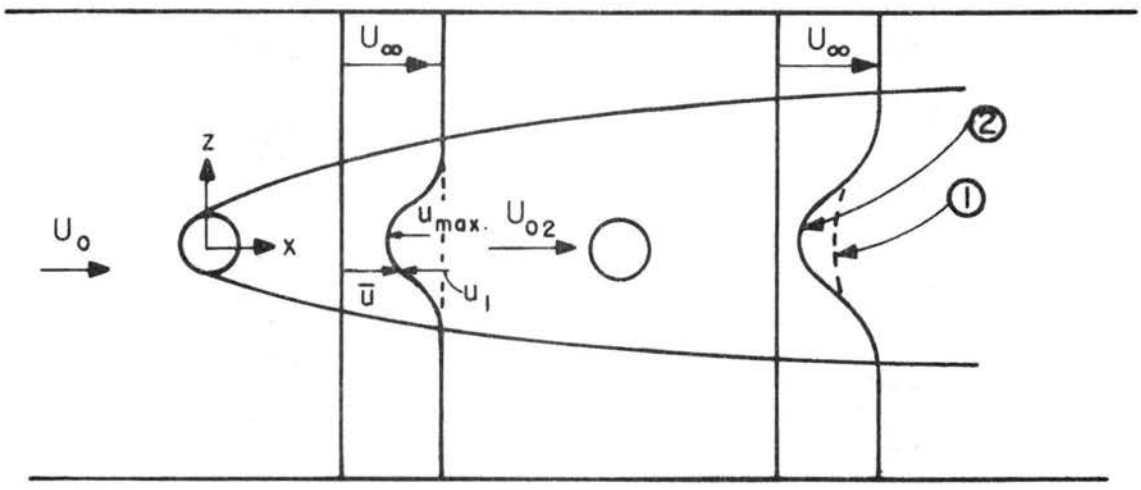

Fig. 2.4. Velocity Profile in Wakes.

From continuity equation

$$Q = U_o\, WD = D \int_W \bar{U}(x,z)\, dz$$

$$= D \int_W [U_\infty(x) + u_1(x,z)]\, dz$$

$$= D\, U_\infty(x)\, W + D \int_W u_1(x,z)\, dz$$

and will then result in

$$U_\infty(x) = U_o - \frac{1}{W} \int_W u_1(x,z)dz \qquad (2.21)$$

where D is the depth of flow, W is the width of the channel and U_o is the mean velocity based on the flow area. From Eqs. (2.20) and (2.21) one can compute the velocity distribution in the wake.

2. Multiple Cylinders Distributed in a Given Pattern:

a) Petryk's Method:

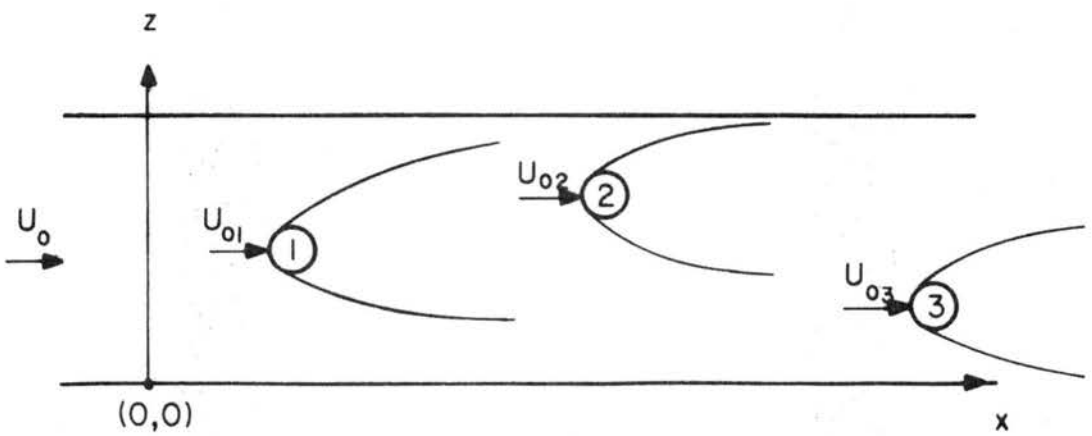

Fig. 2.5. Multiple Cylinder Wake.

Referring to Fig. 2.5, the coordinates of ith cylinder are expressed as (x_i, z_i) and the approached velocity of the first cylinder is taken to be $U_{o1} = U_o$ (the upstream undisturbed flow velocity).

The cylinder diameter is assumed to be small enough to be considered as a point in comparison with the whole channel width, and the approached velocity U_{o2} for the second cylinder can be evaluated according to the single cylinder wake solution, or

$$\begin{aligned} U_{o2} &= \bar{U}(x_2,z_2) \\ &= U_\infty(x_2) + u_1[(x_2-x_1),(z_2-z_1)] \end{aligned} \tag{2.22}$$

where

$$U_\infty(x_2) = U_o - \frac{1}{W}\int_W u_1[(x_2-x_1),(z-z_1)]\,dz \quad . \tag{2.23}$$

Now, consider the third cylinder, the velocity defect at point (x_3,z_3) can be expressed as

$$u(x_3,z_3) = u_1[(x_3-x_1),(z_3-z_1)] + u_2[(x_3-x_2),(z_3-z_2)]$$

then

$$\begin{aligned} U_{o3} &= \bar{U}(x_3,z_3) \\ &= U_\infty(x_3) + u(x_3,z_3) \\ &= U_\infty(x_3) + u_1[(x_3-x_1),(z_3-z_1)] + u_2[(x_3-x_2),(z_3-z_2)] \end{aligned} \tag{2.24}$$

and

$$\begin{aligned} U_\infty(x_3) &= U_o - \frac{1}{W}\int_W u(x_3,z)\,dz \\ &= U_o - \frac{1}{W}\int_W u_1[(x_3-x_1),(z-z_1)]\,dz \\ &\quad - \frac{1}{W}\int_W u_2[(x_3-x_2),(z-z_2)]\,dz \end{aligned} \tag{2.25}$$

where u_1 is the velocity defect due to the first cylinder and u_2 is that due to the second. With known U_{o1} and U_{o2}, one can solve U_{o3} by Eqs. (2.24) and (2.25).

Similarly, for the nth cylinder

$$U_{on} = U_{\infty}(x_n) + \sum_{i=1}^{m} u_i[(x_n - x_i),(z_n - z_i)] \tag{2.26}$$

$$U_{\infty}(x_n) = U_o - \frac{1}{W} \sum_{i=1}^{m} \int_W u_i[(x_n - x_i),(z - z_i)]\, dz \tag{2.27}$$

where m is the number of cylinders which have had influence on the nth cylinder and where $x_i < x_n$ and $u_{imax}/U_{oi} \geq 0.02$. It is arbitrarily assumed that when $u_{imax}/U_{oi} \leq 0.02$ the wake effect due to the ith cylinder has been completely dissipated.

When the wake spreads to the edge of the channel, the wake is constricted by the wall, the integration limits in Eq. (2.27) should not be greater than the width of the flume.

b) Yano's Method: To use superposition of momentum defects (Eq. 2.15) instead of velocity defects (Eq. 2.19), one can follow the similar procedures for establishing Petryk's method and obtain

$$U_{on} = U_{\infty}(x_n) - \sqrt{\sum_{i=1}^{m} u_i^2[(x_n - x_i),(z_n - z_i)]} \tag{2.28}$$

$$U_{\infty}(x_n) = U_o + \frac{1}{W} \int_W \sqrt{\sum_{i=1}^{m} u_i^2[(x_n - x_i),(z - z_i)]}\, dz \tag{2.29}$$

3. An Iterative Solution to Find the Resistance to Flow for a Given Cylinder Distribution: From the above analysis, the model predicts the velocity at any point in the channel. That is, the approach velocity to every cylinder is known. The drag on each cylinder is also known from

$$F_i = \frac{1}{2} C_d \rho U_{oi}^2 d_i D \tag{2.30}$$

where:

d_i = diameter of the ith cylinder

D = depth of flow

F_i = drag on the ith cylinder

C_d = local drag coefficient or the drag coefficient on an individual cylinder without any influence from other cylinders.

Take a channel section with some cylinder distribution as shown in Fig. 2.6, assuming uniform flow, momentum considerations give:

Weight of fluid between section 1 and 2 x slope =

$$\underset{\text{II}}{\int_{A'} \tau_w dA'} + \underset{\text{III}}{\Sigma \text{ (Drag forces on the cylinders)}} \qquad \underset{\text{I}}{} \qquad (2.31)$$

where τ_w is the shear stress on the channel walls, A' is the differential element of area of the channel wall, and the Roman numerals refer to the different terms in Eq. (2.31).

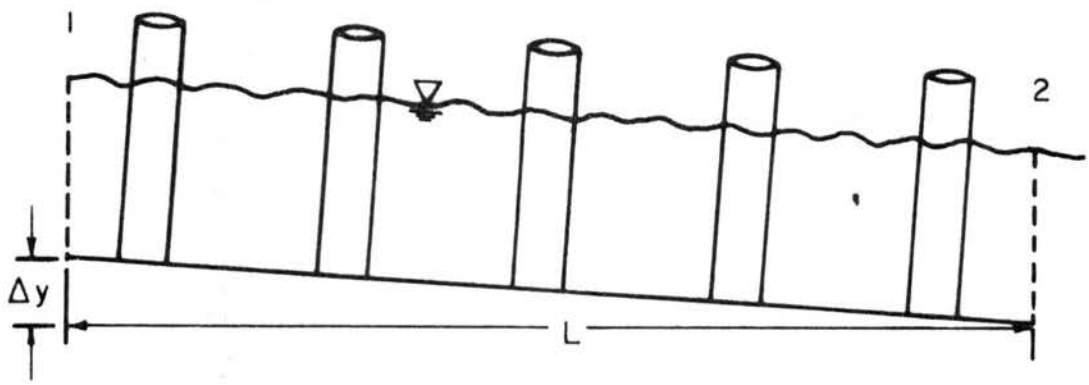

Fig. 2.6. Cylinders in a Channel

An estimate of $\int_{A'} \tau_w dA'$ may be made by assuming that the normal channel friction factor is applicable to estimate friction losses on the walls. For smooth walled channels Tracey and Lester (1961) give the following formula:

$$\frac{1}{\sqrt{f}} = -1.30 + 2.03 \log_{10} R_c \sqrt{f} \qquad (2.32)$$

where

$f = 8S_o gR/U_o^2$ = friction factor

R = hydraulic radius = A/P_r

S_o = energy slope due to friction on the channel walls

A = area of channel flow

P_r = perimeter of flow, excluding cylinders

$U_o = Q/DW$ = average velocity

D = depth of flow

W = width of channel

$R_c = 4RU_o/\nu$ = channel Reynolds number

ν = the kinematic viscosity of water

Equation (2.31) will be satisfied for only one depth of flow in the channel. To obtain this solution, the following procedure is used.

i) Find the first estimate of flow depth by using Eq. (2.32), i.e., neglect the effect of the cylinders.

ii) Having a first estimate of depth, the drag of the cylinders is included, neglecting the effect of wake interference, i.e., the drag force on each cylinder is based on the mean velocity U_o. Term II is solved from Eq. (2.32); its magnitude is based on the mean velocity of flow. Iteration proceeds until Eq. (2.31) is satisfied with a second estimate of depth.

iii) Having a second estimate of depth, the drag of each cylinder with wake interference is calculated according to the method outlined previously. Term II is calculated as given in ii) above. Iteration proceeds until the required depth satisfies Eq. (2.31).

In summary, the required data for the problem is discharge, width of channel section, slope of channel, size of each cylinder, and the location of each cylinder in terms of the x , z coordinate system.

C. Experimental Program and Data Reduction

An extensive experimental program was carried out in this study for two main purposes. The first one was to verify the mathematical model, determine what limitations would have to be imposed, determine what was the accuracy of the model and compare the two superposition methods. The second one was to determine the drag characteristics of two cylinders placed at different positions relative to each other.

To investigate the mathematical model, different multi-cylinder distributions were placed in the facility described by Petryk (1969a). The cylinder's Reynolds numbers were low enough so that each cylinder was in the subcritical regime of flow. The cylinders were made of standard steel conduit pipe, except for the drag measuring cylinder which was made of plexiglass.

The drag force on only one cylinder in the multi-cylinder distribution was measured by the drag balance as described in section II-C. The measured mean drag coefficient was then compared with the computed mean drag coefficients for each cylinder pattern.

The mean drag coefficients were computed by two superposition methods, by Yano's method and by Petryk's method. In each method the computed drag force was calculated by Eq. (2.30).

The local drag coefficient, C_d, which is based on the approached velocity to the cylinder, was assumed to be constant at 1.2. The mean drag coefficient is defined as

$$\overline{Cd_i} = \frac{F_i}{\frac{1}{2}\rho U_o^2 d_i D} = \frac{\frac{1}{2} C_d \rho U^2_{oi} d_i D}{\frac{1}{2}\rho U_o^2 d_i D}$$

$$\overline{Cd_i} = \frac{U_{oi}^2}{U_o^2} C_d \quad . \tag{2.33}$$

The testing conditions were: i) 21 different cylinder patterns of parallel, staggered and random distribution, ii) the ranges of flow conditions ; $2.25 \leq D \leq 11.5$ inches , $0.75 \leq U_o \leq 3.37$ ft/sec , and iv) two sizes of cylinder diameters of two inches and 4-1/2 inches. A total of 113 sets of data were obtained and a more detailed description of the testing conditions is given by Petryk (1969a).

D. Discussion of Results

1. Comparison of Mathematical Models with Experimental Results:

The agreement between computed mean drag coefficients and the measured mean drag coefficient is generally good for both Petryk's and Yano's methods (Fig. 2.7 shows the comparison for Petryk's method). The deviations are generally within ± 30%. Satisfactory agreement is also found when the computed velocity distribution across the channel is compared with the measured values as shown by Petryk (1969a). However, experimental results indicate that for certain cylinder patterns, Yano's superposition method is better than Petryk's method and vice versa. The following tentative conclusions were reached as to which method is better for a given cylinder pattern:

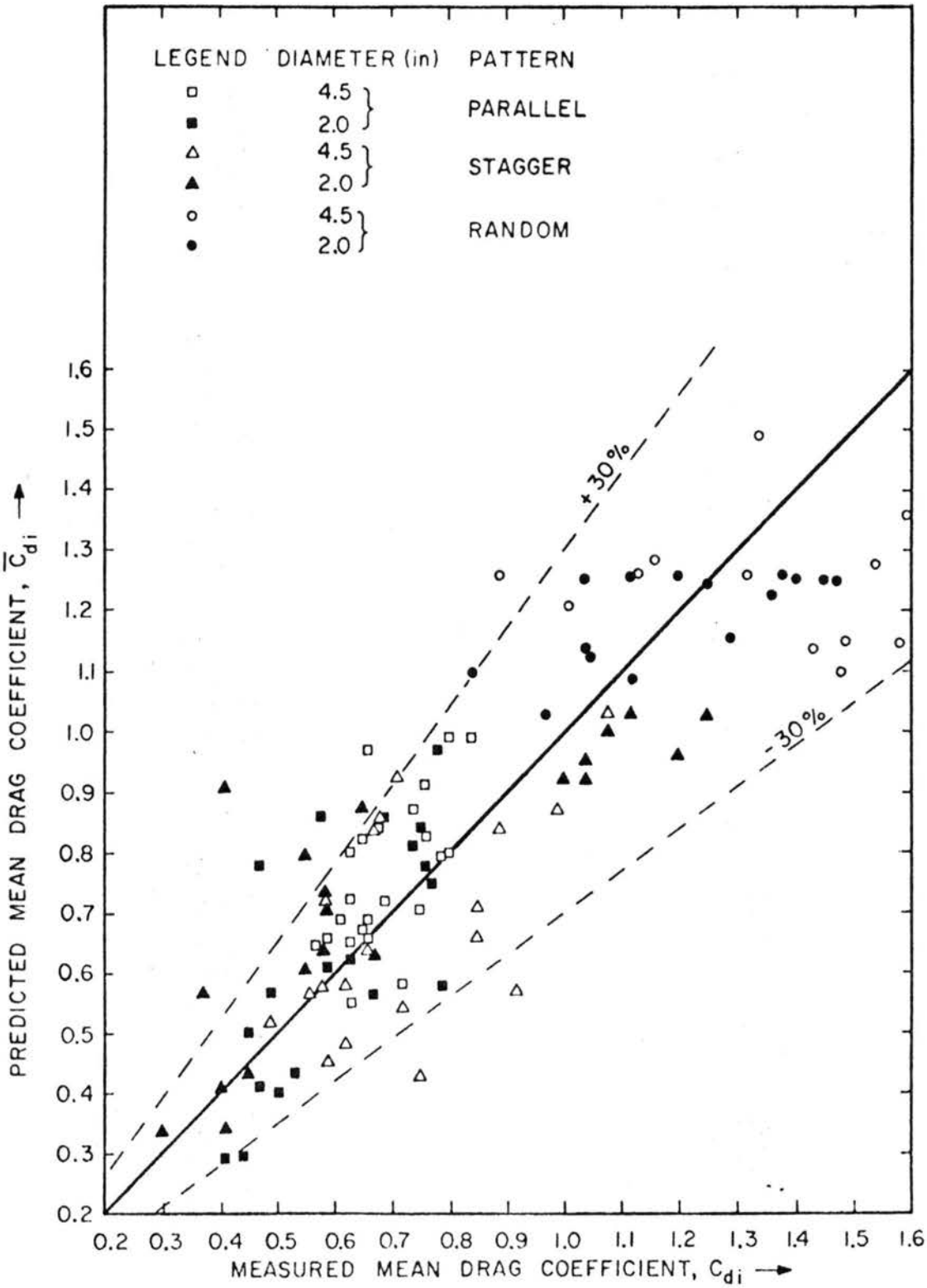

Fig. 2.7. Comparison of Predicted Mean Drag Coefficients (Petryk's Method) With Measured Mean Drag Coefficient

i) Yano's method is better for in-line relatively close cylinder spacing of six to ten diameters. This is due to the invalidity of the assumptions of u_1/U_o being small in Petryk's method.

ii) Petryk's method is generally better for flow situations where the cylinders are distributed only along one side of the channel.

iii) Either method can be used for other conditions within the limits of the mathematical model. However, Petryk's method is preferred over Yano's method.

The experimental $\overline{C_d}$ values varied with different flow conditions, and, in general, $\overline{C_d}$ decreased with the increase of the average velocity U_o, which agrees with the computed results. Figure 2.8 shows the relationship between computed mean drag coefficient and average velocity for selected runs.

The scatter of measured data (as shown in Fig. 2.7) can be explained by any of the following reasons:

i) The local drag coefficient C_d varies with flow conditions. This point was investigated later and the results are presented in section III-D-5 of this chapter.

ii) Some of the runs were close to the point where aeration behind the cylinder almost occurred, and where wave drag and blockage were important.

iii) The cylinder Reynolds number may have been high enough to place the cylinder in the critical regime of flow and hence the drag is reduced.

iv) Under different flow conditions, a different degree of "channeling" may have occurred as shown by Chen (1968).

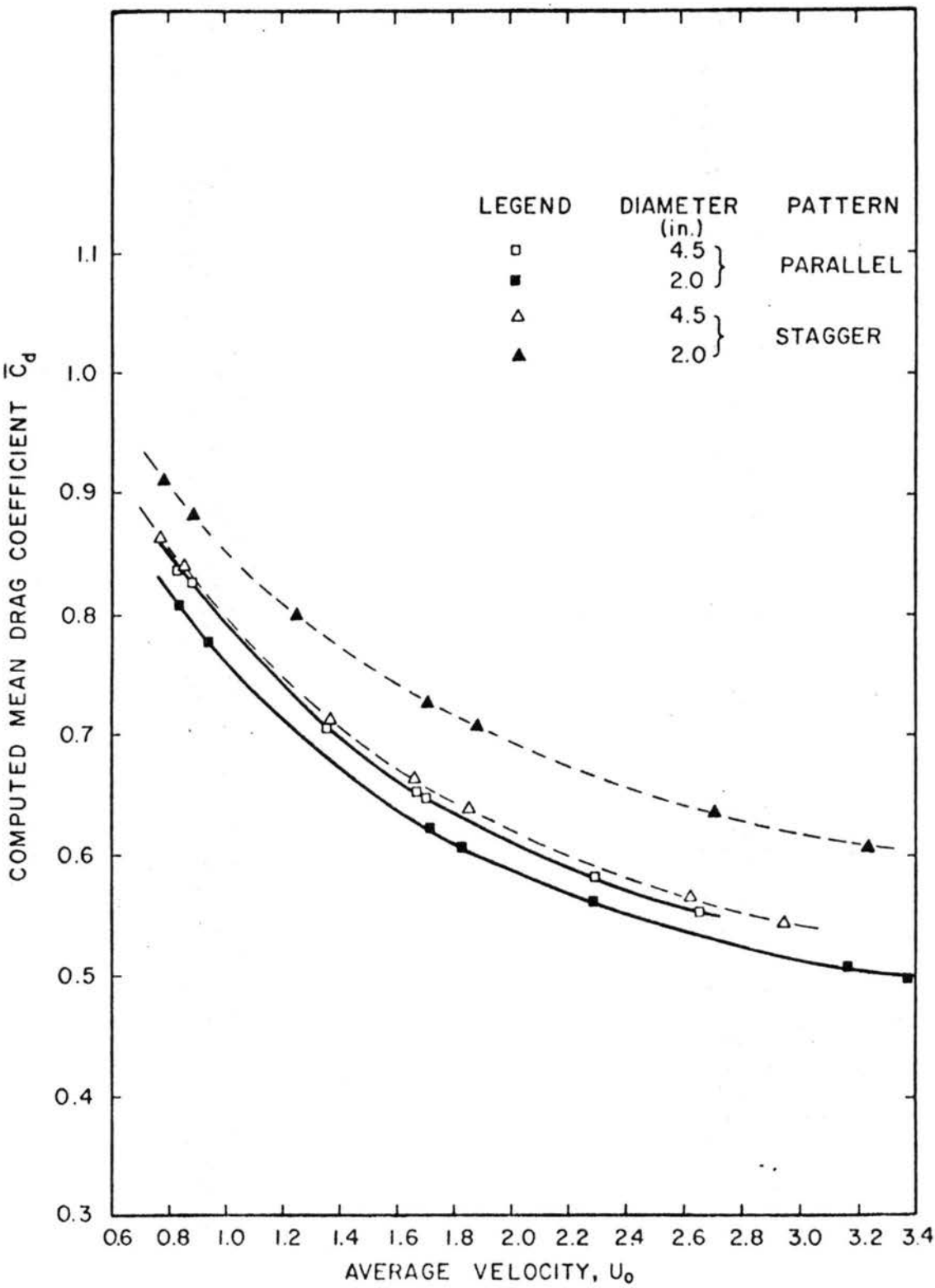

Fig. 2.8. Relation Between Computed Mean Drag Coefficient and Average Velocity For Selected Runs

v) Waves formed in the channel at certain flow conditions when the cylinder vortex shedding frequency corresponded to a natural wave frequency in the channel.

vi) Another instability, which could have existed in the channel, may have been some form of secondary flow.

vii) The maximum velocity defect decayed more quickly for a cylinder placed close to the wall than for the cylinder placed in the center of the channel as shown by Eskinazi (1959).

All of the above effects, which contributed to the experimental variation in the mean drag coefficient magnitudes, were also important in contributing to the deviations of the computed values from the experimental values.

It was found that the measured velocity distributions are similar for both subcritical flow and supercritical flow in the channel portion which is free of cylinder. This indicates that the model is at least qualitatively applicable to flood flow conditions, where the flow in the main channel section may be supercritical while the flow in the vegetated flood-plain section may be quiescent and subcritical. Similarity in the velocity distributions across the channel occurs when the ratio of friction factor remains constant.

2. Limitations and Criticisms of Mathematical Models: The mathematical model, in its present form, is applicable to flow situations where the following limitations apply:

i) The flow in the channel is uniform.

ii) The spacing between cylinders is at least six diameters in the downstream direction or three diameters in the crosswise direction.

iii) The flow around each cylinder is such that free surface effects are small, i.e., outside of the wave drag region, and outside of the region where aeration affects the drag coefficients.

The agreement between the computed mean drag coefficients and the measured mean drag coefficients is approximately within 30% of the measured values.

It should be noted that the model was verified experimentally for only subcritical cylinder Reynolds numbers. However, it should also be valid for critical and supercritical Reynolds numbers if the proper local drag coefficient is known or can be estimated. The mathematical model does not consider the important free stream turbulence effects on wake characteristics. If there is a large scale and high intensity turbulence created by the upstream cylinder, the computed superposition solution would likely yield poor agreement with actual cases.

Another criticism of the model is that it does not give satisfactory velocity distributions near a cylinder. The regions where velocity distributions are not provided include: i) the near-wake region between the cylinder and the area where wake theory is applicable and ii) the area to the front and sides of the cylinder where potential flow theory can be applied as a first approximation.

3. Increase in Depth of Flow Owing to the Presence of Cylinders in an Open Channel: Normal flow depth computations for a particular channel without cylinders and with different cylinder patterns were made by Petryk (1969a). The comparison of computed results shows that the presence of cylinders in an open channel increased the flow depth substantially and the effect of local drag coefficient on flow depth computation is not too sensitive. If an error of 30% is

made in estimating the local drag coefficient, the error in predicting the flow depth by the proposed model should be less than 30%.

4. Drag Characteristics of Two Cylinders Placed at Different Positions Relative to Each Other: Figure 2.9 shows F/F_{sc} plotted as a function of Δ/d and ϕ. The cross hatched cylinder, shown in the figure was the one on which the drag force F was measured. The data shows the following drag characteristics for the two cylinders.

i) The effect of a directly downstream cylinder ($\phi=0$) is to reduce the drag force on the upstream cylinder by as much as about 10 to 15%. Figure 2.9 shows that some drag reduction occurs for all Δ/d ratios up to 4.0 for values of ϕ from 0° to 45°.

ii) From ϕ = 60° to 90°, an increase in drag occurs. For small Δ/d values, the reason for the increase in drag force is that the body formed by two cylinders is "bluffer" than a single cylinder. "Bluffer" means less streamlined; i.e., when two cylinders are placed together crosswise in a stream, the drag due to the positive pressure coefficient along the front portion of the cylinder is likely higher than for a single cylinder in a stream. For small values of Δ/d the increased drag force is due to blockage effects caused by the neighboring cylinder.

iii) It is interesting to note the large change in drag characteristics from ϕ = 90° to 105° for Δ/d approximately equal to .75.

iv) The maximum increase in drag force occurs at small Δ/d ratios for ϕ = 120° and 135°. The maximum increase in drag is of order 300% over the single cylinder drag force. The large increase in drag is assumed to be caused by the high velocity fluid, coming from the upstream cylinder, which impinges on the downstream cylinder as shown in Fig. 2.10.

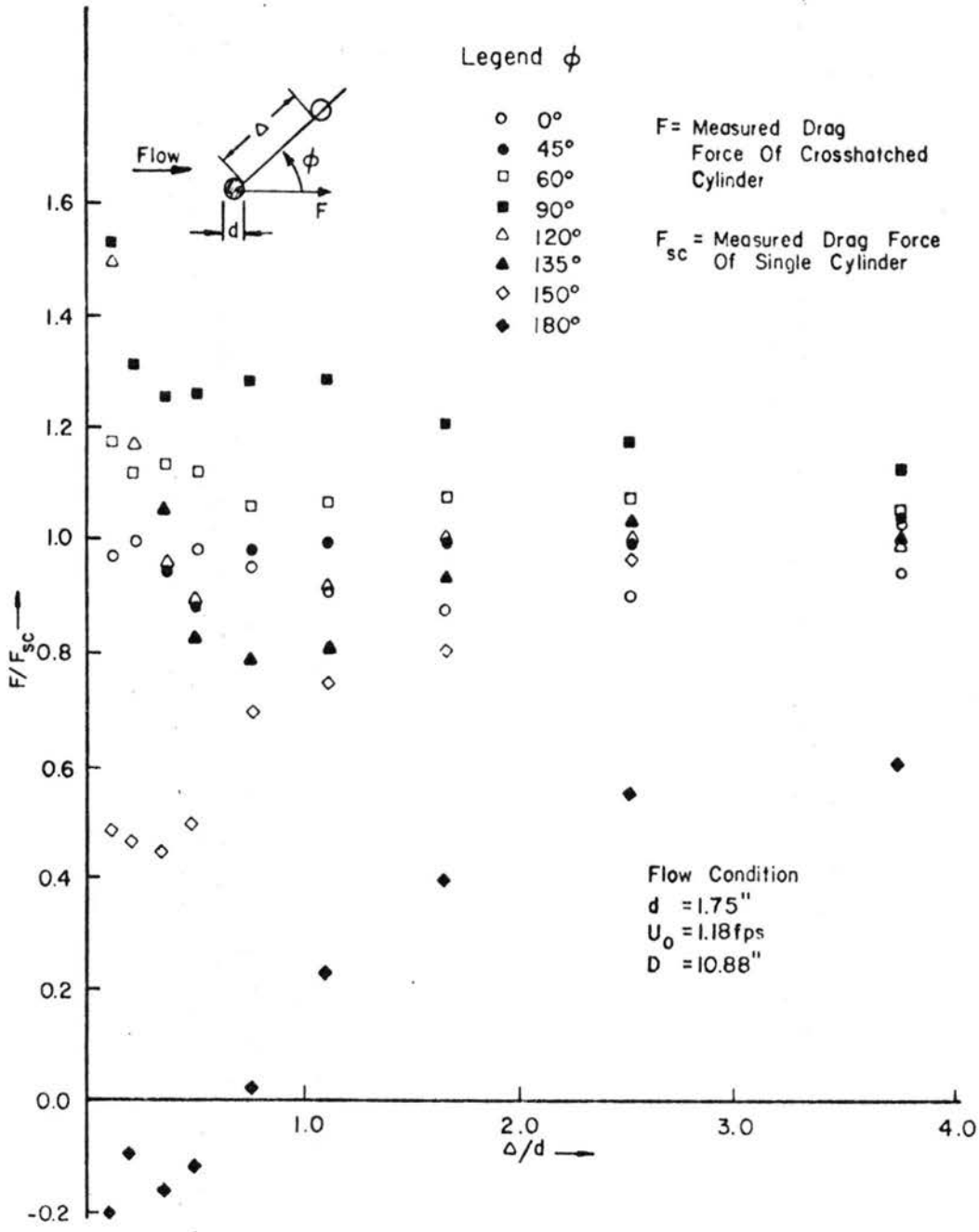

Fig. 2.9. Drag Correlation For Two Cylinders

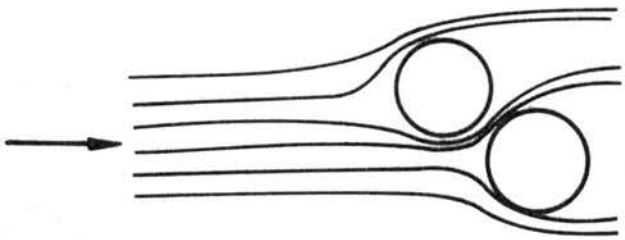

Fig. 2.10. Flow Through Two Adjacent Cylinder Sketch.

v) These experimental results show that a large drag force on two cylinders exists for two cylinder arrangements:

a. For the cylinder arrangements discussed in iv) above, the total drag force on two neighboring cylinders is 150% higher than two times the drag force on a single cylinder.

b. At $\phi = 90°$ and Δ/d less than 0.1, the total drag force on two neighboring cylinders is 65% higher than two times the drag force on a single cylinder.

Figure 2.11 shows the effect a neighboring cylinder placed in line with the flow direction. It was placed directly downstream ($\phi = 0$ or in the positive x direction) and then directly upstream ($\phi = 180°$ or in the negative x direction).

From Fig. 2.11 the following drag features are noted in addition to comments made at the beginning of this section:

i) The effect of an upstream cylinder on a downstream cylinder is felt for a long distance, as indicated from the experimental data and the wake superposition solutions from the mathematical model. At 80 diameters there is still a noticeable reduction in drag.

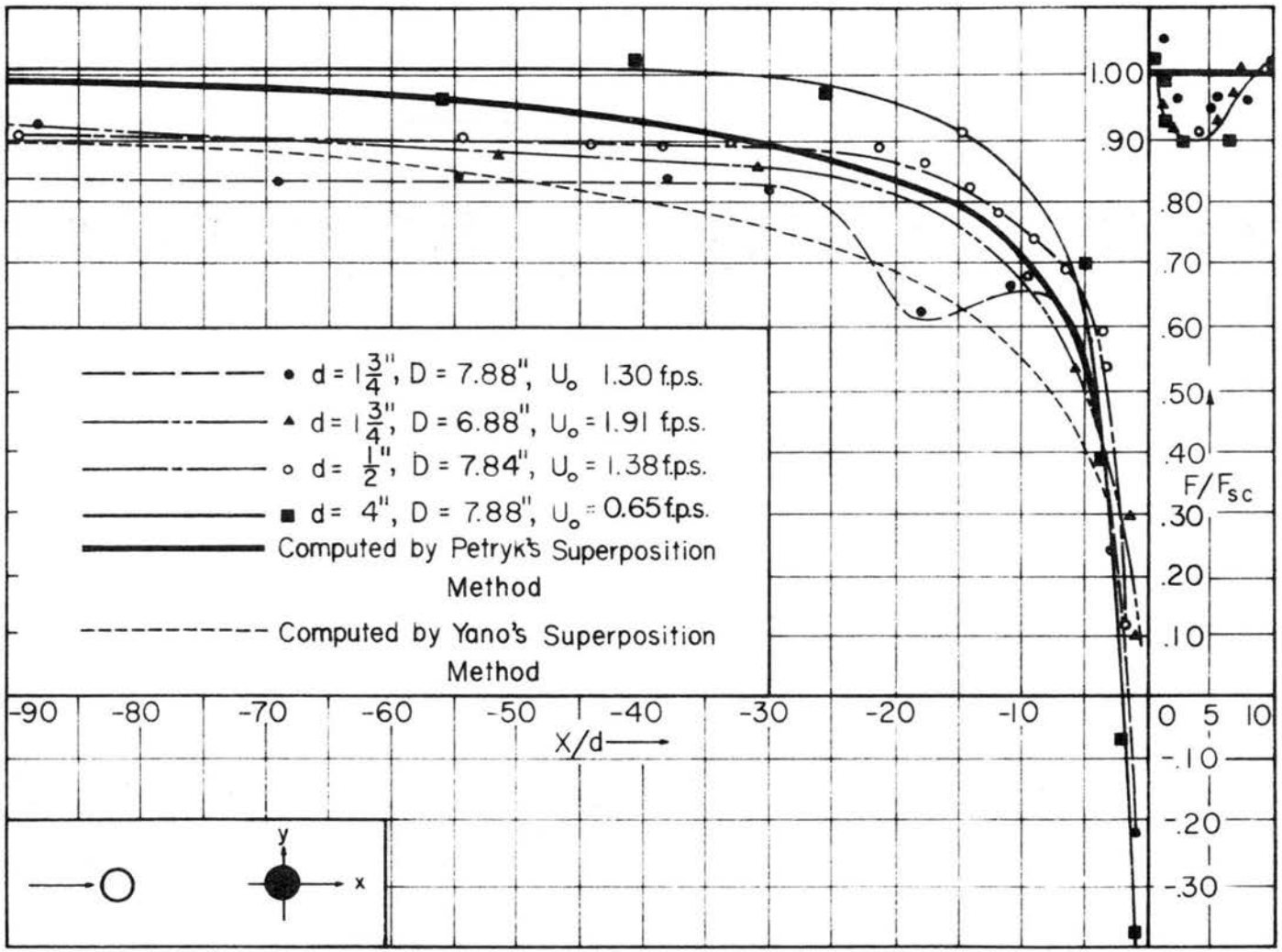

Fig. 2.11. Effect of Upstream or Downstream Cylinder on Drag

ii) The drop in drag force with more negative x values was unexpected for the run with the 1-3/4 inch cylinder at 1.30 fps (at $x/d \simeq -20$). Similar qualitative behavior has been reported by Bierman and Herrnstein (1933). The drag behavior may be explained by the vortex shedding pattern from the upstream cylinder, and the manner in which the vortices pass by the downstream cylinder. The vortices passing the downstream cylinder may effectively reduce the approach velocity.

iii) At low cylinder Froude numbers negative values of drag force are experienced by the downstream cylinder at small x/d values, similar to the results presented by Bierman and Herrnstein (1933).

5. Local Drag Coefficient of a Single Cylinder in a Group of Cylinders: As discussed in Section II-3 of this chapter, the best estimate of the drag coefficient for an individual cylinder is the two-dimensional value of 1.2 provided that i) no aeration exists behind the cylinder, ii) there is no blockage effect, and iii) it is a subcritical flow range. As stated in Section III-D-1, this local drag coefficient C_d could be different for a single cylinder in a multiple cylinder arrangement.

In our experiment, F_i , ρ , d_i and D are all known for all runs and it is found that the minimum f occurs at $C_d \simeq 1.1$ where

$$f = \sum_{i=1}^{n} (\bar{C}_{d_i} - C_{d_i})^2 \qquad (2.34)$$

and

$$C_{d_i} = \frac{F_i}{\frac{1}{2} \rho U_o^2 d_i D} \quad . \qquad (2.35)$$

and $\bar{C}_{d_i}$ is the computed mean drag coefficient by Eq. (2.33) and C_{d_i}

is the measured mean drag coefficient computed by Eq. (2.32) with measured drag force F_i .

The conclusion is to use $C_d = 1.2$ for the local drag coefficient in Eq. (2.30) since there is no strong evidence to prove otherwise.

6. Effect of Cylinder Patterns and Spacings on the Mean Drag Coefficient: There are two basic regular patterns: parallel and staggered and the effects of these two cylinder patterns at different spacings on drag coefficients were studied. Figure 2.12 shows that the mean drag coefficients are increased with increasing spacing for parallel patterns, but, the trend is reversed for staggered patterns for a particular flow condition.

7. The Variation of Drag Coefficient for a Single Row of Cylinders: Figure 2.13 shows a single row of cylinders with coordinates of ith cylinder being (x_i , z_i) and $z_1 = z_2 = z_3 = \ldots = z_n = 0$.

The approaching velocity for the first cylinder is the average velocity U_o , i.e.,

$$U_{o_1} = U_o \quad . \tag{2.36}$$

From Eq. (2.22) the approaching velocity for the second cylinder is

$$U_{o_2} = U_\infty(x_2) + u_i(x_2-x_1,0) \quad . \tag{2.37}$$

From Eq. (2.23)

$$U_\infty(x_2) = U_o - \frac{1}{w}\int_w u_i(x_2-x_1,z)dz \tag{2.38}$$

in which (according to Eq. 2.1)

$$\int_w u_1(x_2-x_1,z)dz = \int_w \frac{1}{2}\, u_1(x_2-x_1,0)\left[1 + \cos\frac{\pi z}{2b_{\frac{1}{2}}(x_2-x_1)}\right] dz$$

For $2b_{\frac{1}{2}}(x_2-x_1) \leq \frac{w}{2}$

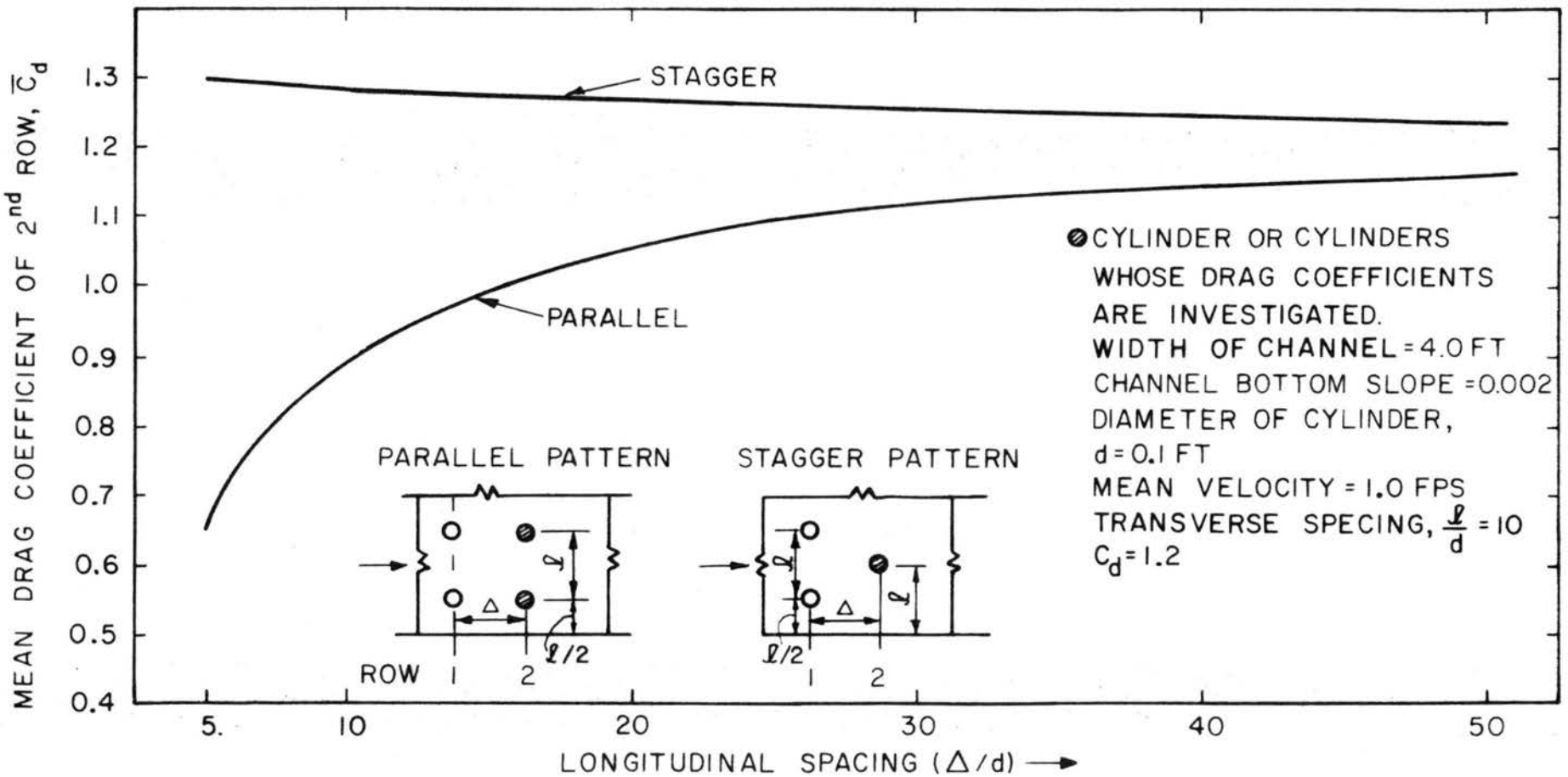

Fig. 2.12. Example of Relation Between Spacings and Mean Drag Coefficient

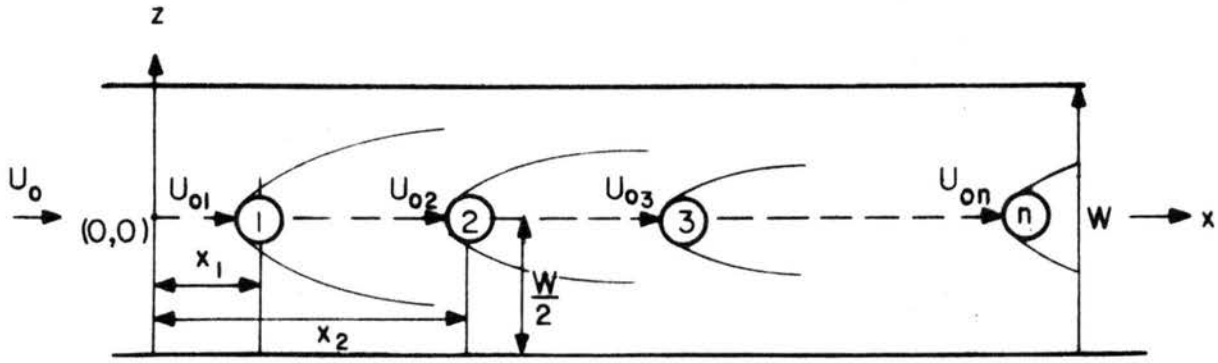

Fig. 2.13. A Single Row of Cylinders

$$\int_w u_1(x_2-x_1,z)dz = \int_{-2b_{\frac{1}{2}}(x_2-x_1)}^{2b_{\frac{1}{2}}(x_2-x_1)} \frac{1}{2}\, u_1(x_2-x_1,0)[1 + \cos \frac{\pi\, z}{2b_{\frac{1}{2}}(x_2-x_1)}]dz$$

$$= \frac{1}{2}\, u_1(x_2-x_1,0) \cdot 4b_{\frac{1}{2}}(x_2-x_1)$$

$$= 2\, u_1(x_2-x_1,0)\, b_{\frac{1}{2}}(x_2-x_1) \quad . \tag{2.39}$$

For $2b_{\frac{1}{2}}(x_2-x_1) > \frac{w}{2}$, the wake spreads to the wall and is constricted; then

$$\int_w u_1(x_2-x_1,z)dz = \int_{-\frac{w}{2}}^{\frac{w}{2}} \frac{1}{2}\, u_1(x_2-x_1,0)[1 + \cos \frac{\pi\, z}{2b_{\frac{1}{2}}(x_2-x_1)}]dz$$

$$= \frac{1}{2}\, u_1(x_2-x_1,0)[w + \frac{4b_{\frac{1}{2}}(x_2-x_1)}{\pi} \sin (\frac{\pi\, w}{4b_{\frac{1}{2}}(x_2-x_1)})]$$

$$= \frac{w}{2}\, u_1(x_2-x_1,0)[1 + \frac{4b_{\frac{1}{2}}(x_2-x_1)}{\pi\, w} \sin (\frac{\pi\, w}{4b_{\frac{1}{2}}(x_2-x_1)})]$$

(2.40)

From Eqs. (2.37), (2.38), (2.39) and (2.40) for $2b_{\frac{1}{2}}(x_2-x_1) \leq \frac{w}{2}$

$$U_{o_2} = U_o + u_1(x_2-x_1,0)[1 - \frac{2}{w}\, b_{\frac{1}{2}}(x_2-x_1)] \tag{2.41}$$

and, for $2b_{\frac{1}{2}}(x_2-x_1) > \frac{w}{2}$

$$U_{o_2} = U_o + u_1(x_2-x_1,0)\left[\frac{1}{2} - \frac{4b_{\frac{1}{2}}(x_2-x_1)}{\pi\, w} \sin\left(\frac{\pi\, w}{4b_{\frac{1}{2}}(x_2-x_1)}\right)\right] \quad . \quad (2.42)$$

From Eq. (2.19)

$$U_{o_3} = U_\infty(x_3) + u_1(x_3-x_1,0) + u_2(x_3-x_2,0) \quad (2.43)$$

and

$$U_\infty(x_3) = U_o - \frac{1}{w}\int_w [u_1(x_3-x_1,z) + u_2(x_3-x_2,z)dz \quad (2.44)$$

in which

$$\int_w [u_1(x_3-x_1,z) + u_2(x_3-x_2,z)]dz$$

$$= 2[u_1(x_3-x_1,0)\; b_{\frac{1}{2}}(x_3-x_1) + u_2(x_3-x_2,0)\; b_{\frac{1}{2}}(x_3-x_2)]$$

$$\text{for } 2b_{\frac{1}{2}}(x_3-x_1) \leq \frac{W}{2} \quad (2.45)$$

$$= \frac{w}{2}\{u_1(x_3-x_1,0)\left[1 + \frac{4b_{\frac{1}{2}}(x_3-x_1)}{\pi\, w} \sin\left(\frac{\pi\, w}{4b_{\frac{1}{2}}(x_3-x_1)}\right)\right]$$

$$+ u_2(x_3-x_2,0)\left[1 + \frac{4b_{\frac{1}{2}}(x_3-x_2)}{\pi\, w} \sin\left(\frac{\pi\, w}{4b_{\frac{1}{2}}(x_3-x_2)}\right)\right]$$

$$\text{for } 2b_{\frac{1}{2}}(x_3-x_2) > \frac{W}{2} \quad (2.46)$$

$$= \frac{w}{2}\, u_1(x_3-x_1,0)\left[1 + \frac{4b_{\frac{1}{2}}(x_3-x_1)}{\pi\, w} \sin\left(\frac{\pi\, w}{4b_{\frac{1}{2}}(x_3-x_1)}\right)\right]$$

$$+ 2\, u_2(x_3-x_2,0)\; b_{\frac{1}{2}}(x_3-x_2)$$

$$\text{for } 2b_{\frac{1}{2}}(x_3-x_2) \leq \frac{W}{2} \text{ and } 2b_{\frac{1}{2}}(x_3-x_1) > \frac{W}{2} \quad . \quad (2.47)$$

From Eqs. (2.43), (2.44), (2.45), (2.46) and (2.47)

$$U_{o_3} = U_o + u_1(x_3-x_1,0)\left[1 - \frac{2}{w}\, b_{\frac{1}{2}}(x_3-x_1)\right.$$

$$+ u_2(x_3-x_2,0)\left[1 - \frac{2}{w}\, b_{\frac{1}{2}}(x_3-x_2)\right]$$

$$\text{for } 2b_{\frac{1}{2}}(x_3-x_2) \leq \frac{W}{2} \quad (2.48)$$

$$U_{o_3} = U_o + u_1(x_3-x_1,0)\left[\frac{1}{2} - \frac{4b_{\frac{1}{2}}(x_3-x_1)}{\pi w} \sin\left(\frac{\pi w}{4b_{\frac{1}{2}}(x_3-x_1)}\right)\right]$$

$$+ u_2(x_3-x_2,0)\left[\frac{1}{2} - \frac{4b_{\frac{1}{2}}(x_3-x_2)}{\pi w} \sin\left(\frac{\pi w}{4b_{\frac{1}{2}}(x_3-x_2)}\right)\right]$$

$$\text{for} \quad 2b_{\frac{1}{2}}(x_3-x_2) > \frac{W}{2} \text{ , and} \tag{2.49}$$

$$U_{o_3} = U_o + u_1(x_3-x_1,0)\left[\frac{1}{2} - \frac{4b_{\frac{1}{2}}(x_3-x_2)}{\pi w} \sin\left(\frac{\pi w}{4b_{\frac{1}{2}}(x_3-x_1)}\right)\right]$$

$$+ u_2(x_3-x_2,0)\left[1 - \frac{2}{w} b_{\frac{1}{2}}(x_3-x_2)\right]$$

$$\text{for} \quad 2b_{\frac{1}{2}}(x_3-x_2) \leq \frac{W}{2} \text{ and } \quad 2b_{\frac{1}{2}}(x_3-x_1) > \frac{W}{2} \text{ .} \tag{2.50}$$

Similarly for the nth cylinder

$$U_{o_n} = U_o + \sum_{i=1}^{n-1} u_i(x_n-x_i,0)\ B_i(x_n-x_i) \tag{2.51}$$

where

$$u_i(x_n-x_i,0) = u_i max(x_n-x_i)$$

$$= -0.9\ \left(\frac{x_n-x_i}{C_d\ d}\right)^{-0.7}\ \left(\frac{1}{1 + \frac{gS_o(x_n-x_i)}{\frac{U_{o_i}^{\ 2}}{2}}}\right)^{3/2}\ U_{o_i} \tag{2.52}$$

$$B_i(x_n-x_i) = 1 - \frac{2}{w}\ b_{\frac{1}{2}}\ (x_n-x_i)$$

$$\text{for} \quad 2b_{\frac{1}{2}}(x_n-x_i) \leq \frac{w}{2} \tag{2.53}$$

$$B_i(x_n-x_i) = \frac{1}{2} - \frac{4b_{\frac{1}{2}}(x_n-x_i)}{\pi w} \sin\left(\frac{\pi w}{4b_{\frac{1}{2}}(x_n-x_i)}\right)$$

$$\text{for} \quad 2b_{\frac{1}{2}}(x_n-x_i) > \frac{W}{2} \tag{2.54}$$

$$b_{\frac{1}{2}}(x_n-x_i) = 0.24\ (x_n-x_i)^{0.59}\ (C_d d)^{0.41} \tag{2.55}$$

The mean drag coefficient based on U_o of the nth cylinder is

$$\bar{C}_{d_n} = \frac{U_{o_n}^2}{U_o^2} C_d \quad . \tag{2.56}$$

From Eq. (2.52), one can see that the magnitude of the velocity defect u_i increases with increasing approaching velocity which, in turn, increases with increasing average velocity. From Eq. (2.51) this will result in the decrease in the approaching velocity of the next cylinder and, therefore, the mean drag coefficient is decreased with increasing average flow velocity.

A flow condition with a channel width of 4.0 ft, a channel bottom slope of 0.002, a cylinder diameter of 0.1, a mean velocity of 1.0 ft/sec and a drag coefficient for a single cylinder of 1.2 was selected to illustrate this effect. Figure 2.14 shows that the mean drag coefficient becomes approximately constant for larger distances. These asymptotic mean drag coefficients are increased with increasing cylinder spacing and these asymptotic values are generally reached at approximately 200 diameters from the first cylinder.

8. Variation of Drag Coefficients in a Multiple Row of Cylinders in Parallel and in Staggered Patterns: The asymptotic mean drag coefficient of a staggered type distribution is generally greater than that of a parallel type distribution (as shown in Fig. 2.15). The asymptotic mean drag coefficient for a parallel and staggered type distribution with different cylinder spacings for a selected flow condition is shown in Fig. 2.16.

IV. CONCLUSIONS.

The conclusions drawn from this study can be summarized as follows:

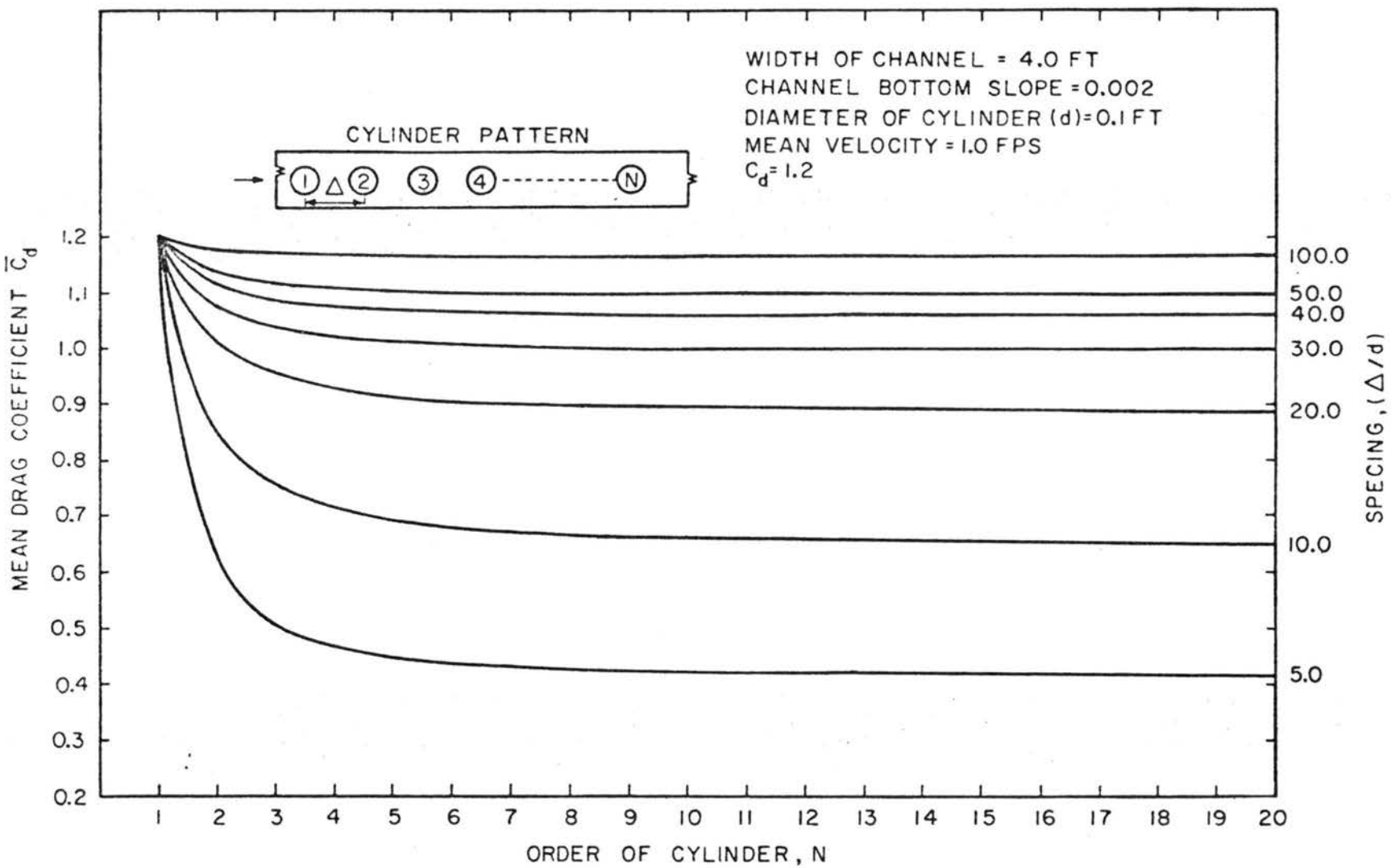

Fig. 2.14. Example of Mean Drag Coefficient Distribution in Open Channel Flow

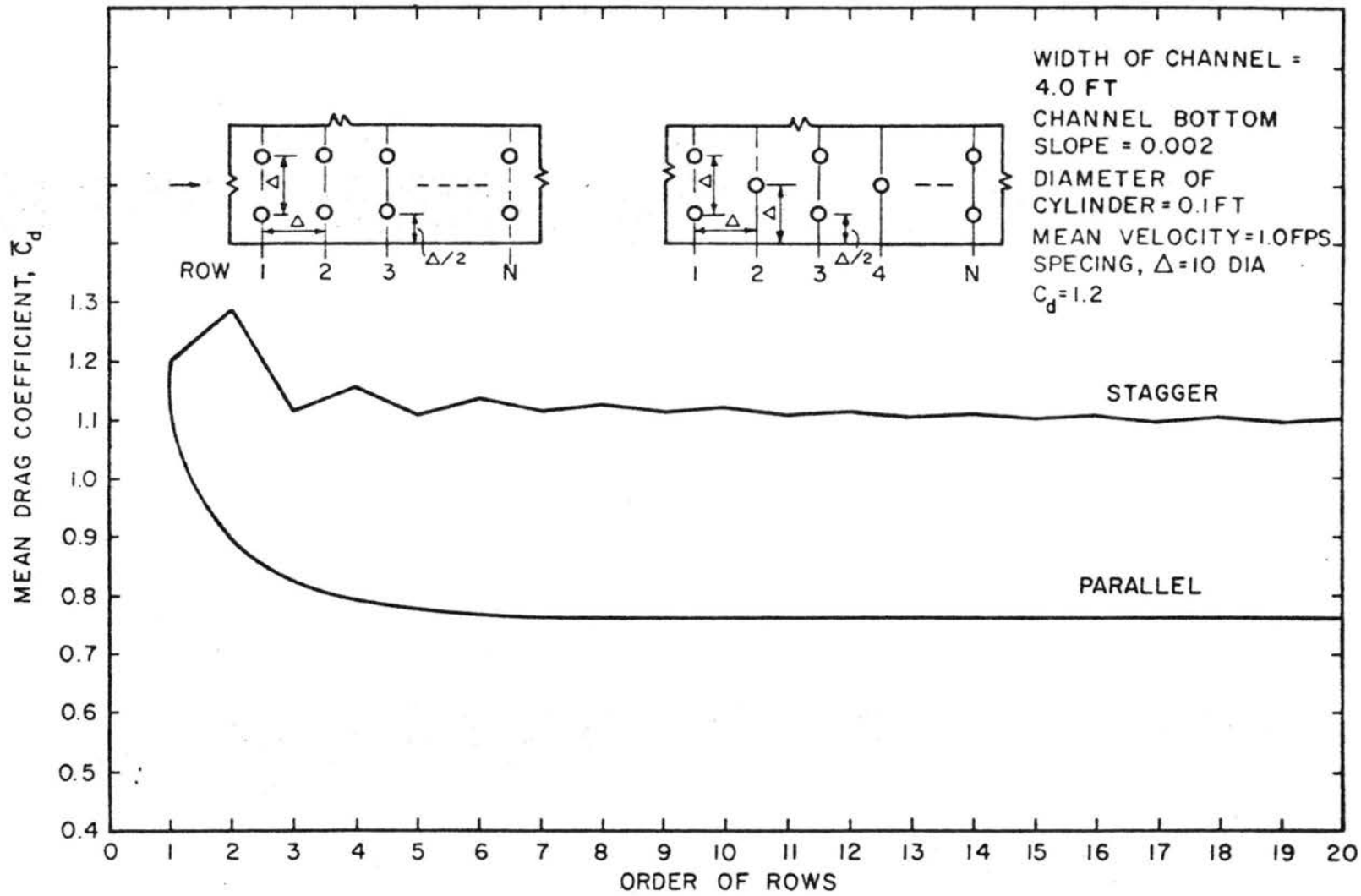

Fig. 2.15. Example of Mean Drag Coefficient Distribution in Open Channel Flow For Different Cylinder Patterns

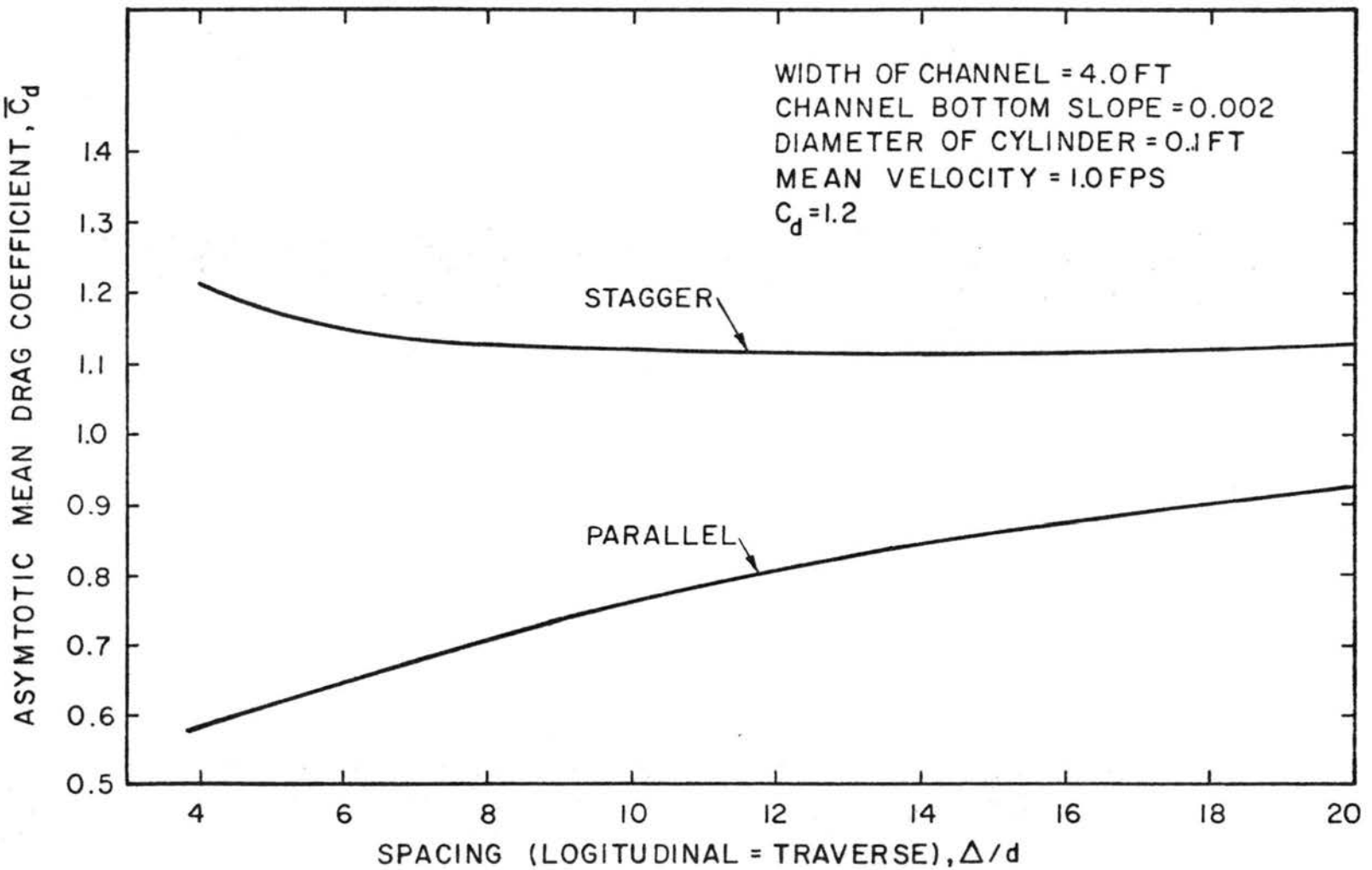

Fig. 2.16. Example of Relation Between Spacings and Asymtotic Mean Drag Coefficient

A. Wakes in Open Channels

1. The secondary flow in the near-wake region may be downward depending on the depth-to-diameter ratio and the structure of flow in the separated region back of the cylinder. This is contrary to all other reported observations which always found secondary flow in the direction of increasing free stream velocity behind a cylinder in shear flow.

2. When the velocity in the wake region is averaged over the depth of flow: i) the shape of the wake is Gaussian, and ii) the wake spreads and decays more rapidly than a two-dimensional wake with a non-turbulent free stream.

3. The detailed characteristics of the mean velocity field in channel wakes is a complex function of the free surface effects (mostly dependent on the cylinder Froude number), and secondary flow patterns ahead and back of the cylinder. Owing to the three-dimensional nature of the flow, it is not possible to describe the flow downstream as a function of the flow existing upstream at a certain height above the flume floor.

B. Cylinder in an Open Channel at Subcritical Cylinder Reynolds Numbers

1. Wave drag for a cylinder can be neglected if the depth-to-diameter ratio is greater than or equal to about four. However, for relatively shallow flows, where the depth-to-diameter ratio is less than about four, wave drag may be important, depending on the Froude numbers based on cylinder size and the Froude number based on depth of flow. If aeration does not occur behind the cylinder, maximum wave drag occurs

for cylinder Froude numbers between .5 and .9 at channel Froude numbers greater than or equal to about .5. The largest increase of the drag coefficient from the two-dimensional value of 1.2 was about 60% due to wave drag and a blockage ratio less than 10%.

2. Blockage effects appear to increase the drag coefficient more in an open channel than in a corresponding two-dimensional flow case.

C. Cylinder in an Open Channel at High Reynolds Numbers

1. The transition cylinder Reynolds number is found to be 9.0×10^4 for a cylinder in an open channel with a fully developed mean velocity profile.

2. The effect of blockage and wave drag seems to be much greater for a cylinder in the critical regime than in the subcritical regime.

3. Owing to the boundary layer and free surface effects, large pressure gradients and secondary flows occur in the longitudinal direction at about 90° and 180° relative to the forward stagnation point.

D. Open Channel Flow with a Multi-Cylinder Distribution

1. A mathematical model, based on wake superposition, provides a technique for predicting the resistance to flow in a channel with any cylinder distribution. The only restriction on it is that the spacing between the cylinders should be at least about six diameters in the downstream direction and three diameters in the crosswise direction. Wake superposition predicts the drag on each cylinder to within an accuracy of about 30% of the measured value, and predicts the velocity

distribution across the channel to an accuracy of about 15% of the measured values. The Pier Reynolds number must be in the subcritical range.

One of two wake superposition methods can be used in the model: i) Yano's wake superposition method which superimposes the momentum defects of upstream wakes, or ii) Petryk's superposition method, based on Reichardt's theory of turbulence, which superimposes the velocity defects of upstream wakes. For relatively close in-line cylinder spacing, or five to ten diameters, the model is more accurate with Yano's wake superposition method. However, when the cylinders are spaced farther apart or when the cylinders are placed on one side of the channel only, then Petryk's method appears to be more accurate.

2. The drag of an individual cylinder, in close proximity to a neighboring cylinder, may be 300% higher than the drag force on a single cylinder placed in open channel flow.

3. The total drag force on two neighboring cylinders may be 150% higher than two times the drag force on a single cylinder in an open channel.

4. The mean drag coefficients are increased with increasing spacing for parallel patterns but the trend is reversed for staggered patterns and the mean drag coefficient converges to asymptotic values at approximately 200 diameters from the first cylinder for regular cylinder patters.

V. REFERENCES - CHAPTER 2

1. Achenbach, E., 1968, Distribution of local pressure and skin friction around a circular cylinder in crossflow up to $\overline{R} = 5 \times 10^6$, Journal of Fluid Mechanics, Vol. 34, pp. 625-639.

2. Allen, H.J., and W.G. Vincenti, 1944, Wall interference in a two-dimensional flow wind tunnel with consideration of the effect of compressibility, NACA Report 782.

3. Apelt, C.J., and L.T. Isaacs, 1968, Bridge piers-hydrodynamic force coefficients, Journal of the Hydraulics Division, ASCE, Vol. 94, No. HY1, January, pp. 17-30.

4. Baines, W.D., 1965, Effect of velocity distribution on wind loads and flow patterns on buildings, Wind Effects on Buildings and Structures, Vol. 1, Her Majesty's Stationary Office, London, England, pp. 197-224.

5. Bearman, P.W., 1968, The flow around a circular cylinder in the critical Reynold's number regime, NPL-Aero 1257, also see STAR No. N69-13290.

6. Bergelow, O.P., G.A. Brown, H.L. Hull and F.W. Sullivan, 1950, Trans. ASME 72, 881.

7. Bierman D., and W.H. Herrnstein, Jr., 1933, Interference between struts in various combinations, NACA Report No. 468.

8. Chen, Y.N., 1968, Flow-induced vibration and noise in tube bank heat exchanges due to Von Karman vortex streets, Journal of Engineering for Industry, ASME, Vol. 90, Series B, No. 1, February, pp. 134-146.

9. Chilton, T.H., and R.P. Genereaus, 1933, Trans. AICLE 29, 161.

10. Colman, E.A., 1953, Vegetation and watershed management, Ronald Press

11. Dalton, C., and F.D. Masch, 1968, Influence of secondary flow on drag forces, Journal of Engineering Mechanics Division, ASCE, Vol. 94, No. EM5, Proc. Paper 6193, October.

12. Eskinazi, S., 1959, Mixing of wakes in a turbulent shear flow, NASA TN-D-83.

13. Gran Olsson, R., 1936, Geschurndigkeits - and Temperaturver - teilung hinter einum Gitter bei turbulenter Strümung. S. für Angew Math. Mech 16, pp. 257-274.

14. Grimson, E.D., 1937, Trans. ASME 59, 583.

15. Gunter, A.Y., and W.A. Shaw, 1945, Trans. ASME 67, p. 643.

16. Hays, A.D., 1947, Flow around semi-submerged cylinders of finite length, Princeton School of Engineering, Princeton, New Jersey.

17. Hill, P.G., U.W. Schaub and Y. Senoo, 1963, Turbulent wakes in pressure gradients, Journal of Applied Mechanics, Vol. 30, pp. 518-524.

18. Hoerner, S.F., 1958, Fluid dynamic drag, published by author.

19. Hsieh, T., 1964, Resistance of cylinder piers in open-channel flow, Journal of the Hydraulics Division, ASCE, Vol. 90, pp. 161-173.

20. Isaacs, L.T., 1965, Hydrodynamic forces on surface piercing circular cylinders and flat plates, Thesis presented to University of Queensland at St. Lucia, Brisbane, Australia, in partial fulfillment of the requirements for the degree of Master of Science in Engineering.

21. Jakob, M., 1938, Trans. ASME 60, 381.

22. Kays, W.M., A.L. London and R.K. Lo, 1954, Trans. ASME 76, 387.

23. Knudsen, J.G., and D.L. Katz, 1958, Fluid dynamics and heat transfer, McGraw-Hill Co.

24. Laird, A.D.K., C.S. Johnson and R.W. Walders, 1959, Water forces on accelerated cylinders, Journal of Waterways and Harbors Division, ASCE, Vol. 85, March, pp. 99-119.

25. Masch, F.D., and W.L. Moore, 1963, Drag forces in velocity gradient flow, ASCE, Vol. 128, Part 1, pp. 48-64.

26. Mattingly, G.E., 1962, An experimental study of the three-dimensionality of the flow around a circular cylinder, Institute of Fluid Dynamics and Applied Mathematics, University of Maryland, Tech. Note BN-295.

27. Molchanov, A.A., 1963, The hydrological role of forest, Israel program for Scientific Translations, Jeruseleum.

28. Petryk, S., 1969, Drag on cylinders in open channel flow, Dissertation presented at Colorado State University, Fort Collins, Colorado, in partial fulfillment of the requirements for the degree of Doctor of Philosophy.

29. Petryk, S., 1969, Discussion of Dalton and Masch's paper, Journal of Engineering Mechanics Division, ASCE, Vol. 95, No. EM5, October, pp. 1288-1289.

30. Petryk, S., and H.W. Shen, 1971, Direct measurement of shear stress in a flume, Journal of the Hydraulics Division, ASCE, Vol. 97, HY6, Tech. Notes, June.

31. Posey, C.J., 1949, Why bridges fail in floods, Civil Engineering, Vol. 19, February, pp. 42-90.

32. Reichardt, H., 1943, New theory of free turbulence, Royal Aeronautical Society Journal, Vol. 47, pp. 167-176.

33. Roper, A.T., 1965, Wake region of a circular cylinder in a turbulent boundary layer, Thesis presented at Colorado State University, Fort Collins, Colorado in partial fulfillment of the requirements for the degree of Master of Science.

34. Roper, A.T., 1967, A cylinder in a turbulent shear layer, Dissertation presented at Colorado State University, Fort Collins, Colorado, in partial fulfillment of the requirements for the degree of Doctor of Philosophy.

35. Roper, A.T., Schneider, V.R., and Shen, H.W., 1967, Analytical approach to local scour, Pre-Congress Vol. 3, Proceedings Paper No. C18, June, for XII Congress of International Association for Hydraulic Research, Fort Collins, Colorado, September.

36. Roshko, A., 1961, Experiments on the flow past a circular cylinder at a very high Reynolds number, Journal of Fluid Mechanics, Vol. 10, pp. 345-356.

37. Roshko, A., 1954, A new hodograph for free-streamline theory, NACA TN31608, July.

38. Schlichting, H., 1960, Boundary layer theory, McGraw-Hill Co., 4th Edition, pp. 590-604.

39. Schlichting, H., 1968, Boundary layer theory, McGraw-Hill Co., 6th Edition.

40. Schwind, Richard G., 1962, The three-dimensional boundary layer near a strut, Gas Turbine Laboratory Report No. 67, Massachusetts Institute of Technology, May.

41. Sevik, M., 1966, Effect of turbulence on vortex shedding from circular cylinders, Meeting on Ground Wind Load Problems in Relation to Launch Vehicles, NASA Langley Research Center, June, pp. 22.1-22.19.

42. Shen, H.W., V.R. Schneider and S. Karaki, 1969, Local scour around bridge piers, Journal of the Hydraulics Division, ASCE, Vol. 95, No. HY6, November.

43. Townsend, A.A., 1956, Structure of turbulent shear flow, Cambridge University Press, London, 315 pp.

44. Tracy, H.J., and C.M. Lester, 1961, Resistance coefficients and velocity distribution in a smooth rectangular channel, U.S. Geological Survey Water Supply Paper 1592-A.

45. Wallis, R.P., 1939, Photographic study of fluid flow between banks of tubes, Engineering 148, October 13, pp. 423-425.

46. Yano, M., 1966, Turbulent diffusion in a simulated vegetative cover, Dissertation presented at Colorado State University, Fort Collins, Colorado, in partial fulfillment of the requirements for the degree of Docotor of Philosophy.

VI. LIST OF SYMBOLS - CHAPTER 2

Symbol	Definition
A'	Wetted area on the channel walls
b	A dimension expressing wake width
$b_{1/2}$	One-half of wake width at half depth of the velocity defect
C_1, C_2	Constants
C_d	Local coefficient of drag based on U_{oi}
$\bar{C}_d$	Mean coefficient of drag
C_{di}	Measured mean drag coefficient based on the measured drag force
d	Diameter of cylinder
D	Depth of flow
f	Friction factor
F_d	Froude number based on cylinder size
F_D	Froude number based on depth of flow
F_i	Drag force on ith cylinder
F_{sc}	Measured drag force on a single cylinder in the flume
g	Gravitational constant
P_r	Perimeter of channel flow area
Q	Total discharge
R	Hydraulic radius
R_c	Channel Reynolds number
$\bar{R}$	Cylinder Reynolds number based on U_o
S_o	Energy slope due to friction losses on the channel walls
u_1	Defect velocity in a wake
$\overline{u'^2}$	Turbulent intensity of fluid
u_{max}	Maximum defect velocity at the center of the wake, averaged over the depth of flow

Symbol	Definition
u_{total}	Total velocity defect due to upstream cylinders, averaged over depth of flow
$\bar{U}$	Average velocity of flow averaged over the depth of flow
U_o	Mean velocity of flow based on the channel flow area
U_{oi}	The average approach velocity to the ith cylinder
U_∞	Reference free stream velocity from which the velocity defects are subtracted to obtain the actual velocity
W	Width of flume
x	Longitudinal direction respective to flow
y	Vertical direction respective to the channel bottom
z	Transverse direction respective to flow
Δ	Inside distance between cylinders
γ	Specific weight of fluid
ϕ	The angle defined in the conventional polar coordinate system
ρ	Density of fluid
ν	Kinematic viscosity of water
θ	Angle on the cylinder measured from the forward stagnation point
τ	Shear stress
τ_w	Shear stress on the channel wall at a given point
ℓ	Turbulent mixing length

Appendix 2-A

RESISTANCE OF OPEN CHANNEL FLOW OVER LARGE STAGGERED ROUGHNESS

I. INTRODUCTION

Robinson and Albertson (1952), the U.S. Waterways Experimental Stations (1953), Sayre and Albertson (1961) and Koloseus and Davidian (1966) all made extensive experimental studies into the resistance of open channel flow over large rigid roughness. Unfortunately, until now, no general relationship has been found to determine the variation of the resistance factor for a combination of flow and roughness properties.

II. ANALYSIS

As shown in Fig. A.1, the dimensions of the roughness elements are a , b and c in height above the floor, perpendicular to the flow direction and in the longitudinal flow direction respectively. The lateral spacing between two roughness elements (center to center) is t and the longitudinal spacing between two successive roughness elements (center to center) is ℓ . The only pattern considered in this study is the staggered pattern because it is by far the most commonly used type.

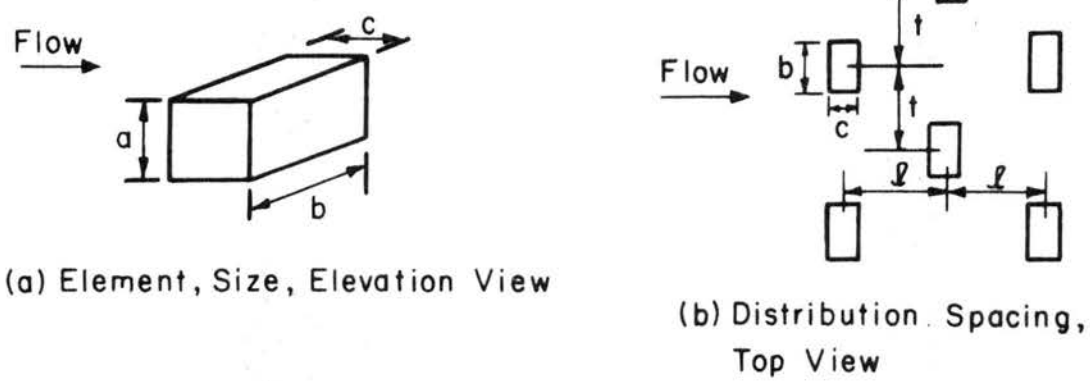

Fig. A.1. Roughness Elements.

For a completely rough boundary with small roughness, the Darcy-Weisbach friction factor, f (as written in terms of V/V_*, where V is the average turbulent flow velocity and V_* is the shear velocity) is a function of the relative roughness y_n/a where y_n is the average flow depth and a is the representative height of the roughness element. Therefore, it is assumed that (note that $V/V_* = \sqrt{8/f}$),

$$\frac{V}{V_*} = \beta_o + \beta_1 \ln \left(\frac{y_n}{a}\right) + \beta_2 \ln \left(\frac{t}{b}\right) + \beta_3 \ln \left(\frac{\ell}{b}\right)$$

$$+ \beta_4 \ln \left(\frac{c}{b}\right) + \beta_5 \ln \left(\frac{a}{b}\right) + \ln \varepsilon \qquad \text{(A.1)}$$

Table A.1 gives a summary of the data used in the multi-variate regression analysis.

The procedure of "all possible regressions" is used to find the most significant regression equation. The highest multiple correlation coefficient within each possible set of combinations of independent variables in a regression equation is summarized in Table A.2.

Table A.2 indicates that the successive addition of the variables c/b and a/b when y_n/a, t/b and ℓ/b are already in the regression equation will remove very little of the unexplained variance. This is clearly shown by the very slight increase in R from set 3 to sets 4 and 5. The criterion for deciding the significant terms in the regression equation can be obtained by successive partial F-test as follows:

i) Partial F-test to test the significance of adding a/b into the equation already with y_n/a, t/b, ℓ/b and c/b (β_o, β_1, β_2, β_3, β_4, and β_5 refer to y_n/a, t/b, ℓ/b, c/b and a/b respectively)

Table A.1. Summary of Roughness Geometry of Data Used in Analysis.

Investigators	Roughness Size (inches)			Spacings (inches)		Roughness Concentration
	a	b	c	ℓ	t	$\lambda = ab/t\ell$
Robinson & Albertson (1952)	1/2	2	1/2	5.5	1.5	0.121
	1	4	1	11	3	0.121
Sayre & Albertson (1961)	1.5	6	0.05	3.05	11.85	0.249
	1.5	6	0.05	9.05	11.85	0.084
	1.5	6	0.05	27.05	11.85	0.028
	1.5	6	0.05	3.05	23.7	0.125
	1.5	6	0.05	9.05	23.7	0.042
	1.5	6	0.05	27.05	23.7	0.014
Koloseus & Davidian (1966)	3/16	3/16	3/16	3	3	0.004
	3/16	3/16	3/16	1.5	1.5	0.016
	3/16	3/16	3/16	3/4	3/4	0.063
	3/16	3/16	3/16	3/4	3/4	0.063
	3/16	3/16	3/16	3/8	3/8	0.250
Waterways Experimental Station, U.S. Army Corps of Engineers (1953)	3/4	3/4	3/4	2	4	0.070
	3/4	3/4	3/4	1.5	3	0.125
	3/4	3/4	3/4	1	2	0.281
	3/4	3/4	3/4	2	1	0.281
	1/2	1/2	1/2	1.25	2.5	0.080
	3/8	3/8	3/8	6	12	0.002
	3/8	3/8	3/8	1	2	0.070
	3/8	3/8	3/8	2	1	0.070
	3/8	3/8	3/8	2	2	0.035
	3/4	3/8	3/8	6	12	0.004
	3/4	3/8	3/8	1	2	0.141
	3/4	3/8	3/8	0.5	1	0.563

Notes: 1) Total percent of floor area occupied by roughness 0.002-0.563
2) t/b between 0.75 to 32 , ℓ/c between 1.3 to 541 , a/b between 0.008 to 1
3) y_n/a between 1.4 to 51.5

$$F = \frac{\text{MS due to } \hat{\beta}_5 | \hat{\beta}_o , \hat{\beta}_1 , \hat{\beta}_2 , \hat{\beta}_3 , \hat{\beta}_4}{\text{MS Residual}} = 2.403$$

$$< F(1,322,0.95)$$

Therefore the addition of a/b is not worthwhile for test size $\alpha = 0.05$.

Table A.2. Examination of "All Possible Regressions."

	Set	Variables in Equation with Highest Multiple Correlation Coefficient Within Each Set	Multiple Correlation Coefficient
A:	One independent variable	$V/V_* =$ function (y_n/a)	0.532
B:	Two independent variables	$V/V_* =$ function $(y_n/a$, $t/b)$	0.940
C:	Three independent variables	$V/V_* =$ function $(y_n/a$, t/b , $\ell/b)$	0.946
D:	Four independent variables	$V/V_* =$ function $(y_n/a$, t/b , ℓ/b , $c/b)$	0.946
E:	Five independent variables	$V/V_* =$ function $(y_n/a$, t/b , ℓ/b , c/b , $a/b)$	0.946

ii) Similarly for c/b

$$F = \frac{\text{MS due to } \hat{\beta}_4 | \hat{\beta}_o , \hat{\beta}_1 , \hat{\beta}_2 , \hat{\beta}_3}{\text{MS Residual}} = 4.512$$

$$< F(1,323,0.975)$$

Thus, the addition of c/b is again not worthwhile for test size 0.025.

iii) Similarly for ℓ/b

$$F = \frac{\text{MS due to } \hat{\beta}_3 | \hat{\beta}_o , \hat{\beta}_1 , \hat{\beta}_2}{\text{MS Residual}} = 74.083$$

$$> F(1,324,0.975)$$

Therefore the addition of ℓ/b is worthwhile for test size $\bar{\alpha} = 0.025$.

The regression result of the multiple regression model of Eq. (A.1) is (multiple correlation coefficient 0.945, standard error of estimate 1.269)

$$\frac{V}{V_*} = -0.0229 + 2.917 \ln \left(\frac{y_n}{a}\right) + 1.871 \ln \left(\frac{t}{b}\right) + 1.229 \ln \left(\frac{\ell}{b}\right) \qquad (A.2)$$

Let Ω denote a dimensionless parameter to describe roughness geometry

and let $\textcircled{H} = y_n/a$, the relative roughness height. Then, Eq. (A.2) can be expressed as

$$\sqrt{\frac{8}{f}} = \frac{V}{V_*} = 2.917 \ln \left(\frac{\textcircled{H}}{\Omega}\right) \tag{A.3}$$

Compare Eqs. (A.2) and (A.3) and one can obtain the roughness geometry descriptor Ω as

$$\Omega = 1.008 \left(\frac{t}{b}\right)^{-0.641} \left(\frac{\ell}{b}\right)^{-0.421} \tag{A.4}$$

All data are plotted in Fig. A.2 with V/V_* vs $\textcircled{H}/\Omega$. One must remember that in a regression curve such as that presented by Eq. (A.3) is, at best, applicable only to the flow and roughness conditions within the range of experimental data of which it is derived.

III. DISCUSSIONS

A.

Chezy resistance coefficient is defined as

$$C = \sqrt{\frac{8g}{f}}$$

where g is the gravitational acceleration and from Eq. (A.3)

$$C = 2.917 \sqrt{g} \ln \left(\frac{\textcircled{H}}{\Omega}\right) \quad . \tag{A.4}$$

B.

From the regression analysis, y_n/a, t/b and ℓ/b appear to exert strong influence on the development of the friction factor. The roughness dimension c has an insignificant effect for $\ell/c > 1.3$ (in that case $t/b = 2.67$). Conceivably, when ℓ/c and t/b reach some lower limits then below these limits the friction factor will decrease with a further decrease in c and b. Ultimately, when $c = \frac{1}{2}\ell$ and $t = b$ the boundary becomes smooth.

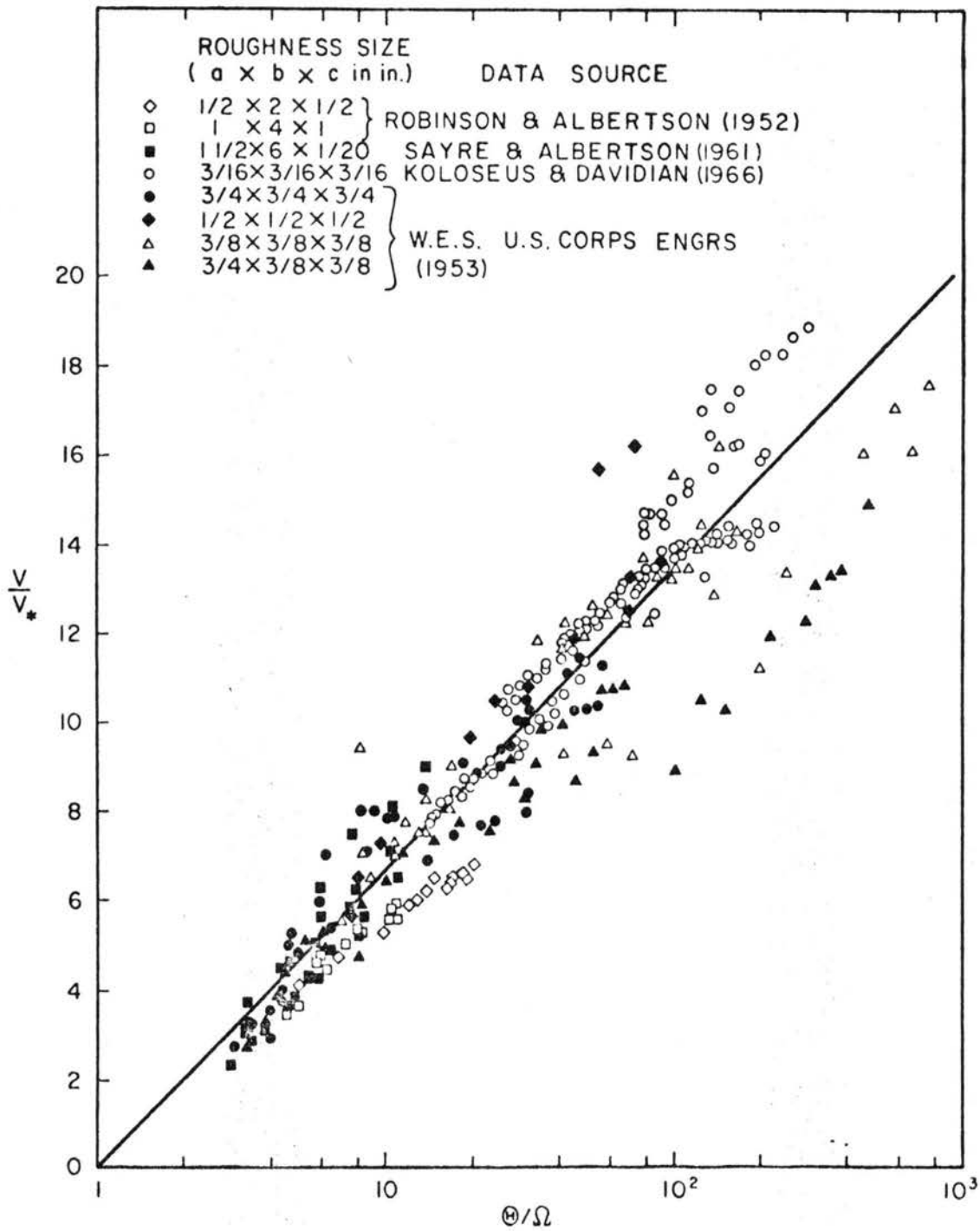

Fig. A-2. $\frac{v}{v_*}$ vs $\frac{\Theta}{\Omega}$ For Rigid Roughness Elements

C.

It is hoped that Eqs. (A.2), (A.3) and (A.4) can be applied to flexible roughness such as vegetation. The only reliable data (known to us) is by Kouwens (1970) and these data points are plotted on Fig. A.3. For flexible roughness, $\textcircled{H}$ is taken to be y_n/h and Ω is defined by Eq. (A.4) (h is the roughness height after bending). Data points indicate that for $h/a < 0.5$, the flow resistance seems to be lower than the corresponding rigid resistance value for the same flow condition. This is reasonable because the concentration of the bending roughness elements should decrease the friction, i.e., ultimately, when the density of the roughness element increases to equal the floor area, the boundary could become smooth, as discussed previously. For $h/a > 0.5$, the flow resistance is higher than the corresponding rigid resistance value for the same flow condition. This may be due to the vibration of flexible roughness. An estimation of correction factors incorporated into Eq. (A.3) with the form $V/V_* = 2.917\ \ell n(\textcircled{H}/\alpha\Omega)$ are determined as shown in Fig. A.3. More data on the development of the friction factor for flexible roughness is needed for further analysis.

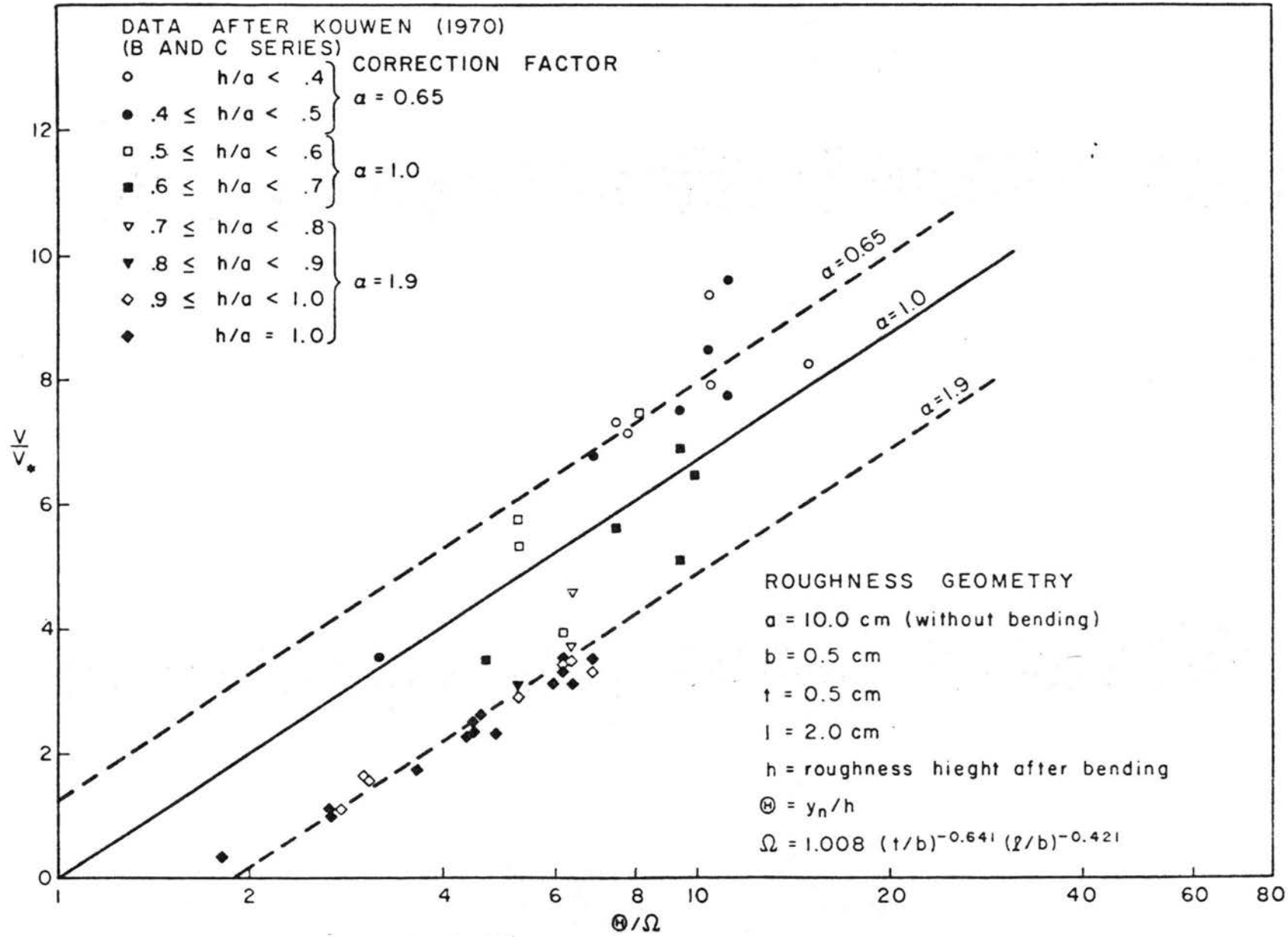

Fig. A-3. $\frac{v}{v_*}$ vs $\frac{\Theta}{\Omega}$ For Artificial Flexible Roughness Elements

III. REFERENCES - APPENDIX 2-A

1. Koloseus, H.J., and J. Davidian, 1966, Free surface instability corrections and Roughness-concentration effects on flow over hydrodynamically rough surfaces, Laboratory studies in open channel flows, U.S. Geological Survey Water-Supply Paper 1592-C,D, U.S. Government printing office, Washington, D.C.

2. Kouwen, N., 1970, Flow retardance in vegetated open channels, Thesis presented to the Faculty of Graduate Studies of the University of Waterloo in partial fulfillment of the requirements for the degree of Doctor of Philosophy in Civil Engineering.

3. Robinson, A.R., and M.L. Albertson, 1952, Artificial roughness standard for open channels, Trans., American Geophysical Union, Vol. 33, No. 6, December, pp. 881-888.

4. Sayre, W.W., and M.L. Albertson, 1961, Roughness spacing in rigid open channels, Journal of the Hydraulics Division, ASCE, Vol. 87, No. HY3, May, pp. 121-150.

5. Waterways Experiment Station, 1953, Roughness standards for hydralic models report No. 4 study of finite boundary roughness in rectangular flumes, U.S. Army Corps of Engineers, Vicksburg, Mississippi, Tech. Memorandum No. 2-364.

IV. LIST OF SYMBOLS - APPENDIX 2-A

Symbol	Definition
a	Height of roughness element above the floor
b	Width of roughness element perpendicular to the flow direction
c	Thickness of roughness element longitudinal to the flow direction
C	Chezy resistance
f	Darcy-Weisbach friction factor
g	Gravitational acceleration
h	Roughness height after bending
ℓ	Longitudinal spacing between two successive roughness elements
t	Lateral spacing between two roughness elements
V	The average turbulent flow velocity
V_*	Shear velocity
y_n	The average flow depth
α	Correction factor
$\bar{\alpha}$	Test size in hypothesis testing
β_i	Regression coefficient in regression equation
Ω	Roughness geometry descriptor
$\textcircled{H}$	Relative roughness height

Appendix 2-B

VIBRATION OF CYLINDER IN FLUID STREAM

Alternating forces acting on a structure in the presence of a fluid stream, may seldom be considered independent of the vibration of the structure itself, as it should be in the case of forced vibrations. Insteady, a certain interaction between the flow-produced forces and the structure deformation is almost always to be expected.

This interaction (which has been called, according to the cases, aeroelasticity, hydroelasticity or, more generally, fluidelasticity) becomes particularly important when the oscillation of the structure (initiated by some casual perturbation) is the necessary condition for the generation of the exciting forces. In such a case (self-excited vibrations), the alternating force always has the frequency equal to the natural frequency of the structure, as for example in the flutter of wings.

More often, however, the alternating exciting force exists independently of the movement of the structure, but its characteristics are more or less influenced by the movement itself (self-controlled vibrations). One of the best known sources of these latter forces is the periodic alternating shedding of the Bénard-von Kármán eddies into the wake of a body immersed in a stream. These vortices are due to the instability of the shear layers delimiting the wake, and the vortices are shed also in the absence of movement of the body.

Di Silvio (1969) concluded from a study sponsored by this grant that the variation of the wake width as a consequence of the transversal motion is recognized by many writers to be the most important feature of

the self-controlled vibration related to the von Kármán vortex shedding. In his model the wake width appears to be controlled by the position of the edge at the so-called "vortex-origin time."

The results of his approach seem to match better with the experiments than the results of the theory according to which the wake width is merely controlled by the over-all displacement; in particular, his model is able to reproduce a certain narrowing of the wake (that is an increase in the shedding frequency) when the stream velocity is lower than the resonance velocity.

A numerical sounding showed that if the damping ratio is below a certain critical value and the stream velocity is sufficiently high, there are three distinct solutions of the problem. Two of these solutions yield frequencies always very close to the natural frequency of the body and vibrational amplitudes increasing without bound when the velocity increases. (The same result is exhibited by the over-all-displacement-theory, but the critical value of the damping ratio is higher in this case.) The third solution always yields oscillation amplitudes which decrease when velocity increases.

At any rate, the possible existence of almost permanent resonsnce-conditions when the damping ratio is low enough, leads to the conclusion that the self-excited vibrations of flexible structures (such as suspension bridges or ice-coated transmission lines) may perhaps be regarded as a case of self-controlled vibration related to the von Kármán vortex shedding.

I. REFERENCES - APPENDIX 2-B

1. DiSilvio, G., 1969, "Self-Controlled Vibration of Cylinder in Fluid Stream," Proc. paper 6498, Jour. of the Engineering Mechanics Division, ASCE, Vol. 95, EM2, April.

Chapter 3

EFFECT OF SEDIMENT YIELD FROM WATERSHED BY RETARDING FLOW RATE DUE TO TALL VEGETATION

I. INTRODUCTION

The effects of vegetation on sediment yield in watersheds are numerous, for instance, large vegetation - a forest could: i) intercept solar radiation and affect soil temperature, ii) diminish wind speed and decrease evaporation, iii) induce rainfall, and iv) reduce sediment yield. Vegetation is a rather effective method to reduce sediment yield by: i) protecting soil from direct rainfall impact, ii) retarding flow rate, iii) increasing soil resistance, and iv) enhancing infiltration and decreasing surface runoff.

Only the effect of reducing sediment yield from watersheds by retarding flow rates due to tall vegetation is discussed here.

II. REVIEW OF LITERATURE

Numerous studies have been made on the effect of vegetation on sediment yield and erosion from watersheds, and, these studies can, in general, be classified into three categories. The first type is to investigate sediment yields and erosion rates from particular watersheds. These types of studies are particularly useful in determining sediment yields and erosion rates from the particular watersheds, but, it is difficult to transfer the knowledge to other watersheds. The second type is to investigate the effect of some selected variables on sediment yields and and erosion rates by regression analysis either from watersheds or large scale experimental plots. These studies can provide an estimate on the effect of changing each variable on sediment yields and

erosion rates for similar watersheds. The third type is to provide a stochastic model for sediment yields from watersheds. This type may, ultimately, provide the correct answer, however, up to now, difficult to apply to special cases.

The following is a list of some recent publications on the effect of vegetation on sediment yields from watersheds.

A. Studies on Particular Watersheds

1. Branson, F.A., and J.B. Owen, 1970, "Plant Cover, Runoff, and Sediment Yield Relationships on Mancos Shale in Western Colorado," Water Resources Research, Vol. 6, No. 3, June.

2. Brown, H.E., 1970, "Status of Pilot Watershed Studies in Arizona," Proc. Paper 7129, Vol. 96, No. IR1, Jour. of Irrigation and Drainage Division, ASCE, March.

3. Lull, H.W., and K.G. Reinhart, 1965, "Logging and Erosion in Rough Terrain in the East," USDA, ARS Misc. Publication No. 970.

4. Ursic, S.J., 1965, "Sediment Yields from Small Watersheds Under Various Land Uses and Forest Covers," USDA, ARS Misc. Publication No. 970.

5. Fredricksen, R.L., 1965, "Sedimentation After Logging Road Construction in a Small Western Oregon Watershed," USDA, ARS Misc. Publication No. 970.

6. Copeland, O.L., 1965, "Land Use and Ecological Factors in Relation to Sediment Yields," USDA, ARS Misc. Publication No. 970.

7. American Geophysical Union, 1965, "Inventory of Representative and Experimental Watershed Studies Conducted in the United States," June.

8. Striffler, W. David, 1964, "Sediment, Streamflow, and Land Use Relationships in Northern Lower Michigan," U.S. Forest Service Research Paper LS-16, October.

B. General Studies

1. Meyer, L.D., 1971, "Soil Erosion by Water on Upland Areas," Chapter 27 of River Mechanics, edited and published by H.W. Shen, P.O. Box 606, Fort Collins, Colorado.

2. Brown, H.E., E.A. Hansen, and N.E. Champagne, Jr., 1970, "A System for Measuring Total Sediment Yield from Small Watersheds," Water Resources Research, June.

3. ASCE Task Committee on Preparation of Sedimentation Manual, 1970, Chapter IV, "Sediment Sources and Sediment Yields," Proc. Paper 7337, Jour. of the Hydraulics Division, ASCE, Vol. 96, No. HY6, June.

4. Mannering, J.V., L.D. Meyer, and C.B. Johnson, 1968, "Effect of Cropping Intensity on Erosion and Infiltration," Agronomy Journal, Vol. 60, pp. 206-209, March-April.

5. McCully, W.G., and W.J. Bowmer, 1967, "Promoting Establishment of Vegetation for Erosion Control," Texas Transportation Institute, Texas A & M University, July.

6. Wischmeier, W.H., 1966, "Relation of Field-Plot Runoff to Management and Physical Factors," Soil Science Society of America proceedings, Vol. 30, No. 2, March-April.

7. Hansen, E.A., 1966, "Suspended Sediment Concentration as Related to Watershed Variables in Central Arizona," presented to the ASCE Hydraulics Conference, Madison, Wisconsin, August.

8. Wischmeier, W.H., and D.D. Smith, 1965, "Predicting Rainfall-Erosion Losses from Cropland East of the Rocky Mountains," Agriculture Handbook No. 282, USDA, ARS.

9. Yong, R.A., C.K. Mutchler and W.H. Wischmeier, 1964, "Influence of Row Direction and Type of Vegetal Cover on the Slope-Soil Loss Relationship," Trans. Am. Society of Agricultural Engineering, Vol. 7, No. 3, pp. 316-320.

10. Mannering, J.V., L.C. Johnson, L.D. Meyer and B.A. Jones, 1964, "The Erosion-Control Effectiveness of Rotation Meadows," Jour. of Soil and Water Conservation, Vol. 9, No. 3, May-June.

11. Meyer, L.D., and J.V. Mannering, 1963, "Crop Residues as Surface Mulches for Controlling Erosion on Sloping Land Under Intensive Cropping," Trans. of Am. Society of Agricultural Engineering, Vol. 6, No. 4, pp. 322-327.

12. Wischmeier, W.H., 1960, "Cropping-Management Factor Evaluation for a Universal Soil-Loss Equation," Soil Science Society of America proceedings, pp. 322-326, July-August.

13. Ree, W.O., 1949, "Hydraulic Characteristics of Vegetation for Vegetated Waterways," Agricultural Engineering, April.

C. Stochastic Model

1. Woolhiser, D.A., and P. Todorovic, "A Stochastic Model for Sediment Yield for Ephermal Streams," Proc. International Association for Statistics in Physical Science Symposium of Hydrology, Tucson, Arizona, August 29-September 2, 1971. Also to be published as a USDA Misc. Publication.

III. ANALYSIS

A. Assumptions Made in This Analysis

1. The flows are steady and uniform.

2. The linear superposition of the velocity defect (as suggested by Petryk and described in Chapter 2) is valid.

3. The turbulent velocity distribution for a completely rough boundary is valid to calculate the boundary shear stress on the bed surface.

4. The form resistance is assumed to be entirely due to vegetation and the bed form and grain resistances on the bed surface are negligible.

5. The boundary shear stress is uniformly distributed across the entire bed.

It must be stressed here that the following analysis is mainly for the comparison of the relative effect of sediment yields by various combinations of tall vegetation and it is not to be used for an accurate prediction of sediment yields. Although assumptions 3 and 5 as listed above may not be exactly true in actual cases, they should be reliable enough to give a qualitative comparison for the effect of various patterns of tall vegetation on sediment yields as described below.

B. Calculation Procedure

Referring to Fig. 3.1

$$(W\ell\ D - \frac{1}{4}\ N\ D\ \pi\ d^2)\gamma\ S_o$$

$$= (W\ell - \frac{1}{4}\ N\ \pi\ d^2)\tau_o + \frac{1}{2}\ \rho\ U_o^2\ D\ d\ \Sigma\ \overline{C_{d_i}} \qquad (3.1)$$

where τ_o is the average boundary shear stress on the bed, W is the width of the plot, ℓ is the length of the plot, D is the depth of the flow, N is the total number of vegetations, d is the diameter of the vegetations (assume that the diameters are equal), γ is the specific weight of the water, S_o is the bottom slope of the plot, ρ is the density of the water, U_o is the average velocity based on the flow area and $\Sigma \overline{C_{d_i}}$ is the sum of the mean drag coefficient.

According to assumption 3

$$\sqrt{\frac{8}{f}} = \frac{U_o}{\sqrt{\frac{\tau_o}{\rho}}} = 2.5 \ln \left(\frac{D}{d_{65}}\right) + 6.0 \qquad (3.2)$$

where d_{65} is the size of the sediment on the bed of which 65% is finer, and f is the Darcy-Weisbach friction coefficient.

Combining Eqs. (3.1) and (3.2), one obtains

$$\left(W\ell D - \frac{1}{4} N D \pi d^2\right)\gamma S_o = \left(W\ell - \frac{1}{4} N \pi d^2\right) \frac{\rho \left(\frac{Q}{WD}\right)^2}{\left[2.5 \ln \left(\frac{D}{d_{65}}\right) + 6.0\right]^2} + \frac{1}{2} \rho \left(\frac{Q}{WD}\right)^2 D d \Sigma \overline{C_{d_i}} \quad . \qquad (3.3)$$

The solution to the above equation is obtained by trial-and-error with an assumed value of the flow depth D. $\Sigma \overline{C_{d_i}}$ is obtained from Petryk's method as given in Chapter 2.

One can use one of the many currently available sediment transport equations to estimate the effect of various vegetation patterns on sediment yield with bed shear stress as calculated from Eq. (3.2) for the value of D as calculated from Eq. (3.3).

C. Examples

The following examples have been worked out to investigate the effect of various vegetation patterns on sediment yield for given flow conditions.

Example-I (with the restriction of certain basic groupings)

As shown in Fig. 3.1, group A consists of basically parallel patterns and group B consists of basically staggered patterns.

The following table (Table 3.1) gives the computation results of the various patterns consisted of the same basic groups.

Table 3.1. Summary of Computation Results

A. Vegetation distributed in parallel pattern and square basic group

Diameter of vegetation: $d = 0.5$ ft

Width of plot: $W = 40.0$ ft

Length of plot: $\ell = 40.0$ ft

Bottom slope of plot: $S_o = 0.002$

Median grain size: $d_{65} = 0.003$ ft

Water discharge: $Q = 208$ cfs

Critical tractive force: $\tau_c = 0.0185$ lb/ft^2 $(\tau_c = 0.06\ (\gamma_s - \gamma)\ d_{65})$

Sediment discharge $Q_s = \dfrac{10(\tau_o - \tau_c) Q\ S_o\ \gamma}{(\gamma_s - \gamma) d_{65}}$

Case	Number of Vegetations N	Flow Depth (ft) D	Average Velocity Based on Flow Area (ft/sec) U_o	Average Boundary Shear Stress (lb/ft^2) τ_o	Sediment Transport Rate (lb/sec) Q_s	Relative Sediment Transport Rate Q_s/Q_{sm}
A-I	64	2.11	2.468	0.0235	4.225	0.047
A-II	0	1.00	5.208	0.1248	89.447	1.000
A-III	32	1.64	3.176	0.0413	19.144	0.214
A-IV	32	1.70	3.064	0.0381	16.469	0.184
A-V	32	1.54	3.382	0.0475	24.378	0.273
A-VI	32	1.71	3.046	0.0376	16.053	0.179
A-VII	32	1.63	3.195	0.0418	19.621	0.219
A-VIII	32	1.69	3.082	0.0386	16.894	0.189

NOTE: Q_{sm} is the maximum sediment transport rate (when there is no vegetation.)

Table 3.1. Summary of Computation Results (cont)

B. Vegetation distributed in staggered pattern and triangular basic group

Diameter of vegetation: $d = 0.5$ ft

Width of plot: $W = 32.5$ ft

Length of plot: $\ell = 40.0$ ft

Bottom slope of plot: $S_o = 0.002$

Median grain size: $d_{65} = 0.003$ ft

Water discharge: $Q = 169$ cfs

Critical tractive force: $\tau_c = 0.0185$ lb/ft^2 $(\tau_c = 0.06\ (\gamma_s - \gamma)\ d_{65})$

Sediment discharge $Q_s = \dfrac{10(\tau_o - \tau_c) Q\ S_o\ \gamma}{(\gamma_s - \gamma) d_{65}}$

Case	Number of Vegetations N	Flow Depth (ft) D	Average Velocity Based on Flow Area (ft/sec) U_o	Average Boundary Shear Stress (lb/ft^2) τ_o	Sediment Transport Rate (lb/sec) Q_s	Relative Sediment Transport Rate Q_s/Q_{sm}
B-I	48	2.36	2.207	0.0184	0.0	0.0
B-II	0	1.00	5.208	0.1248	72.676	1.000
B-III	24	1.77	2.942	0.0348	11.141	0.153
B-IV	24	1.80	2.893	0.0335	10.265	0.141
B-V	24	1.69	3.082	0.0386	13.726	0.189
B-VI	24	1.81	2.877	0.0331	9.984	0.137
B-VII	24	1.76	2.959	0.0353	11.443	0.157
B-VIII	24	1.80	2.893	0.0335	10.265	0.141

From Table 3.1 it may be concluded that:

i) the various patterns or groupings of tall vegetations have a rather significant effect on the retardation of flow rates;

ii) for the same number of tall vegetations or trees, the staggered grouping (Case VI) is the most effective pattern and Case III is the second best pattern in reducing sediment yields;

iii) the staggered grouping (Case VI) is recommended for planting tall vegetation; and

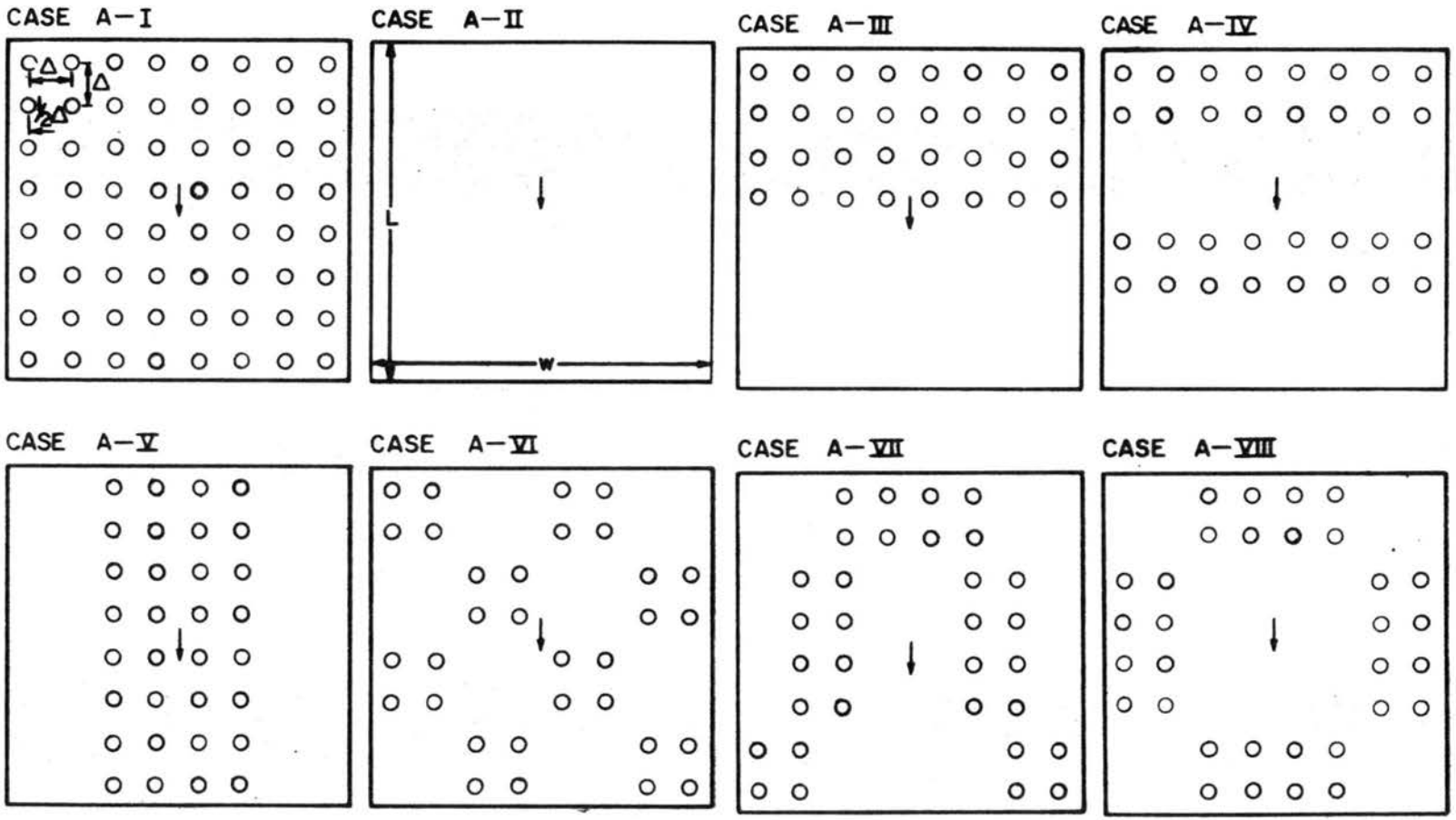

Fig. 3.1. Example-I.

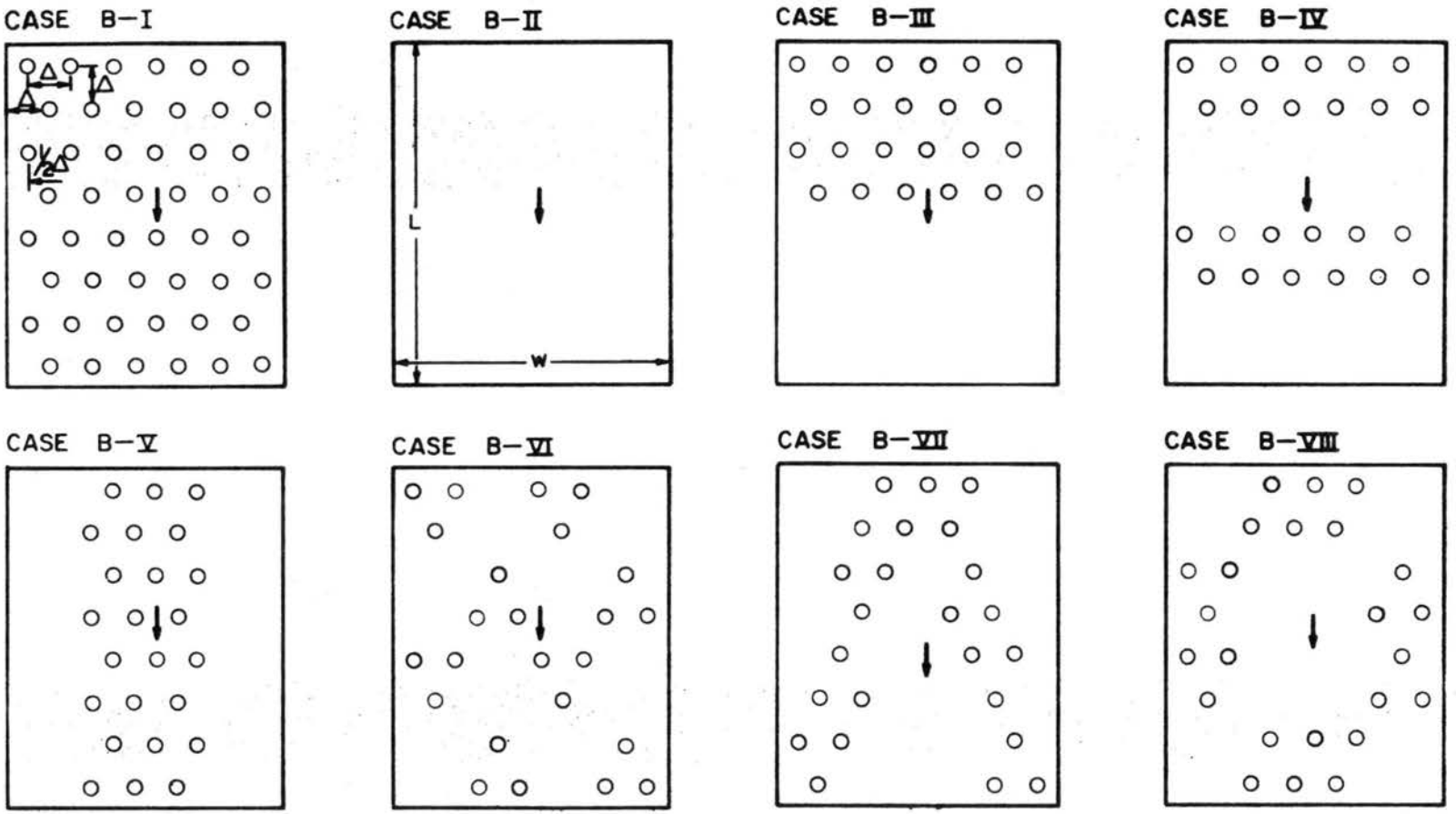

Fig. 3.1. Example-I. (Continued)

iv) the staggered grouping (Case VI) is not economical for the harvest of tall vegetation, in this case, some variation of Case III should perhaps be considered.

2. Example-II (without the restriction of basic grouping)

The most effective patterns for the harvest of 1/4, 1/2, 3/4, 7/8 tall vegetations are given in Fig. 3.2 and their effect in sediment yields are given in the following table (Table 3.2). Flow conditions are the same as Case A-I, Example I (Table 3.1).

Table 3.2. Summary of The Most Effective Pattern For Different Number of Harvesting

Case	Number of Vegetations N	Degree of Harvesting	Flow Depth (ft) D	Average Velocity Based on Flow Area (ft/sec) U_o	Average Boundary Shear Stress (lb/ft^2) τ_o	Sediment Transput Rate (lb/sec) Q_s	Relative Sediment Transput Rate Q_s/Q_{sm}
A-I	64	0	2.11	2.468	0.0235	4.225	0.047
A-IX	68	1/4	1.94	2.685	0.0284	8.298	0.093
A-X	32	1/2	1.75	2.976	0.0357	14.463	0.162
A-XI	16	3/4	1.44	3.617	0.0552	30.842	0.345
A-XII	8	7/8	1.23	4.234	0.0785	50.461	0.564
A-II	0	1	1.00	5.208	0.1248	89.447	1.000

NOTE: Degree of harvesting = $\frac{\text{Number of Vegetation Harvested}}{\text{Total Number of Vegetation Before Harvesting}}$

From this example one may conclude that the degrees of harvesting have a rather significant effect on the retardation of flow. Fig. 3.3 shows the exponential trend of the relationship between relative sediment transport rate and degree of harvesting for the various best effective vegetation grouping as described in Table 3.2. It must be stressed here that the grouping pattern in this example may not be economical. More feasible patterns are already introduced in Example-I.

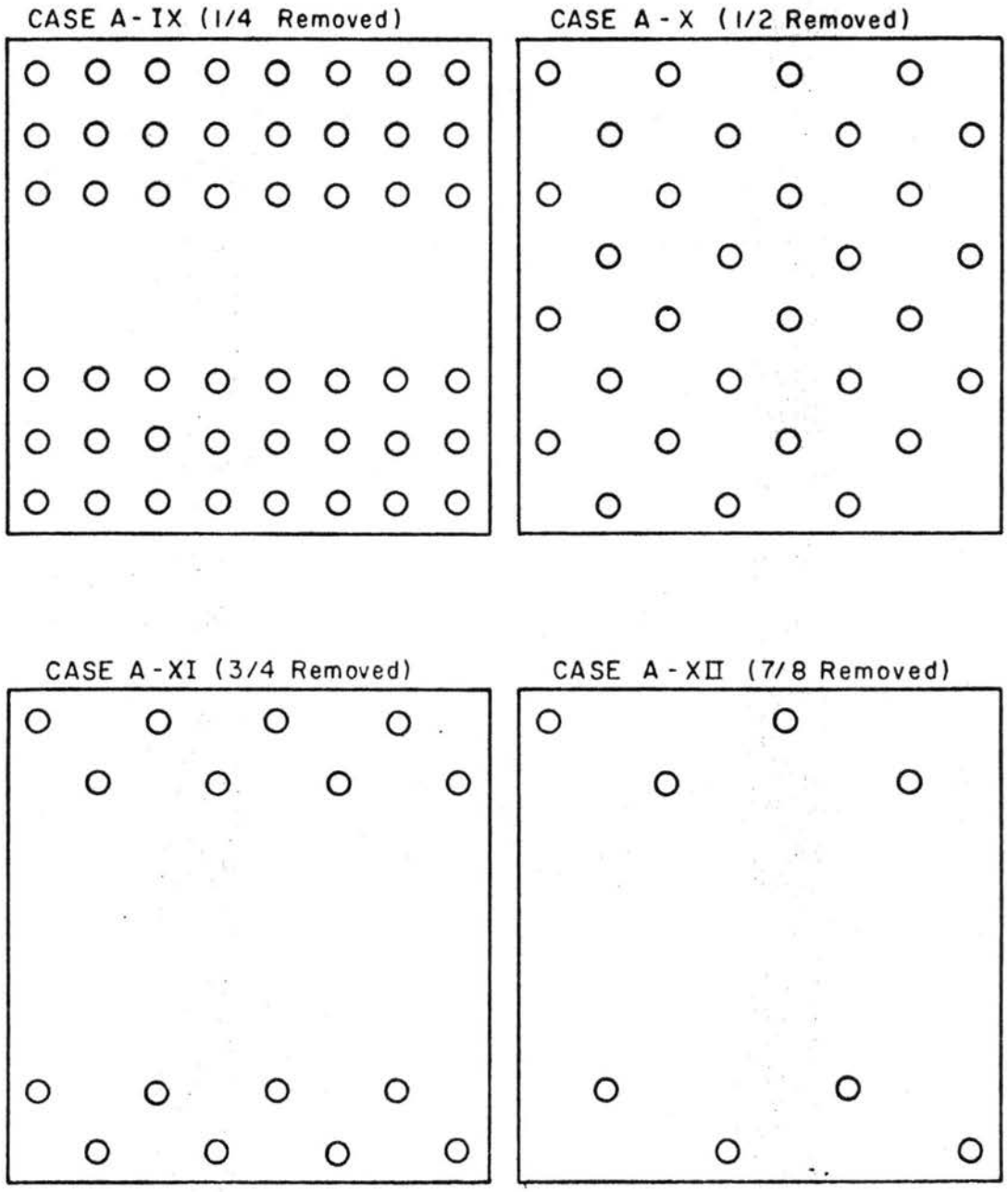

Fig. 3.2. Example - II

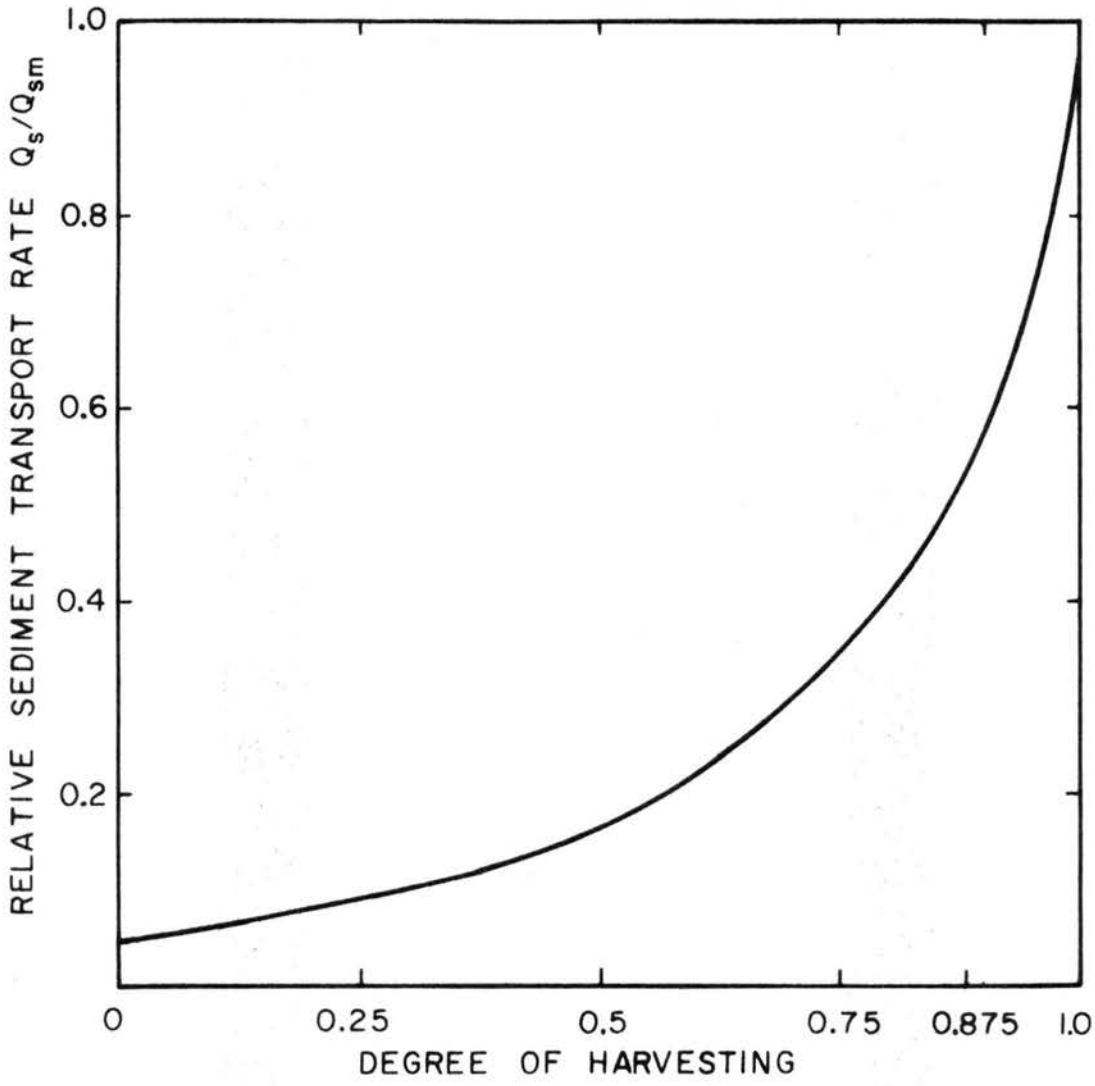

Fig. 3.3. Example of Relationship Between Sediment Yields and Degree of Harvesting for Various Best Effective Pattern Flow Conditions Given in Table 3.2.

3. Example-III. The variations of average boundary shear stress τ_o with i) flow discharge Q, ii) plot bottom slope S_o, iii) size of sediment d_{65}, and iv) diameter of vegetation d).

The vegetation distribution of Case A-XI as shown in Fig. 3.2 is used to examine the variations of τ_o with Q, S_o, d_{65}, and d. The results are shown in Fig. 3.4. From Fig. 3.4 one may draw the following conclusions:

i) the average boundary shear stress is not sensitive to the variation of discharge and sediment size. However, it is much more sensitive to the plot bottom slope and diameter of vegetation

ii) the average boundary shear stress increases with increasing discharge, plot bottom slope and sediment size but decreases with increasing diameter of vegetation (therefore, one may expect that vegetation will have much more effect on sediment yield as trees growing larger).

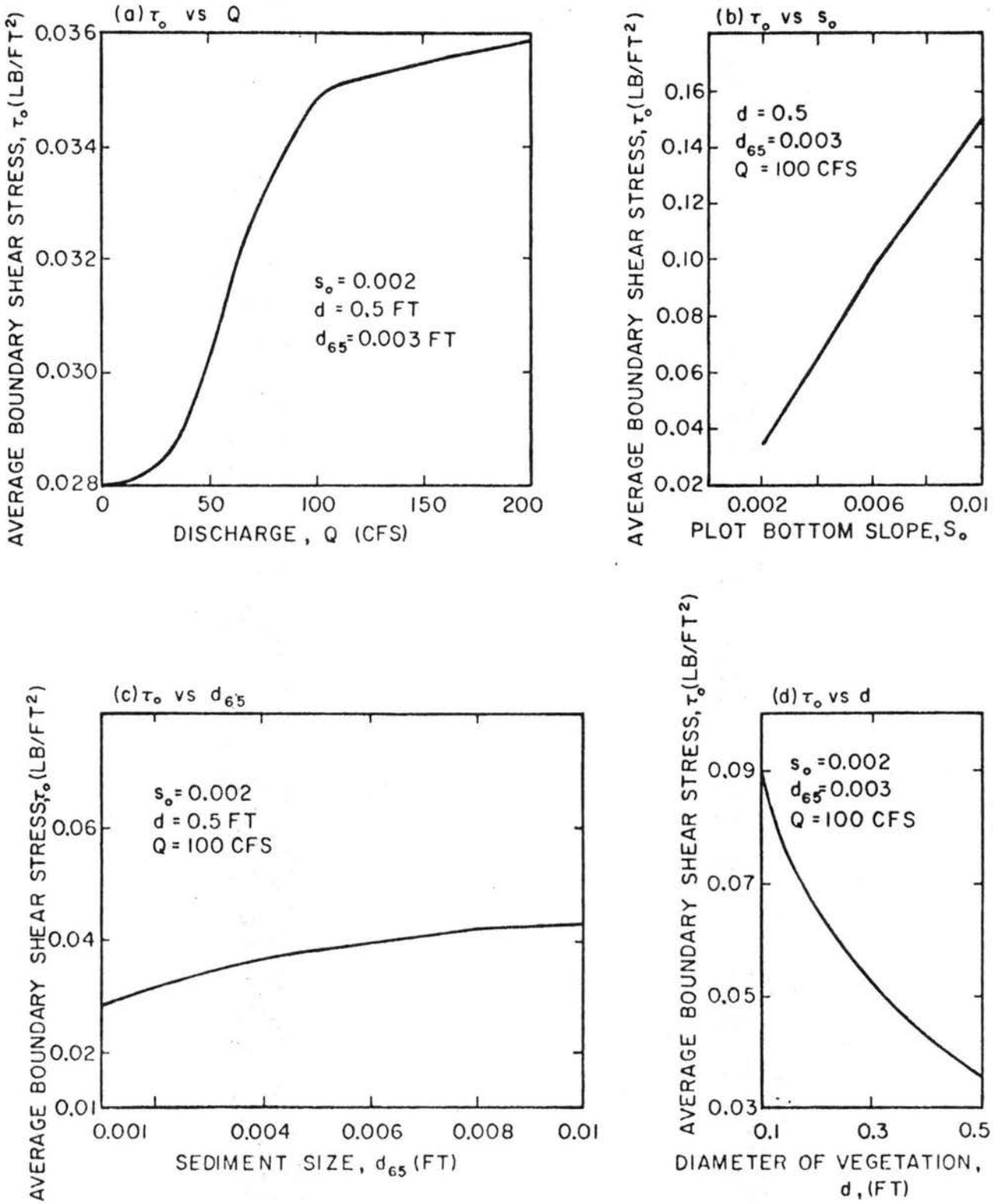

Fig. 3.4. Example of Partial Relationships of τ_o, Q, S_o, d_{65}, and d.

IV. LIST OF SYMBOLS - CHAPTER 3

$\overline{c_{di}}$	mean drag coefficient of wake interference flow
D	depth of flow
d	diameter of vegetation
d_{65}	size of the sediment on the bed of which 65% is finer
f	Darcy-Weisback friction coefficient
ℓ	length of plot
N	total number of vegetation
Q	flow discharge
Q_s	sediment transport rate in weight per unit time
Q_{sm}	maximum sediment transport rate (when there is no vegetation)
S_o	plot bottom slope
U_o	average velocity based on the flow
W	area width of plot
ρ	density of water
γ	specific weight of water
γ_s	specific weight of sediment
τ_c	critical tractive force
τ_o	average boundary shear stress

Chapter 4

EFFECT OF RAINFALL ON SHEET FLOW

I. INTRODUCTION

Steady overland sheet flow with rainfall as a source of lateral inflow is a type of spatially varied, shallow, open channel flow. The steady and unsteady flows of this type are the common flow type which occur in the initial phase of surface runoff in natural watersheds and also in urban drainage. The steady flow is named herein as steady overland sheet flow which is defined as a thin flow over a plane surface caused by constant base flow and constant rainfall in steady-state condition.

With the growing upstream watershed sediment erosion control demands and urban developments there is an apparent need to obtain more information on the mechanics of overland sheet flow. Due to the thin water depth in sheet flow, unlike the conventional open channel flow, the effect of rainfall may play a very important role. Many previous investigators have concluded that rainfall may significantly affect the resistance and other flow characteristics; however, limited work has since been done to quantitatively examine these effects. Indeed, this is a very complicated process and hence no purely theoretical treatment of this problem has been successfully given so far. It is believed that reliable experimental results and simplified assumptions are needed to deal with this problem.

II. REVIEW OF RELATED LITERATURES

The approach to this problem involves the use of the equation of motion, the law of resistance, and the continuity equation. Since it

is impossible to determine the energy dissipation due to rainfall falling on the main flow with current knowledge, the momentum approach appears to be the only feasible method. As shown by Yen and Wenzel (1970), the dynamic equation is

$$\frac{dy}{dx} = \frac{S_o - S_f + \frac{i}{gA}(U \cos \phi - 2 \beta V) - \frac{V^2}{g}\frac{d\beta}{dx}}{\cos \theta - \frac{\beta V^2}{gD}} \qquad (4.1)$$

where x is the distance in the main flow direction, y is the flow depth normal to x, S_o is the channel bottom slope, S_f is the friction slope which is defined as $\tau/\gamma R$, τ is the boundary shear stress, γ is the specific weight of water, $\bar{R}$ is the hydraulic radius which is defined as A/p, A is the channel cross-sectional area, p is the wetted perimeter, i is the lateral inflow rate per unit area, g is the gravitational acceleration, U is the velocity of lateral inflow entering the main flow, ϕ is the angle between the velocity U and the x-direction, β is the momentum coefficient, V is the mean flow velocity, θ is the angle between the x-direction and the horizontal direction, D is the hydraulic depth which is defined as A/T, T is the width of the channel section at the free surface.

A major difficulty in obtaining a solution to Eq. (4.1) is the inability to predict S_f through the law of resistance. The friction factors generally adopted to describe the resistance in open channel flows without rainfall are Darcy-Weisbach's f, Chezy's C and Manning's n. Since Darcy-Weisbach's f value is defined much better than the other two, it has been widely used to investigate the resistance to flow with rainfall. A brief summary of the results of some selected comprehensive studies is given in Table 4.1.

Table 4.1. Summary of Selected Previous Investigations on Darcy-Weisbach Friction Coefficient of Steady Overland Sheet Flow

Investigators	Study Range			Type of Channel Bed	Items Measured	Equations used to Compute f	Presented Related Parameters	Experimental Results
	Reynolds Number N_R	Rainfall Intensity I (in/hr)	Channel Bottom Slope S_o					
Brutsaert (2) (1971)	300 - 2,500	14.3 - 26.8	0.005 - 0.02	Rough (held constant)	Flow Profiles	Eq. 4.2 (with β=1 & ϕ=90°) Eq. 4.4	I , N_R	f increased with increasing I , f varied insignificantly with S_o , f decreased with increasing N_R
Emmett (9) (1970)	5 - 327	3.47 - 11.97	0.0033 - 0.0775	Smooth and Rough	Flow Profiles	Eq. 4.5	N_R, roughness	Rainfall approximately doubled the friction factor but f varied insignificantly with I , f increased with S_o for S_o > 0.055, no systematic changes were observed for smaller slopes. f decreased with increasing N_R f changed with roughness.
Izzard (14) (1944)	40 - 500	1.8 - 3.6	0.001 - 0.04	Rough (held constant)	Flow Profiles	Eq. 4.2 (with β=1 & ϕ=90°) Eq. 4.4	I , S_o , N_R	f increased with increasing I , f increased with increasing S_o , f decreased with increasing N_R
Kisisel, Rao Delleur and Meyer (16) (1971)	66 - 7,000	5.0 - 10.0	0.001 - 0.01	Smooth and Rough	Flow Profiles	Eq. 4.2 (with β=1) Eq. 4.4	I , S_o , N_R	f increased with increasing I , f-values for S_o = 0.001 were considerably less thar those of other slopes but f varied insignificantly for the steeper slopes , f decreased with increasing N_R , f changed with roughness, for higher N_R rainfall effect became insignificant
Woo and Brater (29) (1962)	25 - 192	1.48 - 5.42	0.001 - 0.06	Rough	Flow Profiles		I , S_o , N_R	f increased with increasing I , f decreased with increasing S_o for S_o < 0.008 but varied insignificantly for the steeper slope , f decreased with increasing N_R , f changed with roughness
Yoon (32) (1970) Yoon and Wenzel (33) (1971)	250 - 5,500	0.5 - 18.0	0.001 - 0.03	Smooth	Flow Profiles and Boundary Shear Stresses (τ)	1) Computed f-values Eq. 4.2 (with β=1) Eq. 4.4 2) Measured f-values Eq. 4.6 (used measured τ)	I , S_o , N_R	f increased with increasing I , f increased with increasing S_o , f decreased with increasing N_R , measured f-values gave smoother results, for higher N_R rainfall effect became insignificant
Yu and McNown (34) (1964)	100 - 10,000	0.25 - 10.0	0.005 - 0.02	Rough (held constant)	Flow Profiles	Eq. 4.5	N_R	Rainfall increased f-values but no systematic changes were observed with increasing I , f decreased with increasing N_R

$$Sf = \frac{\tau}{\gamma y} = S_o - \frac{\Delta y}{\Delta x}\left(\cos\theta - \beta\frac{q^2}{qy^3}\right) - \frac{2\beta i q}{qy^2} + \frac{iV}{gy}\cos\phi \qquad (4.2)$$

where q is the flow rate of combined flow per unit channel width and

$$q = q_o + iX \qquad (4.3)$$

where q_o is the base flow rate per unit channel width

$$f = \frac{8gyS_f}{V^2} \qquad (4.4)$$

$$f = \frac{8gyS_o}{V^2} \qquad (4.5)$$

$$f = 8\frac{\tau}{\rho V^2} \qquad (4.6)$$

$$N_R = \frac{Vy}{\nu} \qquad (4.7)$$

where ν is the kinematic viscosity of water.

These studies all indicated that f increased with increasing rainfall intensity and decreased with increasing Reynolds number, but disagreed on the effect of channel bottom slope S_o on f.

In general, all previous investigations indicate that rainfall ratards the flow velocity, deepens the flow depth and increases the turbulent intensity. It also augments the boundary shear stress substantially compared with the case without rainfall. The more comprehensive studies were made by Yoon (1970), Yoon and Wenzel (1971), and Kisisel, et.al. (1971).

A more detailed review of literature is given by Li (1972).

III. PURPOSES OF THE STUDY IN THIS CHAPTER

The examination of previous investigations clearly indicates the necessities of the following research needs (which are also the purposes of this study): i) to establish the variation of friction resistance with different flow conditions by statistical analysis of all available data, ii) to determine the confidence interval and predictability of the friction coefficient with different flow conditions, iii) to estimate the effects of uncertainties in determining the friction coefficient on flow depths and boundary shear stresses, and iv) to provide a simplified procedure to estimate flow depths and boundary shear stresses for straight thin overland flow with rainfall.

Although this study deals with the restricted case of steady flow over smooth boundaries, its results should provide an improved understanding of more complicated cases.

IV. ANALYSIS

A. Basic Equations

As stated in Section II, since it is impossible with the current knowledge to determine the energy dissipation due to rainfall falling on the main flow, the momentum approach appears to be the only feasible method. Under the assumptions that: i) the flow is one-dimensional, i.e., no variation in the transverse direction, ii) hydrostatic pressure distribution is valid across the flow depth, iii) surface tension forces are negligible, iv) the open channel is prismatic, v) the variations of both momentum coefficient (β) and energy coefficient (α) along the x direction are negligible, vi) the channel slope is small so that $\cos\theta \cong 1$ and $\sin\theta \cong \tan\theta = S_o$, and vii) the wind effect and momentum influx of rainfall on the flow are small enough to be neglected, Eq. (4.1) becomes

$$\frac{dy}{dx} = \frac{S_o - S_f - \frac{2\beta V i}{gy}}{1 - \beta \frac{V^2}{gy}} \tag{4.8}$$

where

$$S_f = \tau/\gamma y = f V^2/8gy \quad . \tag{4.9}$$

If Eq. (4.8) is arranged into a finite difference form:

$$\Delta y + \frac{\beta \bar{V} \Delta V}{g} + \frac{\beta \bar{V} i \Delta x}{g\bar{y}} = (S_o - \bar{S}_f) \Delta x \tag{4.10}$$

where

$$\Delta y = y_1 - y_2 \quad , \quad \Delta V = V_1 - V_2 \quad ,$$

$$\bar{y} = \frac{y_1 + y_2}{2} \quad , \quad \bar{V} = \frac{V_1 + V_2}{2} \quad ,$$

$$\bar{S}_f = \frac{S_{f_1} + S_{f_2}}{2} \quad ,$$

and subscripts 1 and 2 indicate the various elements of points 1 and 2 respectively.

B. Boundary Conditions for Different Types of Flow

The thin overland flow may be either laminar or turbulent, or the transition between the two and its flow regime may be either subcritical, critical or supercritical. The flow regime may also change from supercritical to subcritical and vice versa under the influence of rainfall.

There are many possible flow conditions which can occur. Fig. 4.1 shows the seven selected conditions that are investigated here; these are: i) sub-sub, ii) sup-sub, iii) sup-sup, iv) sub-sub-sub, v) sub-sub-sup, vi) sup-sub-sup and vii) sup-sup-sup. The two other possible conditions of i) sub-sup and ii) sub-sup-sup are not studied due to the difficulties in obtaining such flow conditions in a laboratory flume.

There also exist four types of controls which govern the boundary conditions of the seven flow cases as given in Fig. 4.1.

1. Upstream Control (Type 1 Control): In cases iii and vii the flows in the rainfall portion are supercritical, the controls occur at the upstream boundary and the water profile computation should be carried out toward the downstream direction. The flow condition at $x = L$ (See Fig. 4.1) is obtained from the following derived equation with the assumption that a stationary surge occurs at $x = 0$. This is called "Type 1 Control."

$$\frac{(q_o + i\,\Delta x)^2}{gy} - \frac{q_o^2}{gy_o} = y\,(S_o - S_f)\,\Delta x + \frac{y_o^2 - y^2}{2} \quad . \qquad (4.11)$$

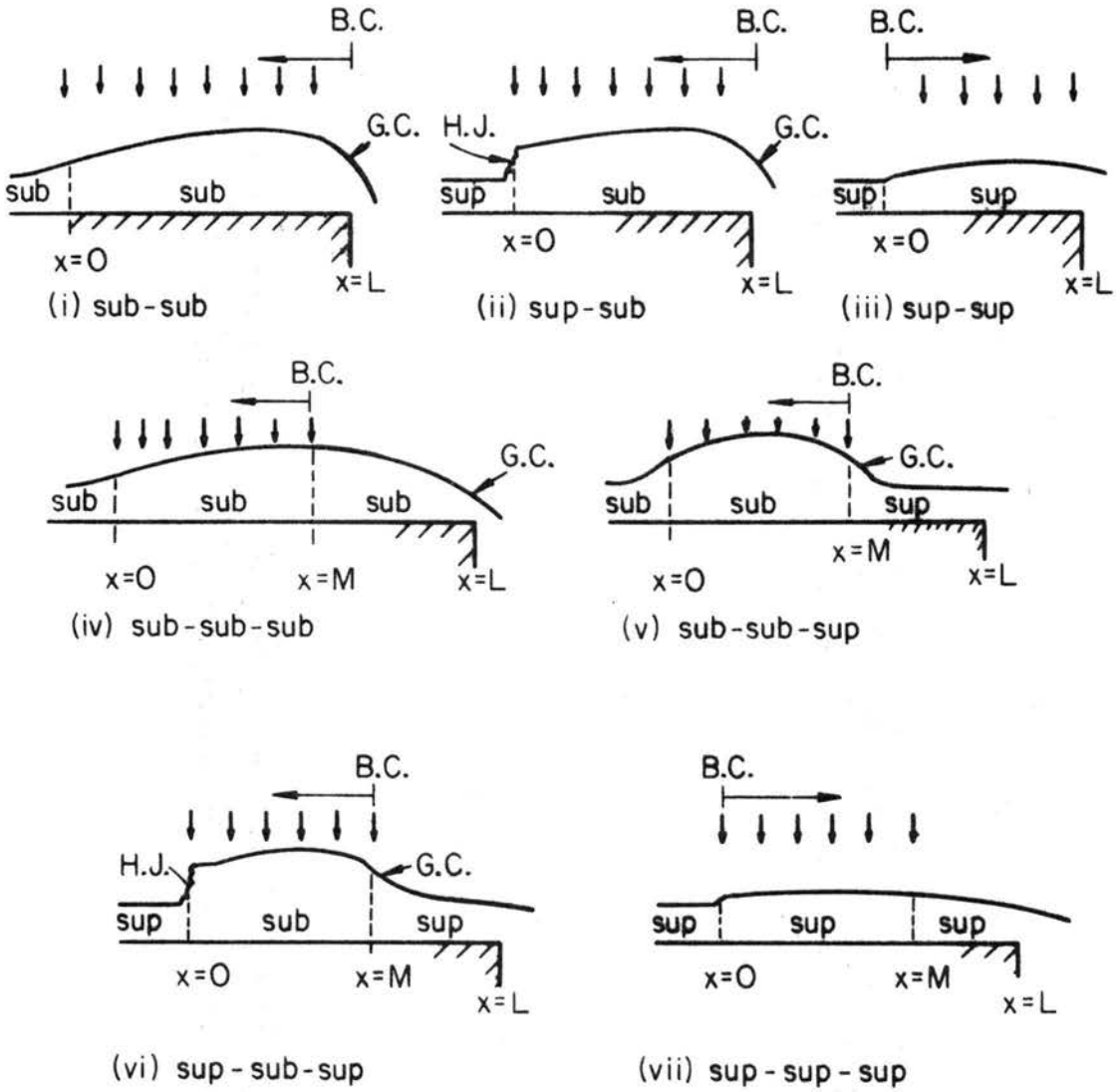

Rainfall Portion as Indicated
All Channel Floors Are Inclined To
The Downstream End

sub = subcritical
sup = supercritical
H.J. = Hydraulic Jump
G.C. = Go Through Critical
B.C. = Boundary Condition

Fig. 4.1 Classification of Flow Regimes

where q_o and y_o are respectively the unit flow discharge and normal flow depth at $x = 0$.

2. Downstream Control (Types 2, 3 and 4 Control): In cases i, ii, iv, v and vi the flows within the rainfall portion are subcritical, the controls occur at downstream ends and the water surface profile computations should be carried out toward the upstream direction. These cases can be further divided into three sub-groups as follows:

a) Type 2 Control: In cases i and ii the critical depths can be assumed to occur at $x = L$ (free overfall) and in cases v and vi the critical depths are assumed to occur at $x = M$. The critical depth is calculated by the following equation that

$$y_c = \left(\frac{q^2}{g}\right)^{1/3} \quad . \tag{4.12}$$

b) Type 3 Control: In cases i and ii the critical depths can also be assumed to occur at $x = L$ over a sharp-crested weir. The equations are then

$$q = \frac{2}{3} C_d \sqrt{2g}\, h^{3/2} \tag{4.13}$$

$$C_d = 0.611 + 0.08\, h/h_o \tag{4.14}$$

$$y = h + h_o \tag{4.15}$$

where h_o is the weir height, h is the head of water above the weir and q is the unit flow discharge.

c) Type 4 Control: In case iv the water surface elevation increases toward the downstream direction in the rainfall portion but decreases gradually downstream from the rainfall portion. Thus, water surface gradient must pass through a zero point at $x = M$.

The flow depth at this boundary point $x = M$ is solved by Eq. (4.8) with $dy/dx = 0$ or

$$S_o - S_f - \frac{2 \beta V i}{gy} = 0 \quad . \tag{4.16}$$

C. Correlation Between Darcy-Weisbach Friction Coefficient and Flow Conditions

Yoon (1970) gives the functional relationship that

$$\tau = \text{function } (V, y, S_o, \bar{\varepsilon}, \nu, I, U, d, \eta, \lambda, g) \tag{4.17}$$

where $\bar{\varepsilon}$ is the boundary roughness, d is the raindrop size, η and λ are parameters describing raindrop pattern, I is the rainfall intensity in length per time, and ν is the kinematic viscosity of the fluid.

The dimensionless parameters are

$$\frac{\tau}{\rho V^2} = \text{function } \left(\frac{Vy}{\nu}, \frac{V}{\sqrt{gy}}, S_o, \frac{Iy}{\nu}, \frac{U}{\sqrt{gy}}, \frac{Id}{\nu}, \frac{\bar{\varepsilon}}{y}, \eta, \lambda\right) \quad . \tag{4.18}$$

Yoon argues further that $\bar{\varepsilon}/y$ can be neglected for smooth boundaries, Iy/ν lacks physical significance. He determined by experimental results that: i) U and raindrop spacing did not affect $\tau/\rho V^2$ if the raindrop size and the I values were kept constant and ii) $\frac{Id}{\nu}$ is proportional to I if the variation of ν is neglected. In addition, the flow Froude number probably can be dropped because it is highly correlated with channel bottom slope S_o. Thus, the relationship as given in Eq. (4.18) becomes

$$f = \frac{8\tau}{\rho V^2} = \text{function } (N_R, S_o, I) \tag{4.19}$$

where f is the Darcy-Weisbach friction coefficient.

D. The Effect of Rainfall on Flow Depth, Mean Velocity and Boundary Shear Stress

In order to describe the effect of rainfall on flow depth, mean flow velocity and boundary shear stress, it would be useful to define some suitable measures which are easy to evaluate and convenient to use.

From the continuity equation of $q = q_o + ix$, one may define (subscript e indicates the element of equivalent flow without rainfall and variables without a subscript indicate elements with rainfall)

$$q = V\,y = V_e\,y_e \tag{4.20}$$

and

$$y_e = \left(\frac{f_e\,q^2}{8\,g\,S_o}\right)^{1/3} \quad . \tag{4.21}$$

These definitions are selected because for the same q, the N_R will be the same for flows with rainfall and without rainfall in a wide channel. It would then be easy to compare the f values (with or without rainfall) with a Moody diagram.

1. The Ratio of Flow Depths With and Without Rainfall:

y/y_e does not give the ratio between the flow depth after the rainfall and the flow depth before the rainfall. y/y_e gives the relative ratio of flow depths for the same unit flow discharge.

With the similar analysis used to obtain Eq. (4.19)

$$\frac{y}{y_e} = \text{function } (N_R,\ S_o,\ I) \quad . \tag{4.22}$$

2. The Ratio of Flow Velocities With and Without Rainfall:

Similar to the ratio of flow depths, V/V_e gives only the ratios of flow velocities with and without rainfall for the same unit flow discharge

$$\frac{V}{V_e} = \frac{y_e}{y} = \text{function } (N_R, S_o, I) \quad . \tag{4.23}$$

3. The Ratio of Boundary Shear Stresses With and Without Rainfall: From Eq. (4.19)

$$\tau = \frac{\rho}{8} f V^2 \quad .$$

Similarly

$$\tau_e = \frac{\rho}{8} f_e V_e^2 \quad , \tag{4.24}$$

$$\frac{\tau}{\tau_e} = \frac{f}{f_e} \left(\frac{V}{V_e}\right)^2 = \frac{f}{f_e} \left(\frac{y_e}{y}\right)^2 \quad . \tag{4.25}$$

4. The Change of Flow Regime:

$$\frac{\text{Froude Number with rainfall}}{\text{Froude Number without rainfall}} = \frac{v/\sqrt{gy}}{ve/\sqrt{gy_e}} = \left(\frac{y_e}{y}\right)^{3/2} \tag{4.26}$$

V. DESCRIPTION OF EXPERIMENTAL DATA

A. Rainfall-Runoff System

A rectangular recirculating flume 1.965 foot wide, 2.5 feet deep and 60 feet long was used. The flume side walls were 0.5 inch thick plexiglass and the bottom was made of 0.25 inch thick stainless steel plate. Two separate recirculating systems were used for rainfall flow and base flow. The rainfall was simulated through a series of 15 rainfall modules similar to those developed by Chow and Harbaugh (1965). These modules, suspended eight feet above the flume bottom and covering 30 feet of flume length, produced an average equivalent raindrop diameter of 3.2 mm. Figures 4.2 and 4.3 show the flume and the water surface respectively under the impacts of raindrops.

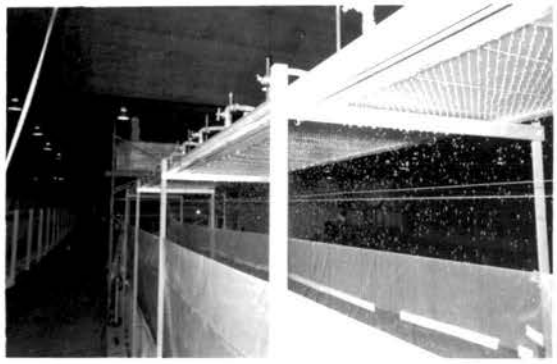

Fig. 4.2. Top View of Experimental Condition

Fig. 4.3. Raindrop impacts on water surface

B. Discharge Measurement

A volumetric tank two feet by 4.5 feet by three feet was connected to the downstream end of the flume for flow discharge measurement.

C. Flow Depth Measurement

A piezometric tap coupled with a PACE pressure transducer (model KP-15), a PACE transducer indicator (model CD25), a Hewlett-Packard digital voltmeter (model 3440A) and a Hewlett-Packard digital recorder (model H75-562A) were used for the flow depth measurement. It is believed that the accuracy of depth measurement is within ± 0.01 inch.

D. Boundary Shear Stress Measurement

The boundary shear stress was measured by a TSI flat surface hot film sensor (model 1237-W) coupled with a DISA constant temperature anemometer (model 55A01), a H-P digital voltmeter (model 3440A), a H-P digital recorder (model H75-562A) and a Moseley autograph (model 680).

The calibration was conducted in flows without rainfall at a six inch diameter and 60 feet long horizontal pipe and also at the flume where experiments were subsequently performed. Results indicated that different constants must be used for boundary shear stress measurements in laminar and turbulent flows. However, there is calibration from pipe flow which agreed very well with that from flume flow. For a detailed description of the calibration the reader is referred to Li (1972). It is important to investigate the following: how much does the raindrop impact affect the reading of flow depth measurement and boundary shear stress measurement in a thin flow with rainfall from the measuring techniques as described above. From a statistical analysis of data (with and without the direct impact of raindrops on the measured points for a rainfall intensity of 17.5 inches per hour) with mean flow depth

0.0157 feet, channel bottom slope 0.0108 and unit flow discharge 0.00715 cfs/ft, it was determined that with 95% confidence level the raindrop impacts do not affect the flow depth and boundary shear measurement readings for the flow condition tested. Four other flow conditions were also investigated for the affect of raindrops on flow measurements and similar results were obtained. In subsequent experiments, the rainfall intensity was kept below or equal to 17.5 inches per hour and most of the flow depths were above 0.0157 feet. However, in the few runs where the rainfall was close to 17.5 inches per hour and the flow depths below 0.0157 feet, the raindrop impacts might have affected the flow depth and boundary shear stress measurements.

Data collected in this study are given by Li (1972).

VI. ANALYSIS OF EXPERIMENTAL DATA AND DISCUSSIONS

A. Variation of Friction Coefficient

Yoon's (1970) data and our data are plotted on Figs. 4.4 and 4.5 respectively. The values of Darcy-Weisbach f were evaluated by Eq. (4.19) with the direct measurements of boundary shear stresses.

Due to the different behavior of data for different ranges of Reynolds number the discussion is divided into three groups:

1. Reynolds number less than 900 (the number 900 is only an approximation): The total friction coefficient with rainfall is assumed to be the sum of the f_o friction coefficient without rainfall and f_R, the added friction due to rainfall, or

$$f = f_R + f_o \tag{4.27}$$

where

$$f_o = \frac{24}{N_R} \tag{4.28}$$

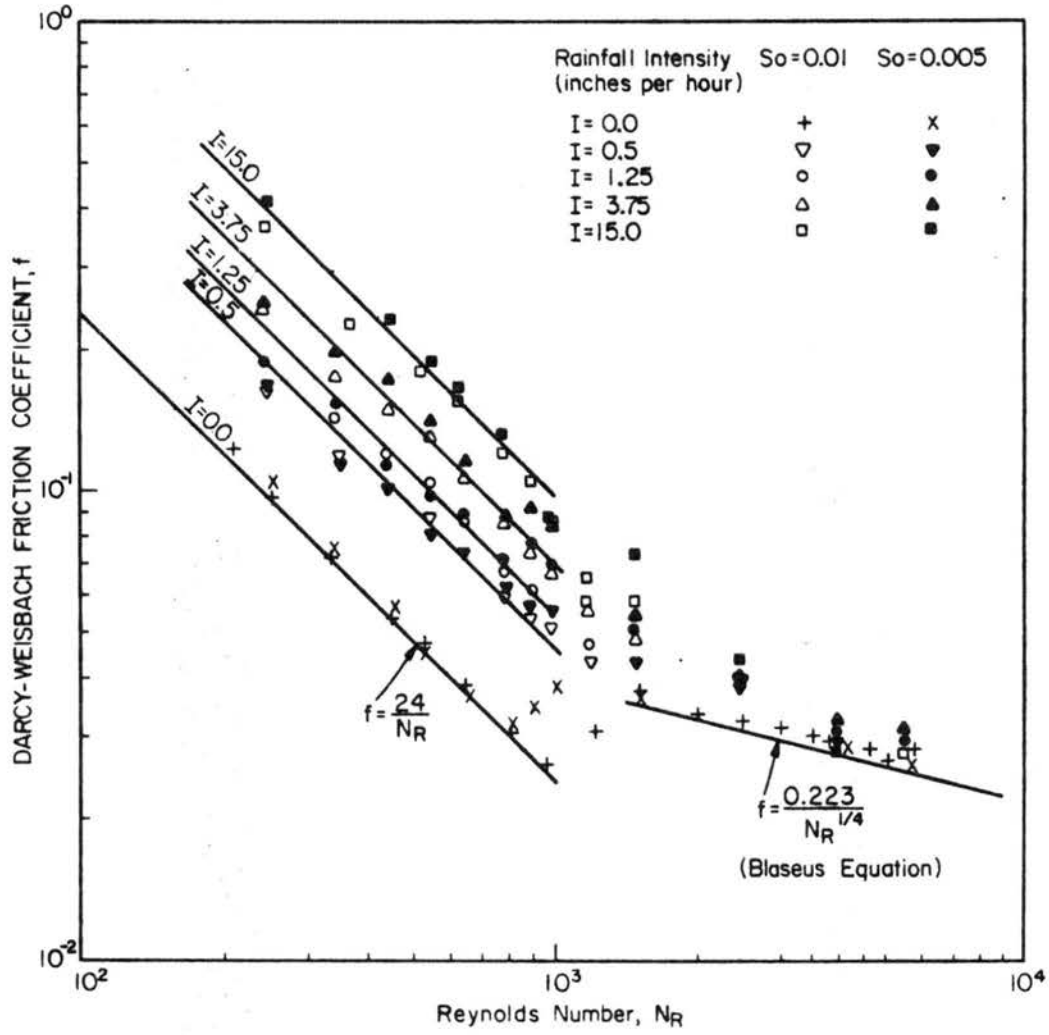

Fig. 4.4 Relationship Among f , N_R , I , S_o [after Yoon (1970)]

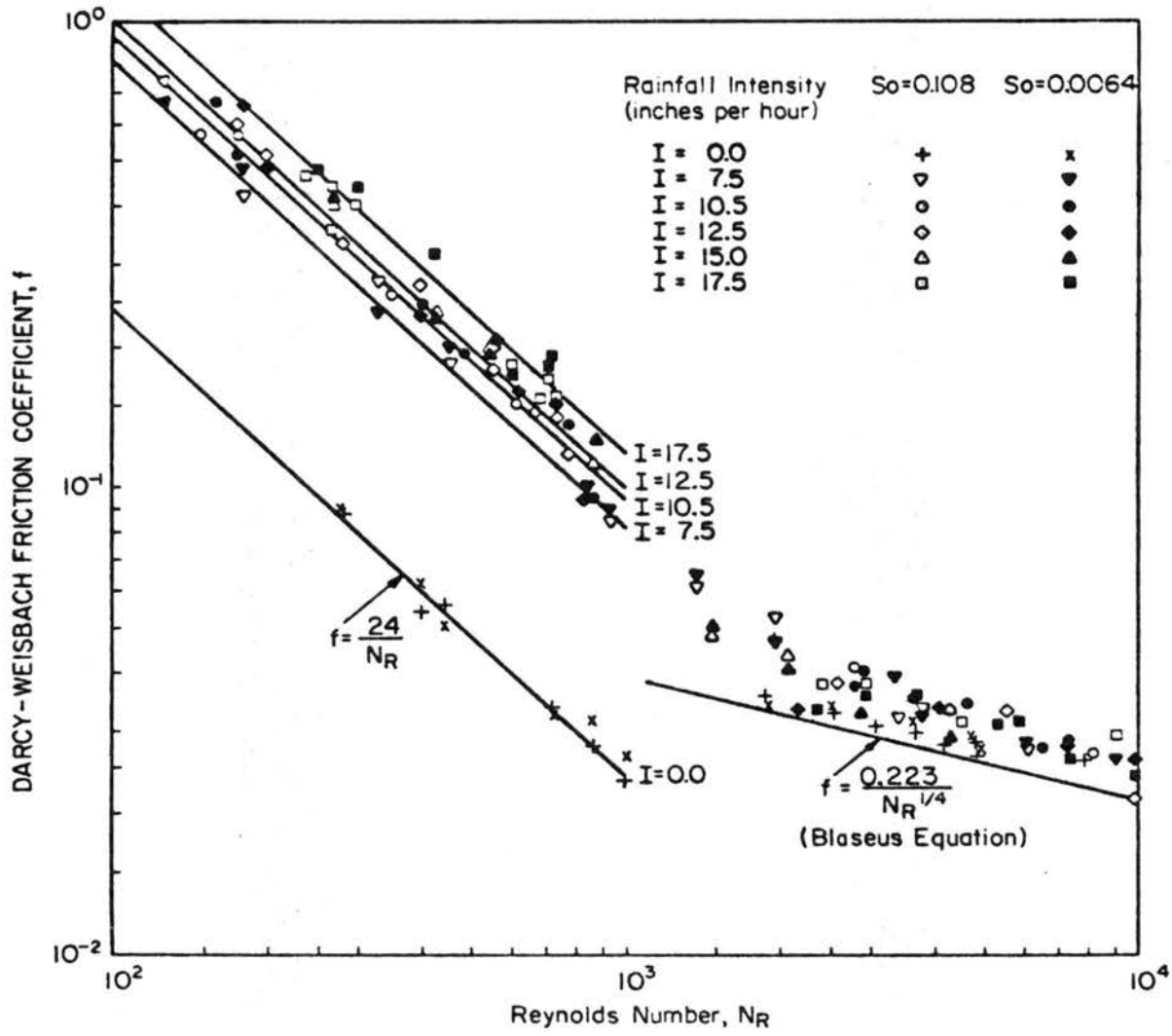

Fig. 4.5. Relationship Among f , N_R , I , S_o (C.S.U. Data)

and therefore

$$f = f_R + \frac{24}{N_R} \tag{4.29}$$

$$f_R = \text{function } (N_R, S_o, I) \quad . \tag{4.30}$$

Since N_R , S_o , and I are all independent variables, the following multiplicative model is assumed

$$f_R = \beta_o N_R^{\beta_1} I^{\beta_2} S_o^{\beta_3} \varepsilon \quad . \tag{4.31}$$

Taking logarithms to the base e in the above equation converts the model into the linear form

$$\ell n\ f_R = \ell n\ \beta_o + \beta_1\ \ell n\ N_R + \beta_2\ \ell n\ I + \beta_3\ \ell n\ S_o + \ell n\ \varepsilon \quad . \tag{4.32}$$

The procedures of "all possible regressions" are used to find the most significant regression equation. The highest multiple correlation coefficient within each possible set of combinations of independent variables in a regression equation is summarized in the following table (Table 4.2).

Table 4.2. Examination of "All Possible Regressions" of $\ell n\ f_R$ with $\ell n\ N_R$, $\ell n\ I$ and $\ell n\ S_o$ for $N_R < 900$.

Set	Variables in Equation with Highest Multiple Correlation Coefficient (R) Within Each Set	Coefficient of Determination (R^2)
A: One independent variable	$\ell n\ f_R$ = function ($\ell n\ I$)	0.5553
B: Two independent variables	$\ell n\ f_R$ = function ($\ell n\ N_R$, $\ell n\ I$)	0.9689
C: Three independent variables	$\ell n\ f_R$ = function ($\ell n\ N_R$, $\ell n\ I$, $\ell n\ S_o$)	0.9702

From Table 4.2 one can see that the addition of the variable $\ell n\ S_o$ when $\ell n\ N_R$ and $\ell n\ I$ are already in the regression equation will remove very little of the unexplained variation in the response. This is clearly shown by the slight increase in R^2 from set B to set C.

The results of the multiple regression are given in Table 4.3. From Table 4.3 one can see that Eq. (4.32) becomes (I in inches per hour)

$$f_R = 13.517\ N_R^{-0.958}\ I^{0.413}\ S_o^{-0.088}\ \varepsilon \quad . \tag{4.33}$$

The assumption of $\ell n\ \varepsilon$ being normally distributed with mean zero was carefully examined from plots of each independent variable with residuals by Li (1972) and no evidence was found to prove otherwise.

Two important observations are noted here from this regression analysis. The first point is the low magnitude of $\hat{\beta}_3$ value and the second point is that $|\hat{\beta}_1|$ is nearly one. Perhaps the following two additional statistical tests should be made to test "whether or not one can assume $\hat{\beta}_3 = 0$ and $\hat{\beta}_1 = -1$."

Testing Hypothesis

(i) partial F-test to test the significance of adding S_o into the equation already with N_R and I

$$F = \frac{\text{MS due to } \hat{\beta}_3 | \hat{\beta}_o, \hat{\beta}_1, \hat{\beta}_2}{\text{MS Residual}} = 4.719 < F(1,110,\ 0.975) \quad .$$

Therefore the addition of S_o is not worthwhile for test size $\alpha = 0.025$.

(ii) student-t test to test the null hypothesis

$$H_o : \beta_1 = -1 \quad \text{vs} \quad H_a : \beta_1 \neq -1$$

$$t = \frac{\hat{\beta}_1 - \beta_1}{(\text{est. stand. error of } \hat{\beta}_1)} = \frac{-0.958 + 1}{0.0245} = 1.727 < t\ (110,\ 0.975)$$

Therefore the null hypothesis is not rejected for test size $\alpha = 0.05$.

Table 4.3. Multiple Linear Regression Results of $\ell n\ f_R$ with $\ell n\ N_R$, $\ell n\ I$ and $\ell n\ S_o$ for $N_R < 900$.

The sample regression line

$$\ell n\ \hat{f}_R = 2.604 - 0.958\ \ell n\ N_R + 0.413\ \ell n\ I - 0.088\ \ell n\ S_o$$

Multiple correlation coefficient 0.985

Standard error of estimate 0.1339

Range of residual 0.674

Transformed regression curve

$$f_R = 13.517\ N_R^{-0.958}\ I^{0.413}\ S_o^{-0.088}$$

Analysis of Variance

Source of Variation	Degree of Freedom	Sum of Squares	Mean Squares	F Ratio
Total (corrected)	113	66.2008	0.5858	
Regression $\mid \hat{\beta}_o$	3	64.2282	21.4094	
Due to $\hat{\beta}_1 \mid \hat{\beta}_o$	1	36.1615	36.1615	2016.8
Due to $\hat{\beta}_2 \mid \hat{\beta}_o, \hat{\beta}_1$	1	27.9821	27.9821	1560.6
Due to $\hat{\beta}_3 \mid \hat{\beta}_o, \hat{\beta}_1, \hat{\beta}_2$	1	0.0846	0.0846	4.719
Residual	110	1.9726	0.01793	

β's are defined by Eq. (4.32)

Additional statistical tests were made by Li (1972) that for constant values of I, the product of $f\ N_R$ and S_o are not correlated.

All these statistical tests seem to establish a simple model that

$$f = \frac{k}{N_R} + \frac{24}{N_R} = \frac{C_L}{N_R} \quad . \tag{4.34}$$

From Yoon's (1970) and CSU's data, regression analysis was conducted to determine that (correlation coefficient 0.9644, standard

error of estimate 0.1375, I in inches per hour).

$$f = \frac{C_L}{N_R} = \frac{27.162\ I^{0.407} + 24}{N_R} \quad . \tag{4.35}$$

The 95% confidence interval and prediction intervals of C_L together with all data points are shown in Fig. 4.6.

Equation (4.35) can also be rewritten as

$$\frac{f}{f_e} = 1.132\ I^{0.407} + 1 \quad . \tag{4.36}$$

2. Reynolds Number Greater than 2000: It is first assumed that

$$C_T = f\ N_R^{1/4} = \text{function } (I) \quad . \tag{4.37}$$

As shown from Figs. 4.4 and 4.5, C_T seems to be a constant for all flows with rainfall when $N_R > 2000$. Total samples of size 81 were divided (Li, 1972) into eight classes: rainfall intensities of 0.5, 1.25, 3.75, 7.5, 10.5 12.5, 15.0 and 17.5 inches/hour. It was found that one cannot reject the null hypothesis that C_T was not a function of rainfall intensity for $I > 0.5$ inches/hour. Li further determined that (standard deviation 0.0201 and 95% confidence intervals $0.222 \leq C_T \leq 0.302$).

$$C_T = 0.262 \quad \text{for} \quad 0.5 < I < 17.5 \text{ inches/hour} \tag{4.38}$$

and $C_T = 0.25$ for $I = 0.0$ inches/hour, then

$$\frac{f}{f_e} = 1.048 \quad . \tag{4.39}$$

If one compares this f vs N_R curve (for flows with rainfall) with the same curve for flows without rainfall, one may speculate that rainfall with intensity somewhere below 0.5 inches/hour would begin to increase the flow resistance. Once the flow resistance is increased by the rainfall, the amount of the increase would be constant and

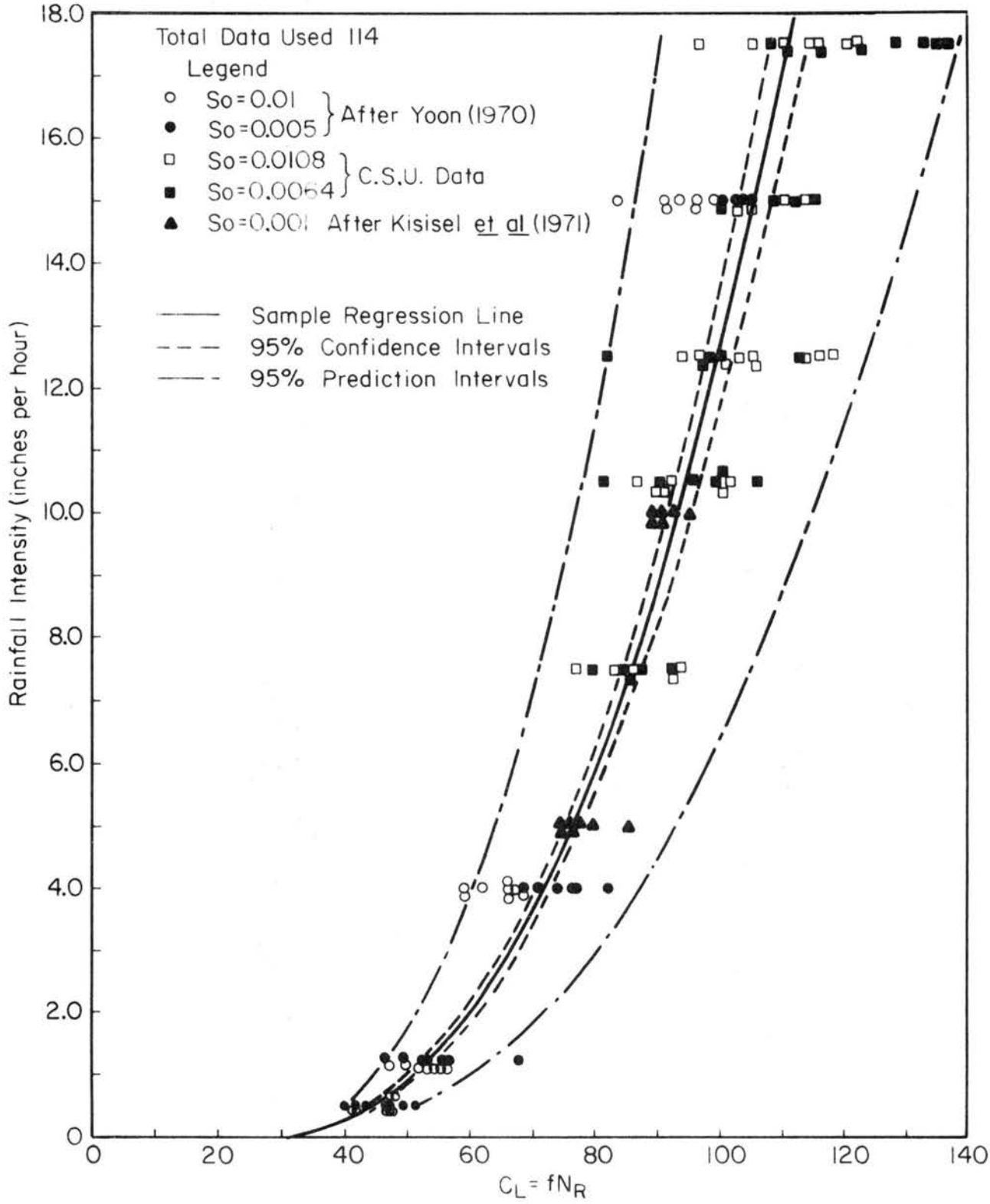

Fig. 4.6 Relationship Between C_L and Rainfall Intensity for $N_R < 900$

independent of any further increase of rainfall up to at least $I = 17.5$ inches/hour.

3. Reynolds Number Between 900 to 2000: Within this range of Reynolds number, the relationship between f and I is difficult to define. For any given amount of rainfall intensity, the f values decrease from that for the laminar flow to its value for turbulent flow as shown in Figs. 4.4 and 4.5. From the linear interpolation of the two end points ($N_R = 900$ and $N_R = 2000$) in the relationship between $\ell n\ f$ and $\ell n\ N_R$, the f value within the range $900 < N_R < 2000$ can be approximated by

$$f = 0.0392\ (\frac{N_R}{2000})^{-1.252\ \ell n\ (0.68 + 0.77\ I^{0.407})} \quad . \qquad (4.40)$$

B. Relative Change of Flow Depth, Mean Flow Velocity and Boundary Shear Stress Due to the Influence of Rainfall

1. $N_R < 900$: From Eq. (4.22)

$$\frac{y}{y_e} = \text{function}\ (N_R,\ S_o,\ I)$$

and as stated previously, y/y_e gives the relative ratio of flow depths with and without rainfall for the same unit flow discharge and also for the same flow Reynolds number if the temperature of the water is held constant. The following multiplicative model is assumed

$$\frac{y}{y_e} - 1 = \beta_o\ N_R^{\beta_1}\ I^{\beta_2}\ S_o^{\beta_3}\ \varepsilon \quad . \qquad (4.41)$$

Following the same procedures made on the investigation on f_R, the examination of "all possible regressions" indicate that $y/y_e - 1$ can be written as a function of I and N_R. However, for practical purposes, the effect of N_R is so small and may be neglected. Then,

$y/y_e - 1$ can be written as a function of I alone, the regression result is (correlation coefficient 0.9426, standard error of estimate 0.1323 from Yoon and CSU data, I in inches/hour)

$$\frac{y}{y_e} = 0.302\ I^{0.305} + 1 \quad . \tag{4.42}$$

The relative change of mean velocity V/V_e (ratio of mean velocities with and without rainfall for the same unit flow discharge and also for the same flow Reynolds number if the temperature of the water is kept constant), can be evaluated by the relationship

$$\frac{V}{V_e} = \frac{y_e}{y} = (0.302\ I^{0.305} + 1)^{-1} \tag{4.43}$$

and the relative change boundary shear stress τ/τ_e is (from Eqs. 4.25 and 4.43)

$$\frac{\tau}{\tau_e} = \frac{f}{f_e}\left(\frac{V}{V_e}\right)^2 = (1.132\ I^{0.407} + 1)\ (0.302\ I^{0.305} + 1)^{-2} \quad . \tag{4.44}$$

These ratios of f/f_e, y/y_e, V/V_e and τ/τ_e are rather useful to design engineers for estimating the effect of rainfall on various flow elements.

2. $N_R > 2000$: An analysis of variance to test the null hypothesis that there is no effect of rainfall intensity on C_T for rainfall intensity between 0.5 to 17.5 inches/hour was made by Li (1972). He found that the null hypothesis was not rejected and for the sample mean

$$\frac{y}{y_e} = 1.0315 \tag{4.45}$$

$$\frac{V}{V_e} = \frac{y_e}{y} = \frac{1}{1.0315} = 0.969 \tag{4.46}$$

$$\frac{\tau}{\tau_e} = \frac{f}{f_e} \left(\frac{y_e}{y}\right)^2 = 1.048\ (0.969)^2 = 0.985 \quad . \tag{4.47}$$

3. $900 < N_R < 2000$: In this flow range, no accepted correlation between flow elements and rainfall intensity was found. However, an estimate can be made by each respective flow element for $N_R = 900$ and $N_R = 2000$ as upper and lower bounds.

C. Discussions

1. Raindrops falling on the flow roughens the water surface, as shown in Fig. 4.2, and retards the main flow velocity, especially the portion near the water surface. The maximum flow velocity thus occurs at a distance below the water surface instead of at the water surface. Since the main velocity is retarded, the flow depth must be increased for the same unit flow discharge. Raindrops also enhance turbulent velocity fluctuations. As shown by Yoon and Wenzel (1971), for flows with lower Reynolds numbers, turbulent fluctuations increased with rainfall intensity throughout the flow depth and for flows with greater Reynolds numbers the effect of rainfall intensity was limited to the region very near to the water surface.

2. Experimental results indicate that the friction slope, S_f, is generally slightly less than channel bottom slope and it decreases as rainfall intensity increases for a constant Reynolds number and channel bottom slope. This effect can also be seen for $N_R < 900$ from Eqs. (4.9), (4.25) and (4.43)

$$\frac{S_f}{S_{f_e}} = \frac{f}{f_e} \left(\frac{y_e}{y}\right)^3 \frac{q^2}{q_e^2}$$

and for the same N_R, $q = q_e$, and from $S_o = S_{f_e}$, thus,

$$\frac{S_f}{S_o} = \frac{f}{f_e} \left(\frac{y_e}{y}\right)^3$$

$$= (1.132\ I^{0.407} + 1)\ (0.302\ I^{0.305} + 1)^{-3} \qquad (4.48)$$

$$\leq 1 \quad .$$

Similarly, for $N_R > 2000$

$$\frac{S_f}{S_o} = (1.048)\ \left(\frac{1}{1.0315}\right)^3 = 0.955 \quad . \qquad (4.49)$$

3. The data collected at Colorado State University appears to scatter little more than that taken by Yoon (1970). This could be due to any of the following possible reasons: i) a TSI probe was coupled with a DISA anemometer for boundary shear stress measurement, with comparatively low power in the DISA anemometer. The maximum overheat ratio used in measurement was limited to 1.03, thus the voltage output was more sensitive to temperature change than the output from using the same system for the probe and the anemometer, ii) surface tension effect might be significant for very thin flow depth measurement by piezometric depth devices, and iii) the flume floor had a slight deformation.

4. From a seperate regression analysis with only data collected by Yoon (1970) to determine the variation of the friction coefficient with: i) rainfall intensity, ii) Reynolds number of the flow, and iii) channel bottom slope, it was found that statistically the channel bottom slope had little effect on the friction coefficient, and this result is contrary to that concluded by Yoon and Wenzel (1971).

VII. APPLICATION OF RESULTS

A. Basic Equations for Water Surface Profiles

From Eqs. (4.3), (4.8), (4.35), (4.39) and (4.40); for $N_R < 900$

$$\frac{dy}{dx} = \frac{S_o - \dfrac{\nu(27.162\ I^{0.407} + 24)\ (q_o + ix)}{8\ gy^3} - \dfrac{2\beta(q_o + ix)i}{gy^2}}{1 - \beta\dfrac{(q_o + ix)^2}{gy^3}} \qquad (4.50)$$

for $900 < N_R < 2000$

$$\frac{dy}{dx} = \frac{S_o - f\dfrac{(q_o + ix)^2}{8\ gy^3} - \dfrac{2\beta(q_o + ix)i}{gy^2}}{1 - \beta\dfrac{(q_o + ix)^2}{gy^3}} \qquad (4.51)$$

and for $N_R > 2000$

$$\frac{dy}{dx} = \frac{S_o - \dfrac{0.262\ \nu^{0.25}}{8\ gy^3}(q_o + ix)^{7/4} - \dfrac{2\beta(q_o + ix)i}{gy^2}}{1 - \beta\dfrac{(q_o + ix)^2}{gy^3}} \qquad (4.52)$$

where I is the rainfall intensity in inches/hour and i is the lateral inflow rate per unit area which is equal to $I/43200$ in feet per second.

B. Comparisons of Water Surface Profile and Boundary Shear Stress as Predicted by Eqs. (4.50), (4.51) and (4.52) with Friction Resistance Determined by Regression Curves against that Collected by Experiment

As shown by Li (1972), the deviations between the flow depths and boundary shear stress as predicted by the above equations are within ± 10% of that measured by experiment in all flow cases as shown by Fig. 4.1.

C. Sensitivity Study and Estimating the Effects of Uncertainties

From

$$\frac{\tau}{\gamma y} = S_f = f\frac{q^2}{8\ gy^3} \qquad (4.53)$$

and also from experimental data $S_f \simeq S_o$, one obtains

$$d\tau \propto S_o \gamma \, dy$$

or

$$\frac{d\tau}{\tau} \simeq \frac{dy}{y} \tag{4.54}$$

and similarly

$$\frac{3\,dy}{y} \simeq \frac{df}{f} \quad . \tag{4.55}$$

In other words, the percentage of variation of τ is about the same as the flow depth and both of these variations are in the order of one-third of the percentage of variation of the friction oefficient. This is good because, if one estimates the friction coefficient incorrectly, the flow depth and boundary shear stress would be influenced to a much smaller magnitude.

There are three possible sources of uncertainties: random error, systematic error and non-homogeneity.

1. Uncertainties due to Random Error:

a) $N_R < 900$: If random error is included, Eq. (4.35) may take the form

$$f = \frac{27.162\ I^{0.407}\ \varepsilon + 24}{N_R} \quad . \tag{4.56}$$

With the assumption that $\ell n\ \varepsilon$ (random error) is normally distributed with $N\ (0, \hat{\sigma}^2)$, the random error will be generated by the Monte Carlo method as follows:

If one lets U_i be identically and independently uniformly distributed random variables with probability density function

$$f_U(u) = \frac{1}{12\ \hat{\sigma}}\ I_{[-6\ \hat{\sigma},\ 6\hat{\sigma}]}\ (u) \tag{4.57}$$

then according to the Central Limit Theorem, $\bar{u}_{12}\ (= \frac{1}{12} \sum_{i=1}^{12} u_i)$ will

distribute approximately normal with $N(0, \hat{\sigma}^2)$. From regression analysis, $\hat{\sigma} = 0.1375$ (for the derivation of Eq. 4.35). The random variables $\ell n\ \varepsilon$ are generated by the arithematic mean of 12 generated random samples of uniform distribution as described above. Computer simulation results for flow with control types 1, 2 and 3 (with only type 3 control flow shown in Fig. 4.7) indicate that the flow depths and boundary shear stresses based on randomly generated f-values are nearly all inside the upper and lower bounds of the computed values based on 95% prediction limits for f . The effect of random error of f on the successive computation is not cumulative. Actually this result is not a surprise, since if a too large f value is chosen for computation of water surface profile, it would result in a larger upstream flow depth for subcritical flows. A large f value and a large water depth would compensate each other as indicated by Eq. (4.8) with S_f equal to $f\ q^2/8\ gy^3$. The upper bound and lower bound of the percentage deviation of flow depths or boundary shear stresses from those computed by the mean value of f for different rainfall intensities are given in Fig. 4.8(a).

b) $N_R > 2000$: Similar to that for $N_R < 900$, the flow depths and boundary shear stresses based on randomly generated f-values within 95% confidence interval fall between +5.2% and -5.2% of their values based on the mean f values (all these deviations are independent of the rainfall intensity).

2. Uncertainties due to Systematic Error: To test the effect of systematic error, one can assign the systematic error as percentage deviation from the mean values of f and the systematic errors are allowed in both positive and negative directions, i.e.,

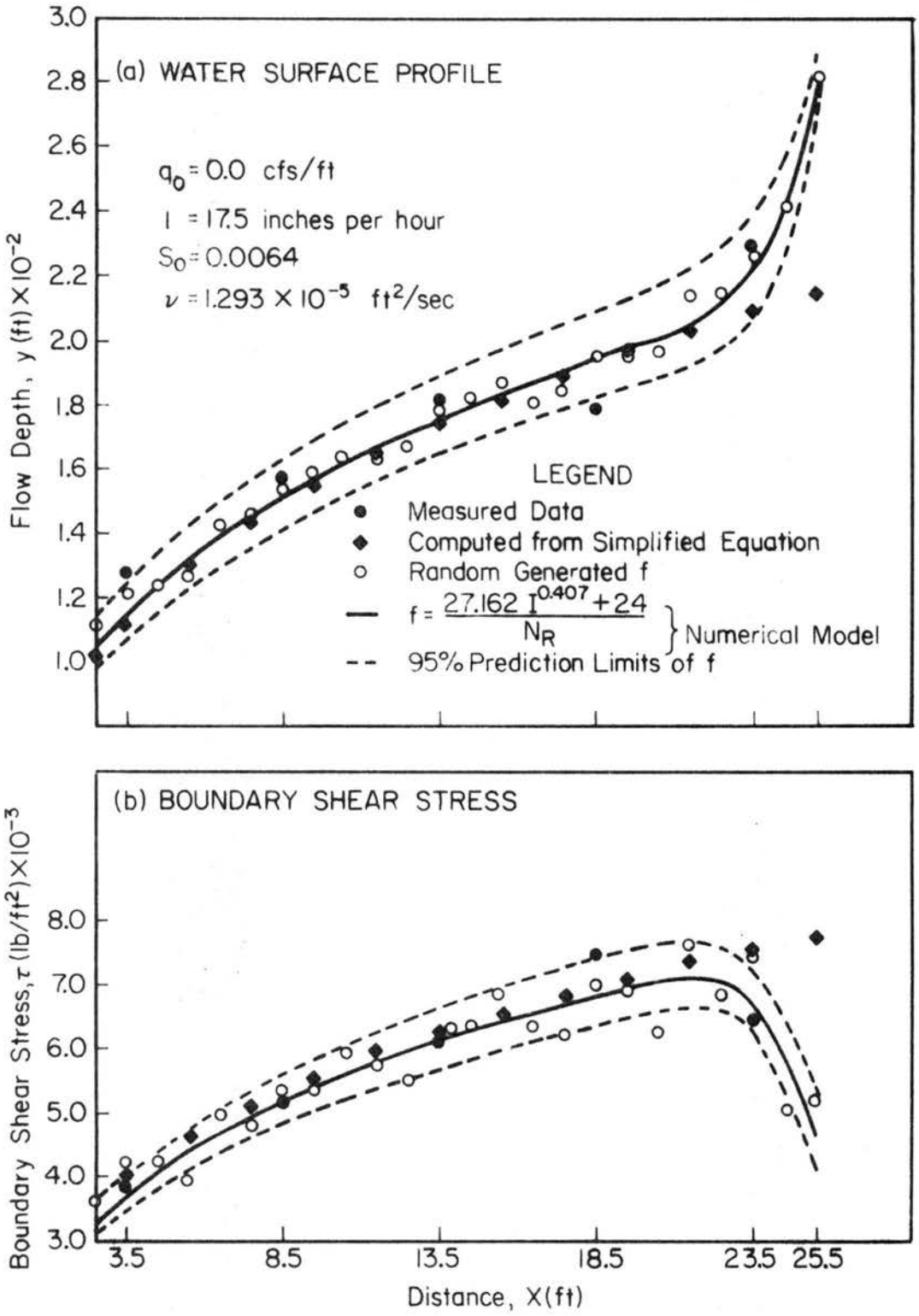

Fig. 4.7. Example of Effect of Random Errors of Darcy-Weisbach f on Water Surface Profile and Boundary Shear Stress for Type 3 Control

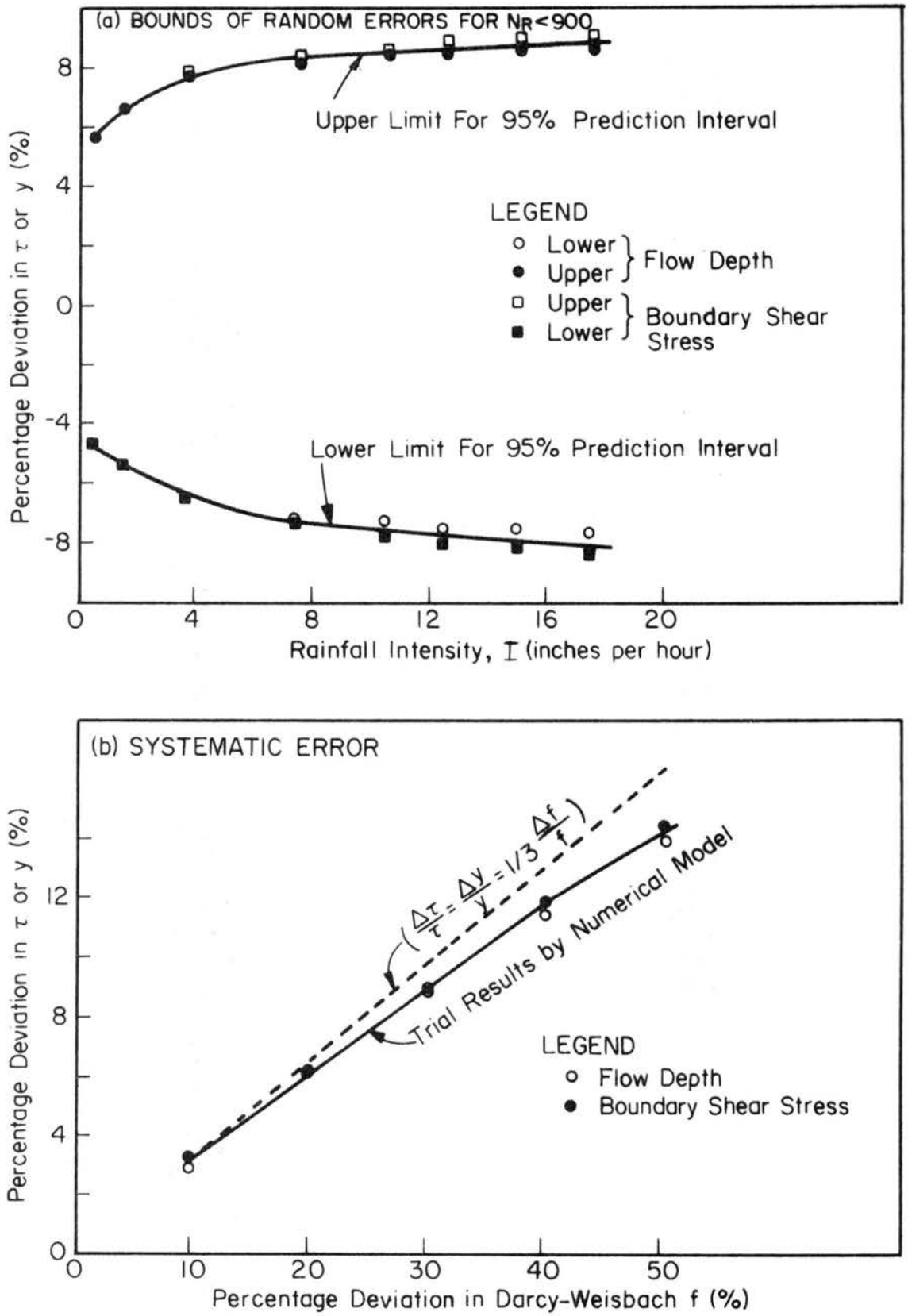

Fig. 4.8. The Effects of Uncertainties of f on Flow Depths and Boundary Shear Stresses

$$f_s = \bar{f} + \varepsilon_s \tag{4.58}$$

where f_s is the f-value with systematic error, ε_s and $\bar{f} = (27.162 I^{0.407} + 24)/N_R$ for $N_R < 900$ and $\bar{f} = 0.262/N_R^{1/4}$ for $N_R > 2000$.

Many flow cases with pre-assigned constant percentage deviations of f were studied (i.e., $\varepsilon_s/f = 10$, 20, 30, 40 and 50 percents). It is found that the percentage deviations of flow depths or boundary shear stresses increase by a constant amount over the entire flow region except at the region where the back water effect is significant if the f value is increased by a constant amount over the entire flow reach. This indicates that the effect of uncertainties is not cumulative. The overall effects of systematic errors of f on the boundary shear stresses and flow depths are given in Fig. 4.8(b). Figure 4.8(b) also indicates that the percentage deviations of shear stresses and flow depths are about one-third of the percentage deviations of friction factor.

3. Uncertainties due to Non-Homogeneity: This source of uncertainties is due to the use of incorrect f-values, for instance, if f value without rainfall is used for flow with rainfall, etc. In this case, one should first determine the correct mean f value for that combination of rainfall and N_R. The next step is to find f/f_e and the last step is to find the percentage deviations of shear stress and flow depth from Fig. 4.8(b) with $f/f_e - 1$ as the percentage increase or decrease of friction value.

D. Simplified Equations

Since there is no closed form solution for the dynamic equations, numerical method through iteration process is necessary to obtain a soltuion. It happens to take a lot of time and effort, thus, simplified

but practical equations to yield approximate solutions are useful for practical engineering use.

Due to thin water depth in sheet flow, unlike conventional open channel flow, the control effect is generally negligible. This special characteristic of sheet flow leads to the possibility of developing the following simplified equation to yield approximate solutions.

For a given base flow (q_o), channel slope (S_o), rainfall intensity (I) and kinematic viscosity of water (ν), one can easily evaluate flow depth, mean velocity and boundary shear stress at some distance x by the following methods.

1. For $N_R < 900$: From Eq. (4.21) the equivalent flow depth at point x is evaluated by

$$y_e = \left[\frac{3\nu\,(q_o + ix)}{g\,S_o}\right]^{1/3} \tag{4.59}$$

then, by using Eq. (4.42), the flow depth at point x can be estimated, i.e.,

$$y = (0.302\ I^{0.305} + 1.0)\left(\frac{3\nu}{g\,S_o}\right)^{1/3}(q_o + ix)^{1/3} \quad . \tag{4.60}$$

Since q is equal to Vy the mean velocity at point x is

$$V = \frac{q}{y} = \frac{q_o + ix}{y}$$

then from Eq. (4.60)

$$V = \frac{\left(\frac{g\,S_o}{3\nu}\right)^{1/3}}{(0.302\ I^{0.305} + 1)}(q_o + ix)^{2/3} \quad . \tag{4.61}$$

The equivalent boundary shear stress at point x is

$$\tau_e = \gamma\, y_e\, S_o = \gamma\left(\frac{3S_o{}^2\nu}{g}\right)^{1/3}(q_o + ix)^{1/3} \quad . \tag{4.62}$$

From Eqs. (4.44) and (4.62), one can easily evaluate boundary shear stress at point x by

$$\tau = \frac{(1.132\ I^{0.407} + 1)}{(o.302\ I^{0.305} + 1)^2}\ \gamma\ (\frac{3\ S_o^2\ \nu}{g})^{1/3}\ (q_o + ix)^{1/3} \quad . \quad (4.63)$$

2. For $N_R > 2000$: Similar to the development for $N_R < 900$, for $N_R > 2000$

$$y = 1.0315\ (\frac{\nu^{1/4}}{32\ g\ S_o})^{1/3}\ (q_o + ix)^{7/12} \quad (4.64)$$

$$V = 0.969\ (\frac{32\ g\ S_o}{\nu^{1/4}})^{1/3}\ (q_o + ix)^{5/12} \quad (4.65)$$

$$\tau = 0.985\ \gamma\ (\frac{S_o^2\ \nu^{1/4}}{32\ g})^{1/3}\ (q_o + ix)^{7/12} \quad . \quad (4.66)$$

The computed values by these simplified equations are found to agree very well with the values predicted by numerical models except some points with significant back water effect as shown in Fig. 4.8(a) and (b). Therefore, these simplified equations have been proven to be powerful tools in the prediction of mechanics of sheet flow. A more detailed comparison of the results is given by Li (1972).

D. Effect of Rainfall on the Mechanics of Base Flow

The effect of rainfall on the base flow has two folds: one is due to the raindrop impact on the flow, the other is the mass inflow adding to the base flow.

The ratio of flow depths with and without rainfall introduced in Section IV gave the relative ratio of mean flow properties for the same unit flow discharge and those may not be functions of distance. The relative quantities introduced here give the ratio between the mean flow

properties after the rainfall and the mean flow properties before the rainfall and these are functions of distance.

With the aid of results obtained in previous sections, the effect of rainfall on the base flow is introduced here. This information should provide a better understanding of the effect of rainfall.

1. For $N_R < 900$ or $q_o + q_i < 0.009$ cfs/ft: The initial normal depth of base flow is

$$y_o = \left(\frac{3 \nu q_o}{g S_o}\right)^{1/3} \tag{4.67}$$

where y_o is the initial normal depth of base flow and q_i is the unit lateral inflow discharge which is equal to ix. From Eqs. (4.59) and (4.67)

$$\frac{y_e}{y_o} = \left(\frac{q_o + q_i}{q_o}\right)^{1/3} . \tag{4.68}$$

From Eqs. (4.68) and (4.42)

$$\frac{y}{y_o} = \left(1 + \frac{q_i}{q_o}\right)^{1/3} (0.302\ I^{0.305} + 1) . \tag{4.69}$$

Similarly, V/V_o can be approximated by

$$\frac{V}{V_o} = \left(1 + \frac{q_i}{q_o}\right)^{2/3} (0.302\ I^{0.305} + 1)^{-1} \tag{4.70}$$

where V_o is the mean velocity of base flow and

$$\frac{\tau}{\tau_o} = \left(1 + \frac{q_i}{q_o}\right)^{1/3} (1.132\ I^{0.407} + 1)\ (0.302\ I^{0.305} + 1)^{-2} \tag{4.71}$$

where τ_o is the boundary shear stress of base flow. Equations (4.69), (4.70) and (4.71) can be used to estimate y, V or τ easily by knowing the rainfall intensity and the discharge ratio (q_i/q_o). Besides these equations can be used to roughly determine where the ratio

is equal to some value. Graphical representation of these equations are given in Figs. 4.9(a), (b) and (c).

2. For $2000 < N_R < 12600$ or $0.02 < q_i + q_o < 0.126$ cfs/ft

$$\frac{y}{y_o} = 1.0315 \left(1 + \frac{q_i}{q_o}\right)^{7/12} \tag{4.72}$$

$$\frac{V}{V_o} = 0.969 \left(1 + \frac{q_i}{q_o}\right)^{5/12} \tag{4.73}$$

$$\frac{\tau}{\tau_o} = 0.985 \left(1 + \frac{q_i}{q_o}\right)^{7/12} \tag{4.74}$$

Figure 4.9(d) shows the trend of these three equations.

VIII. CONCLUSIONS

The conclusions drawn from the present study limiting to some conditions as already described previously with Reynolds numbers in the range of 126 to 12600, channel bottom slope 0.005 to 0.0108 and rainfall intensity 0.5 to 17.5 inches/hour over a smooth surface are:

A.

The water surface and boundary shear stresses for a steady straight flow with rainfall can be studied by a conventional steady spatially varied flow equation derived by the momentum approach with the effect of rainfall included in the variation of friction coefficient (such as Darch-Weisbach f value). Numerical solutions for these dynamic equations agree with measurements rather well.

B.

By regression analysis, the friction coefficient f is found to be a function of both the flow Reynolds number and the rainfall intensity for a flow Reynolds number of less than 900. For a flow Reynolds number

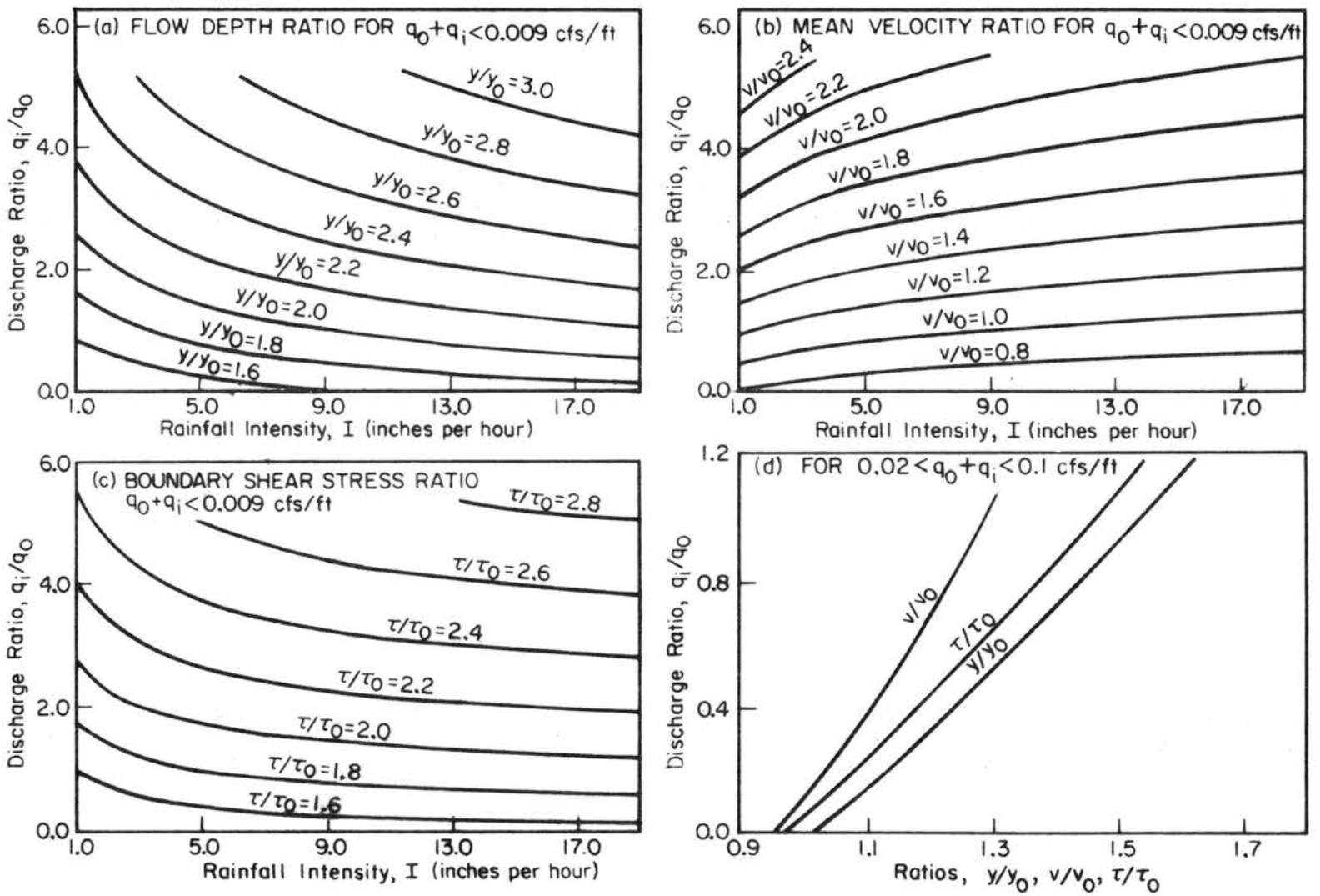

Fig. 4.9. Contour Map of Ratios of Flow Depth, Mean Velocity and Boundary Shear Stress of Flow Before and After Rainfall

greater than 2000, the friction coefficient is only a function of the Reynolds number and is independent of the rainfall intensity. A set of regression curves for the variation of f with rainfall intensity and Reynolds number is determined for $126 < N_R < 12600$.

C.

The effect of uncertainties in selecting friction factors in the computation of flow depths and boundary shear stresses is not too sensitive. If one selects the friction factor with a certain percentage error, k , in calculating boundary shear stresses and flow depths, the calculated boundary shear stress and flow depth would involve an error of one-third of that percentage of $k/3$.

D.

The error of using an incorrect friction factor in the calculations of boundary shear stress and flow depths is not cumulative with steps. In other words, if one selects a too large value of friction factor to calculate the boundary shear stresses and flow depths in an entire back water profile computation, the resultant boundary shear stress and flow depths would deviate from the correct values uniformly over the entire flow region and not to increase with the number of distance steps.

E.

Simplified estimations for the effect of rainfall on flow depths and boundary shear stresses are presented in graphical forms. Very good agreement exists in the calculated values of boundary shear stresses and flow depths between the numerical solutions and the simplified equations.

IX. LIST OF SYMBOLS - CHAPTER 4

Symbol	Description
A	Channel cross-sectional area
C_L	$f N_R$ for $N_R < 900$
C_T	$f N_R^{1/4}$ for $N_R > 2000$
D	Hydraulic depth, A/T
d	Raindrop size
f	Darcy-Weisbach friction coefficient
f_e	Equivalent Darcy-Weisbach friction coefficient
f_o	Darcy-Weisbach friction coefficient without rainfall
f_R	Added Darcy-Weisbach friction coefficient due to rainfall
f_s	Darcy-Weisbach friction coefficient with systematic error
g	Gravitational acceleration
h	Head of water above weir
h_o	Height of weir
I	Rainfall intensity
i	Lateral inflow rate per unit area
N_R	Reynolds number, Vy/ν
P	Wetted parameter
Q	Flow rate of the combined flow
q	Flow rate of combined flow per unit width of channel
q_i	Lateral inflow rate per unit width of channel
q_o	Flow rate of base flow per unit width of channel
R	Multiple regression coefficient
$\overline{R}$	Hydraulic radius, A/P
S_f	Friction slope, $\tau/\gamma y$

Symbol	Description
S_{f_e}	Equivalent friction slope
S_o	Channel bottom slope
T	Width of channel section at the free surface
U	Velocity of lateral inflow entering the main flow
V	Mean flow velocity of combined flow
V_e	Equivalent mean flow velocity
V_o	Mean flow velocity of base flow
x	Distance in the main flow direction
y	Flow depth normal to x of combined flow
y_c	Critical flow depth
y_e	Equivalent flow depth
y_o	Flow depth of base flow
α	Test size of hypothesis testing
β	Momentum coefficient
β_i	Regression coefficient in regression equation
γ	Specific gravity of water
Δx	Increment of x
ε	Error in regression equation
ε_s	Systematic error
$\bar{\varepsilon}$	Characteristic length of roughness element
η	Parameter describing raindrop pattern
θ	Angle between the x-direction and the horizontal direction
λ	Parameter describing raindrop shape
ν	Kinematic viscosity of water
ρ	Density of water
$\hat{\sigma}$	Standard deviation of regression equation

Symbol	Description
τ	Boundary shear stress of combined flow
τ_e	Equivalent boundary shear stress
τ_o	Boundary shear stress of base flow
ϕ	Angle between the velocity U and x-direction

X. REFERENCES - CHAPTER 4

1. Brutsaert, W.F., 1971, "De Saint-Venant Equations Experimentally Verified," Jour. Hydr. Div., ASCE, Vol. 97, No. HY9, September, pp. 1387-1401.

2. Draper, N.R., and Smith, H., 1966, Applied Regression Analysis, John Wiley & Sons, Inc., New York.

3. Emmett, W.W., 1970, "The Hydraulics of Overland Flow on Hill Slopes," USGS Professional Paper 662-A.

4. Henderson, F.M., 1966, Open Channel Flow, Macmillan, New York.

5. Izzard, C.F., 1944, "The Surface Profile of Overland Flow," Trans. AGU, Part IV, pp. 959-968.

6. Kisisel, I.T., Rao, A.R., Delleur, J.W., and Meyer, L.D., 1971, "Turbulence Characteristics of Overland Flow---The Effect of Rainfall and Boundary Roughness," Technical Report No. 28, Water Resources and Hydromechanics Laboratory, Purdue University, Lafayette, Indiana, February.

7. Li, Ruh-Ming, 1972, "Sheet Flow Under Simulated Rainfall," thesis presented to Colorado State University, at Fort Collins, Colo., in partial fulfillment of the requirements for the degree of Master of Science.

8. Woo, D.C., and Brater, E.R., 1962, "Spatially Varied Flow from Controlled Rainfall," Jour. Hydr. Div., ASCE, Vol. 88, No. HY6 pp. 31-56.

9. Yen, B.C., and Wenzel, H.G., Jr., 1970, "Dynamic Equations for Steady Spatially Varied Flow," Jour. Hydr. Div., ASCE, Vol. 96, No. HY3, March, pp. 801-814 and paper presented at the ASCE Hydraulics Division 18th Annual Specialty Conference at Minneapolis, Minnesota, August.

10. Yoon, N.Y., 1970, "The Effect of Rainfall on the Mechanics of Steady Spatially Varied Sheet Flow on a Hydraulically Smooth Boundary," thesis submitted in partial fulfillment of the requirements for the degree of Ph.D., University of Illinois, Urbana, Illinois.

11. Yoon, N.Y., and Wenzel, H.G., Jr., 1971, "Mechanics of Sheet Flow Under Simulated Rainfall," Jour. Hydr. Div., ASCE, Vol. 97, No. HY9, September, pp. 1367-1386.

12. Yu, Y.S., and McNown, J.S., 1964, "Runoff from Impervious Surfaces," Jour. Hydr. Rec., IAHR, Vol. 2, No. 1, pp. 2-24.

Chapter 5

DISPERSION OF CONTAMINANTS ATTACHED TO THE TOP SOIL

I. INTRODUCTION

Contaminants such as herbicides, pesticides and radioisotopes can attach to sediment particles and move as bed load in a flow. Unlike those contaminants which are dissolved in the flow and moved rapidly by the flow velocity, these bed load particles with contaminants, attached are dispersed rather slowly and can be a health hazard. Since sediment movements are a stochastic process, the dispersion of contaminated top soil will be approached stochastically. This study is limited to cohesionless soil.

Stochastic models describing the unidirectional movement of a sediment particle which advances in a series of alternate rest and transport periods have been proposed by a number of investigators, notably Einstein (1937), Hubbell and Sayre (1964), and Yang and Sayre (1971). Current theoretical and experimental evidence indicate that the step lengths are gamma distributed with the shape parameter varying between one and three, and the rest periods are exponentially distributed. The analysis reported here is within the above framework to investigate the concentration distribution function describing the dispersion of contaminated particles released instantaneously and continuously from a line source in the bed of a straight channel with steady, uniform flow.

The first part of this chapter is devoted to the development of a general sediment stochastic model which is much less restrictive than all the other previous available theoretical models. After the completion of this theoretical model, it was found that a large amount of

experimental data must be collected to find the variation of coefficients with different flow conditions in order to calculate sediment transport rate. Attention will then be shifted to the development of an empirical model based on regression techniques for the prediction of sediment bed material load with various flow conditions. The dispersion of contaminated bed load particles will be investigated last.

Since most of the developments are quite theoretical and are published elsewhere, only physical descriptions of these are presented in this report.

II. DEVELOPMENT OF A GENERAL STOCHASTIC SEDIMENT MODEL FOR THE TRANSPORT OF SEDIMENT BED MATERIAL

The stochastic process presented here is a nonhomogeneous compound Poisson process. Parzen (1962) described non-homogeneous Poisson processes in p. 124-126 and compound Poisson processes in p. 128. The stochastic process presented by Sayre and Hubbell (1965) is a compound Poisson process of the homogeneous type. If the presentation given by Sayre and Hubbell were followed in this paper the connection between the two papers would be much clearer.

Let E represent the event a particle begins and terminates a step in the downstream direction. Also let the probability of E occurring while the particle remains within a random length increment $(x, x + \Delta x)$ be $k_1(x)\,\Delta x$ where $k_1(x)$ is a function of x and is independent of the number of times that E has occurred previously. Furthermore let Δx be sufficiently small so that the probability of two or more successive occurrences of E while the particle is in $(x, x + \Delta x)$ is negligibly small with respect to Δx. Let $p_n(x)$

denote the probability that the event E has occurred n times in the interval (0, x) . Then based on the above assumptions the following differential equations are well known to express the relationships among the $p_n(x)$.

$$\frac{dp_n(x)}{dx} = k_1(x)[p_{n-1}(x) - p_n(x)] \ , \ n = 1, 2, \ldots, \tag{5.1}$$

$$\frac{dp_0(x)}{dx} = - k_1(x)\ p_0(x) \tag{5.2}$$

with initial conditions

$$p_0(0) = 1 \text{ and } p_n(0) = 0 \text{ for } n \geq 1 \ . \tag{5-3}$$

The solution to the above set of differential equations is given in Parzen (1962) p. 125-126 in another form. The solution is

$$p_n(x) = \frac{[\Lambda_1(x)]^n \exp[- \Lambda_1(x)]}{n!} \tag{5.4}$$

where

$$\Lambda_1(x) = \int_0^x k_1(s)ds \ . \tag{5.5}$$

If similar assumptions are made concerning the occurrence of the event E in the interval $(t, t + \Delta t)$ and if $q_n(t)$ denotes the probability of the event E occurring n times in the interval (0, t) then

$$q_n(t) = \frac{[\Lambda_2(t)]^n \exp[- \Lambda_2(t)]}{n!} \tag{5.6}$$

for

$$n = 0, 1, 2, \ldots,$$

where

$$\Lambda_2(t) = \int_0^t k_2(s)ds \tag{5.7}$$

and $k_2(t)$ is analogous to $k_1(x)$.

The two processes describing the occurrence of E in space and time are thus both nonhomogeneous Poisson processes. The $k_1(x)$ and $k_2(t)$ correspond to the λ_i's in the first approach. If $k_1(x) = k_1$ and $k_2(t) = k_2$ the Sayre and Hubbell model results.

Now let X_t denote the position of the particle at time t and let y_j denote the distance moved at the jth step. Let N(t) denote the number of steps taken in the interval (0, t) . Then,

$$X_t = \sum_{j=1}^{N(t)} y_j \tag{5.8}$$

a compound Poisson process.

The distribution function of interest is

$$F_t(x) = P[X_t \leq x]$$

$$= \sum_{j=0}^{\infty} P[X_t \leq x | N(t) = j]\ P[N(t) = j]$$

$$= \sum_{j=0}^{\infty} \sum_{k=j}^{\infty} p_k(x)\ q_j(t)$$

$$= \exp\ [-\Lambda_1(x) - \Lambda_2(t)] \sum_{j=0}^{\infty} \sum_{k=j}^{\infty} \frac{[\Lambda_1(x)]^k [\Lambda_2(t)]^j}{k!\qquad j!} \quad . \tag{5.9}$$

Equation (5.9) is the main result of the study by Shen and Todorovic (1971). At this stage, $k_1(s)$ and $k_2(s)$ are not determined and perhaps should be investigated from experimental results. The currently available data obtained by Sayre and Hubbell (1965) and Yang and Sayre (1971) are not sufficient to establish the functional forms of k_1 and k_2 .

The assumptions used in deriving Eq. (5.9) are:

i) The sediment particle moves in a series of alternate rest and transport periods.

ii) The particle always moves in downstream direction.

iii) $\sum_{r=2}^{\infty} P(E_r^{t,t+\Delta t}) = 0(\Delta t)$ as $\Delta t \to 0$.

In other words, the probability to make two or more steps in the time period t to $t+\Delta t$ as $\Delta t \to 0$ should be an infinitesimal or higher order than Δt .

iv) $P(E_1^{t,t+\Delta t} | E_\nu^{t_o,t}) = P(E_1^{t,t+\Delta t})$.

The information that a particle makes exactly a particular number of steps occurring in the time period t_o to t has no influence on the probability of the particle to make a step in the next time period between t to $t+\Delta t$.

v) The duration of moving is insignificant as compared with the rest period.

vi) $P\{X_\nu \leq x | E_\nu^{t_o,t}\} = P\{X_\nu \leq x\}$.

The total distance X_ν traveled by the sediment particle after ν steps should not depend in which time interval (t_o,t) that these ν steps occurred.

As stated previously, $k_1(s)$ and $k_2(s)$ are not known at this stage and the specific physical conditions that they can be different from constants are also not determined. However an interesting and important result can be obtained by assuming that $k_1(s)$ and $k_2(s)$ to be in their simplest possible forms, i.e., $k_1(s) = k_1$, $k_2(s) = k_2$, and k_1 as well as k_2 are constants. From Eq. (5.9) with $t_o = 0$ and $x_o = 0$,

$$F_t(x) = \exp\{-k_1 t - k_2 x\} \sum_{\nu=1}^{\infty} \sum_{j=\nu}^{\infty} (k_1 t)^{\nu} (k_2 x)^{j} / j!\nu! \qquad (5.10)$$

which is the same result as obtained by Einstein (1937) and Sayre and Hubbell (1965). In other words, their result is only a special solution of Eq. (5.9). In their case the average number of steps a sediment particle takes in $(t_o,t]$ and $(x_o,x]$ are respectively $k_1 t$ and $k_2 x$. Thus k_1 is the inverse of the average rest period, and k_2 is the inverse of the average jump length.

A general stochastic sediment transport model based on less restrictive assumptions than those developed previously is formulated. The exact functional form for the probability distribution function to describe the longitudinal displacement of a sediment particle is still not known and, perhaps, should be determined by a comprehensive data collection program.

III. AN ENGINEERING APPROACH TO TOTAL BED-MATERIAL LOAD BY REGRESSION ANALYSIS

We began with the assumption that sediment transport is such a complex phenomenon that no single Reynolds number, Froude number, or combination of them can be found to describe sediment motion under all conditions. Regression method is used to develop a formula based on all available data for immediate engineering purposes. The disadvantage of this approach is, of course, the final flow parameter will probably be dimensional. But, the approach has merit in that if all previous data are found to correlate well, it is likely that other data (within the same range) will follow the same trend. The sediment concentration is selected (bed material load) as the dependent variable

and the fall velocity of the median sediment particle of the bed sample as well as the flow velocity and flow depth are treated as the independent variables. A summary of the data used is given in Table 5.1.

The logarithm of sediment concentration is used as the dependent variable instead of the sediment concentration itself due to the following two reasons:

i) Based on data collected by Guy, Simons and Richardson (1966) the logarithm of the sediment concentration ratio between the mean of several samples plus one standard deviation and the mean concentration is approximately constant (except in low sediment concentration range) and the standard deviation of the measured sediment concentration increases with the concentration.

ii) Ultimately, engineers want a relationship capable of predicting sediment concentration within a certain small percentage of the true sediment concentration for all flow conditions, not within a small absolute magnitude, say 2000 ppm, for the true sediment concentrations for all flow conditions. In other words, an error of 2000 ppm for a true sediment concentration of 500 ppm is not accurate enough, and an error of 2000 ppm for a true 50,000 ppm is not attainable.

The linearization (or Taylor Series) method is selected to estimate the parameters of a non-linear system. It essentially uses the results of linear least squares in a succession of stages. Approximation of the parameters is assumed and the corrections are found. The iteration is then continued until the solution converges, i.e., until the absolute ratios of the corrections to their corresponding previous estimates are less than a certain pre-specified number. The equation is

Table 5.1. Range of Primary Data, After Shen and Hung (1971)

Author	No. of Data	Sed. Conc. by Wt. ppm	Flow Vel. ft/sec	Energy Slope	Flow Depth ft	Channel Width ft	Temp. °C	Flow Dischg. cfs	d_{50} mm
Flume Data:									
Einstein and Chien (1953)	9	2100-16000	3.4-3.6	.0033-.005	~.6	1	9-24	2.2	.13-.37
Nomicos* (1954-55)	1	3600	2.3	.0026	.2	.9	25	.51	.15
Brooks* (1955)	11	200-2700	1.0-2.0	.002-.0035	.15-.3	.9	24	.20-.43	.14
Nomicos* (1956)	11	110-3200	1.0-2.0	.0019-.0027	.24	.9	15-38	.19-.43	.14
Kennedy (1961)	41	490-59000	1.4-4.7	.0016-.027	.07-.36	.9,2.8	23-30	.20-3.3	.23-.55
Stein (1965)	57	93-39000	1.4-6.0	.00061-.017	.3-1.2	4	20-29	2.8-17	.40
Guy, Simons, Richardson (1966)	315	0.2-50000	.7-6.3	.00015-.019	.19-1.3	2, 8	10-34	1.0-23	.18-1.2
Williams (1967)	37	16-15000	1.3-3.5	.0011-.0222	.1-.52	1	12-31	.13-1.3	1.3
USWES, see Toffaleti (1968)	11	120-500	1.2-1.5	.00094-.0017	.42-.53	3	4-27	1.9	.21
Lee (1969)	10	70-1700	1.8-6.5	.00047-.0043	1.0-1.1	8	20-22	15-55	.25
Schneider (1969)	21	18-1800	1.7-5.3	.00014-.0018	1.1-2.8	8	21-22	17-78	.25
River Data:									
Niobrara River, see Colby and Hembree (1955)	18	330-1400	1.8-3.3	.0011-.0016	.9-1.6	69-135	2.2-29	207-350	.15-.25
Middle Loup River, see Hubbell and Matejka (1959)	45	440-2300	2.0-3.7	.00078-.0016	.8-2.1	76-153	0-31	319-500	.14-.30

*See Vanoni and Brooks (1957)

$$\log C = a_0 + a_1 X + a_2 X^2 + a_3 X^3 \tag{5.11}$$

where

$$X = V^{a_4} S^{a_5} W^{a_6} D^{a_7} \tag{5.12}$$

a_0 through a_7 are the parameters to be determined by regression technique, C is the sediment bed material load concentration by weight (wash load is arbitrarily taken to be less than 0.0625 mm), V is the average flow velocity, S is the energy slope, W is the fall velocity of the median size sediment of the bed sample, and D is the flow depth. The sediment particle fall velocity is corrected to that of the actual measured water temperature and no attempt is made to include the effect of heavy sediment concentration (if it exists).

With the total 587 data points in Table 5.1, the final results are a_0 = -107404. 45938164, a_1 = 324214. 74734085, a_2 = -326309. 58908739, a_3 = 109503. 87232539, a_4 = 0. 00750189, a_5 = 0. 00428802, a_6 = -0. 00239974, and a_7 was very small as compared to a_4, a_5 and a_6 and subsequently is dropped from the final analysis.

The standard error of $\log C$ is 0.217 and its standard deviation is 0.972. The correlation coefficient of the fit is 97.5%. The standard error of 0.217 means that on the average, 68% of all the data points fell within 0.217 logarithmic cycles (based on 10) from the values predicted by the recommended curve (Eqs. 5.11 and 5.12 with values of a_0 through a_7 given above), and 95% of all the data points fell within 0.434 logarithmic cycles from the predicted values. In terms of absolute value, 68% of all the data points fell within 0.61 to 1.65 of the values predicted by the recommended curve of 95% of all the data fell within 0.37 to 2.72 of the predicted values. For sediment

transport rate prediction this seems to be quite good. For convenience of application, the following transformation was made: Let

$$Y = X^{1/0.00750189} = \frac{VS^{0.57}}{W^{0.32}} \quad . \tag{5.13}$$

Figure 5.1 shows the recommended curve and its agreement with flume data and river data. Shen and Hung (1972) also showed that the recommended curve agreed with Gilbert's data (1914) rather well by assuming the temperature of flow to be 20°C. However, this curve would predict a much lower sediment bed material load concentration than their corresponding measured values for the Mississippi, Atchafalaya, Red, and Rio Grande Rivers and some large West Pakistan canals. They speculated that this disagreement with large river data may primarily be due to:

i) The sediments used in laboratory studies are usually much more uniform than that in the large rivers. The flow can transport much more non-uniform sediment than the uniform sediment with the same median size. In other words, perhaps using the fall velocity of the median sediment particle of the bed sample cannot adequately describe the characteristic of sediment in terms of its transport rate.

ii) The wash load is taken to be that size sediment which is less than 0.0625 mm, a value arbitrarily chosen by various investigators. A more reasonable criterion, although not necessarily theoretically correct, is to choose say sediment size finer than 10% of the bed sample as the dividing size between wash load and bed material load. If this criterion is selected, the bed material load concentration (coarser than 10% of the bed sample) for these large rivers and canals could easily be reduced by a great deal from the bed material load concentration

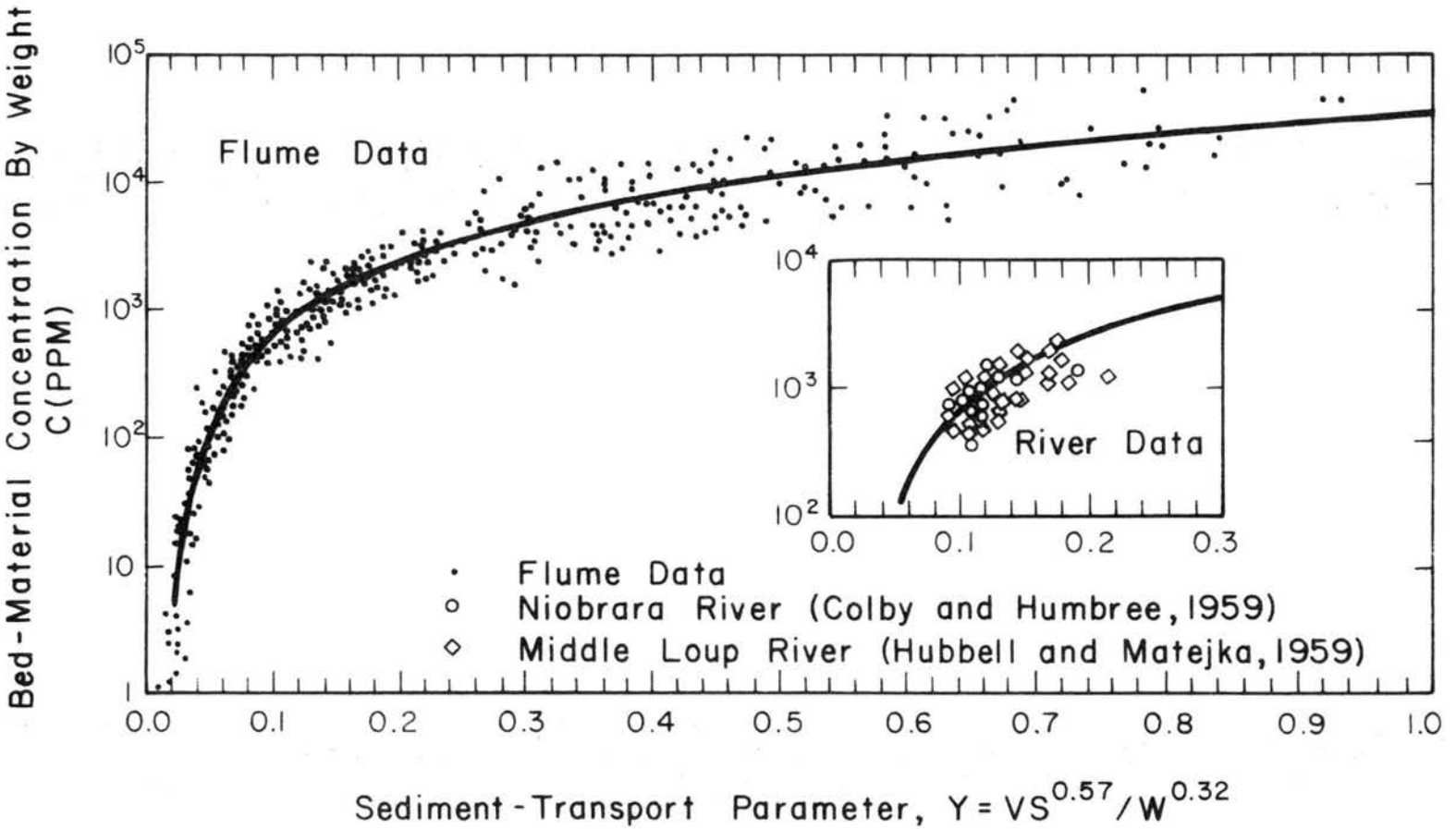

Fig. 5.1 Bed-Material Loads vs Flows (All Primary Data)

(coarser than 0.0625 mm). A similar effect on flume data would not be as great. The division between wash load and bed material load is extremely important and perhaps should be investigated further. If the hypothesis is true that large rivers transport a great deal of wash load even for sizes greater than 0.0625 mm, and only a small amount of bed material load, the consequence is rather alarming. That means one must estimate the total sediment transport rate in these large rivers mainly from their upstream wash load supplies rather than from their capabilities to transport.

IV. DISPERSION OF CONTAMINATED BED-LOAD PARTICLES

A. Instantaneous Injection of Contaminates

Assume a straight alluvial channel where the flow is steady and uniform. Consider a large number of contaminated particles having identical transport characteristics as the sand grains forming the bed to be released instantaneously at a time $t=0$ and at a station $x=0$. The concentration distribution function (Yang and Sayre, 1971) describing the longitudinal dispersion of the contaminated particles is

$$f_t(x) = K_1 e^{-K_1 x - K_2 t} \sum_{n=1}^{\infty} \frac{(K_1 x)^{nr-1} (K_2 t)^n}{\Gamma(nr)\, n!} \tag{5.14}$$

where K_1, K_2 and r are defined by the following probability density functions (where I is the indicator function):

$$f_X(x) = \frac{K_1^r}{\Gamma(r)} x^{r-1} e^{-k_1 x} I_{(0,\infty)}(x) \tag{5.15}$$

$$f_T(t) = K_2 e^{-K_2 t} I_{(0,\infty)}(t) \tag{5.16}$$

where X and T are random variables describing the step lengths and rest periods of a single particle which moves downstream in an alternate sequence of steps and rest periods. $f_t(x)$ indicates the amount of contaminates per unit length downstream at x and time t when a unit amount (either gravimetric or volumetric) of contaminates is injected instantaneously at x=0 and t=0 . Experimental evidence indicate that r is between one and three.

1. Decay of Concentration at x=0 : It is interesting to note that the area under the curve $f_t(x)$ is $(1-\exp(-K_2 t))$, so that the decay of the concentration level at the source is exponential with time.

2. Movement of Mass Center: Under the conditions of steady, uniform flow, the time rate of movement of the mass center, $\bar{x}$, is essentially constant. For the distribution function of Eq. (5.14)

$$\bar{x} = \int_0^\infty x f_t(x) dx = \frac{r K_2 t}{K_1}$$

and

$$\frac{d\bar{x}}{dt} = r \frac{K_2}{K_1} \quad . \tag{5.17}$$

Neither the relationship between the sediment transport rate and the rate of movement of $\bar{x}$ nor the variation of K_1 , K_2 and r for different flow conditions are well understood at present. Einstein (1937) attempted to relate the rate of movement of the mass center with the sediment transport rate as follows:

for uniform sediment sizes $\frac{d\bar{x}}{dt} \approx q_s^{2/3}$ and (5.18)

for non-uniform sizes $\frac{d\bar{x}}{dt} \approx q_s$ (5.19)

where q_s is the sediment transport rate in liters per meter per unit time. Sayre and Hubbell (1965) suggested the following relationship between the mass center and sediment discharge:

$$q_s = \gamma_s (1-\alpha) h \frac{\bar{x}}{t} \tag{5.20}$$

where q_s is the sediment transport rate per unit width, γ_s is the specific weight of the sediment, α is the porosity of the bed and h is the depth of the zone of particle movement. However, the evaluation of h requires a knowledge of bedforms which is not known.

3. Migration of the Concentration Distributions: One can discuss the movement and attenuation of the concentration peak by considering first the case of $r=1$. Equation (5.14) may be written as:

$$f_t(x) = K_1 e^{-K_1 x - K_2 t} \left[\frac{\sqrt{K_2 t}}{\sqrt{K_1 x}} \right] I_1(2\sqrt{K_1 K_2 x t}) \tag{5.21}$$

where $I_1(\,)$ is the modified Bessel function of the first kind of order one.

Shen and Cheong (1971) proved that for sufficiently large t, $\bar{x} = \frac{K_2 t}{K_1} \simeq x_p$ and for $y_p \simeq 2 K_2 t$,

$$\frac{f_t(x_p)}{K_1} \simeq \frac{e^{y_p}}{\sqrt{2\pi y_p}} \exp\,[-y_p]$$

$$\sim \frac{1}{\sqrt{4\pi K_2 t}} \tag{5.22}$$

in agreement with a similar result by Hubbell and Sayre (1964). At large dispersion times, the peak concentration varies inversely as the square root of the dispersion time. At smaller and intermediate dispersion times, the decrease

rapid as shown in Fig. (5.2).

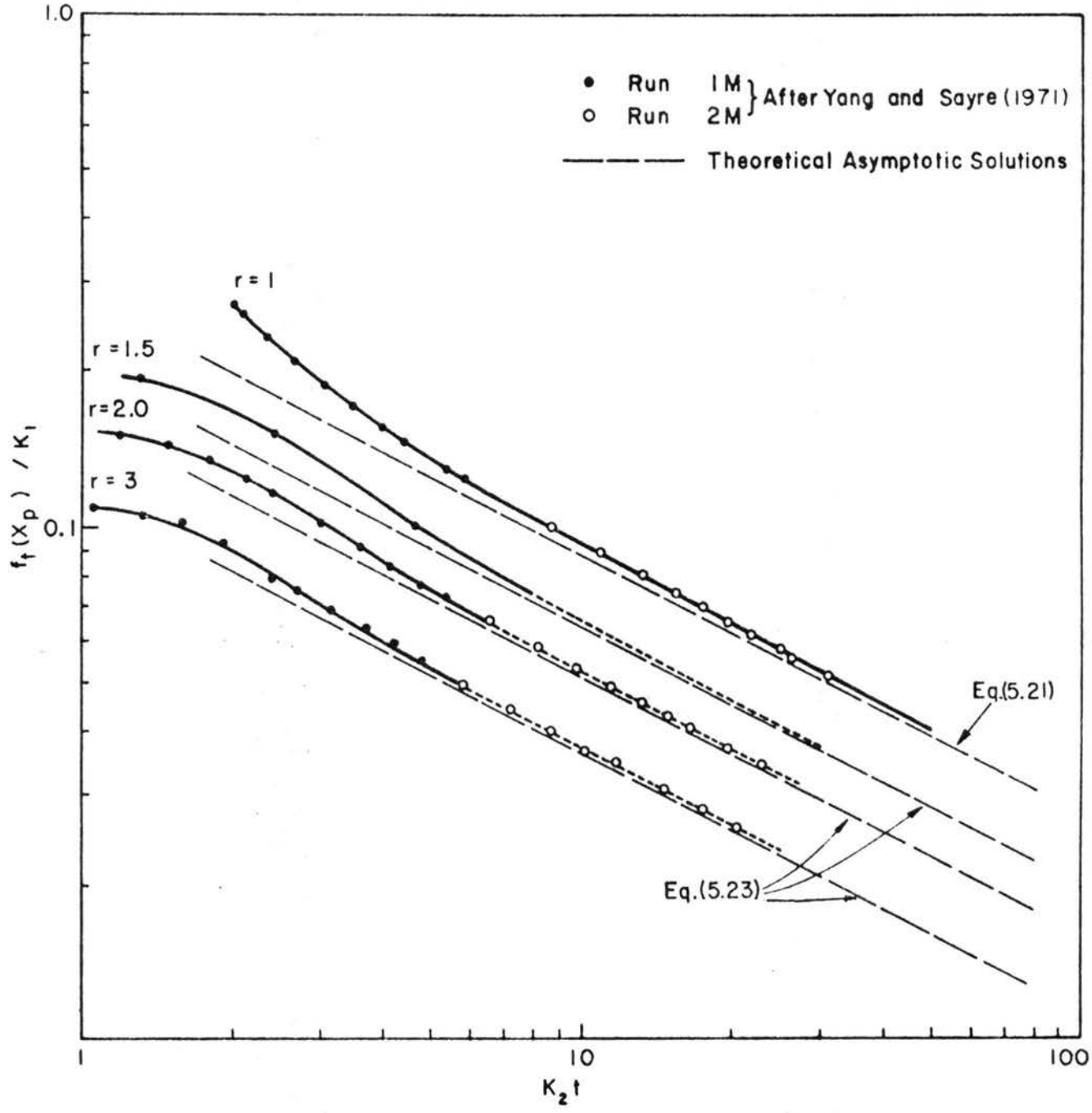

Fig. 5.2. Decay of Peak Concentration (After Shen and Cheong (1971))

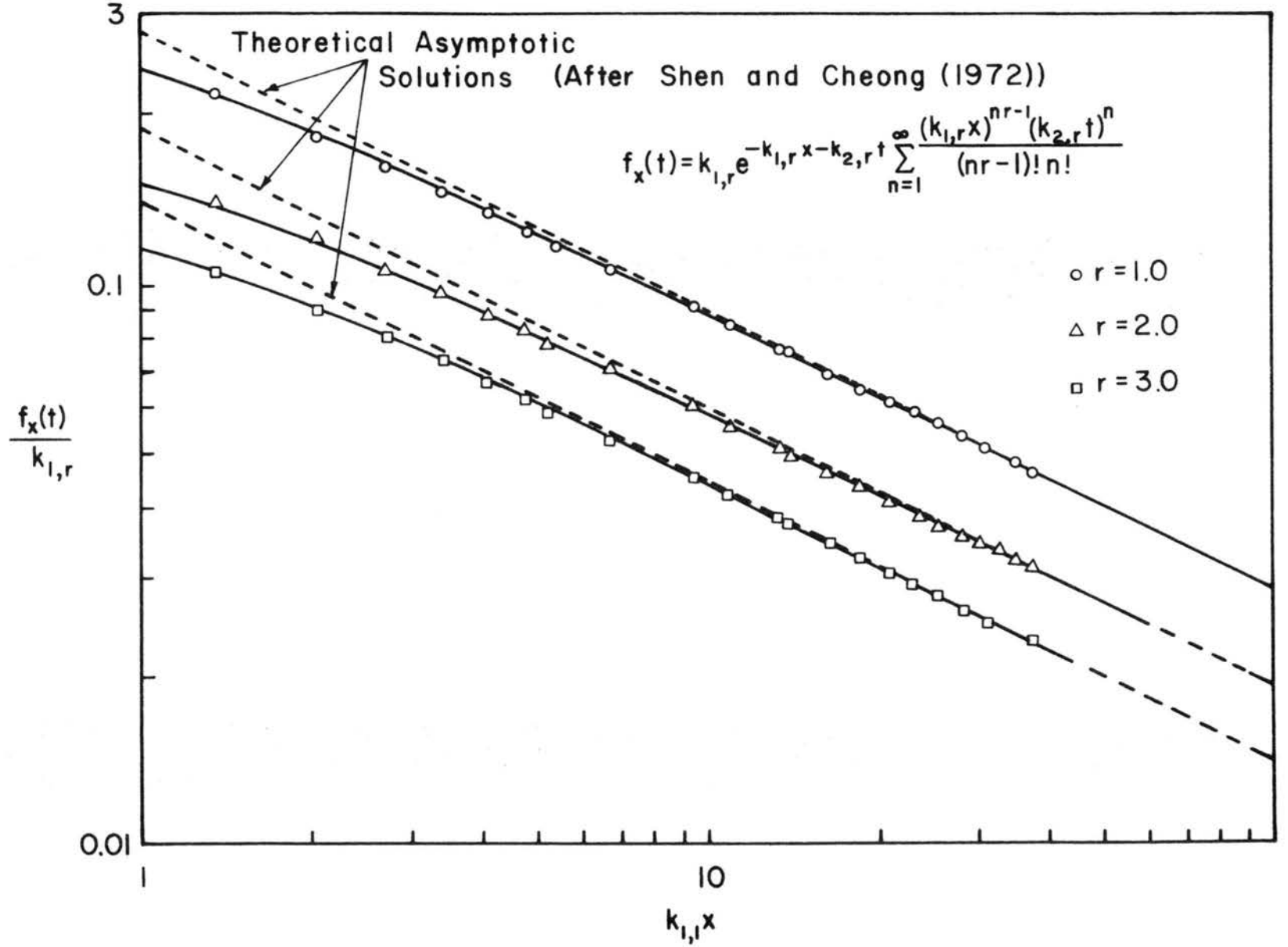

Fig. 5.3 Attenuation Of The Peak Of The Time-Concentration Functions

Shen and Cheong (1971) also determined that for any $r \geq 1$, the asymptotic expression for the attenuation of the peak is

$$\frac{f_t(x_p)}{K_1} \sim \frac{1}{\sqrt{2\pi r(r+1)t_*}} \tag{5.23}$$

and the asymptotic expression for the position of the peak is

$$x_p \sim \frac{rK_2 t}{K_1} \quad . \tag{5.24}$$

Thus, in general, after a sufficiently long time (say $t_* > 10$), the peak concentration decreases inversely as the square root of the dispersion time (Fig. 5.2).

A similar theoretical asymptotic solution between $f_x(t_p)/K_{1,r}$ vs $K_{1,1}x$ is found as shown in Fig. 5.3.

The longitudinal position of the mode approaches the mass center of the distribution function as shown in Fig. 5.4.

4. Envelope of the Concentration Distributions: The curves of $f_t(x)$ with x as the abscissa for different times are shown in Figs. 5.4, 5.5, 5.6, 5.7, 5.8 and 5.9. Figures 5.4, 5.5 and 5.6 are based on the experimental values of $\frac{dx}{dt}$ and $\frac{d\sigma^2}{dt}$ of Run 1M obtained by Yang and Sayre (1971) for selected values of $r=1,2$ and 3 and

$$\frac{d\sigma^2}{dt} = \frac{r(r+1)K_2}{K_1^2} \tag{5.25}$$

where $\frac{d\sigma^2}{dt}$ is the rate of spread of the tracer. Similarly, Figs. 5.7, 5.8 and 5.9 are based on the results of Run 2M. Runs 1M and 2M represent that lowest and highest rates of dispersion, respectively. Pertinent hydraulic data for both runs are given in Table 5.2.

It is interesting to note that the envelopes of $f_t(x)$ with $r=1$, 2 and 3 for each run appear to collapse into a single curve.

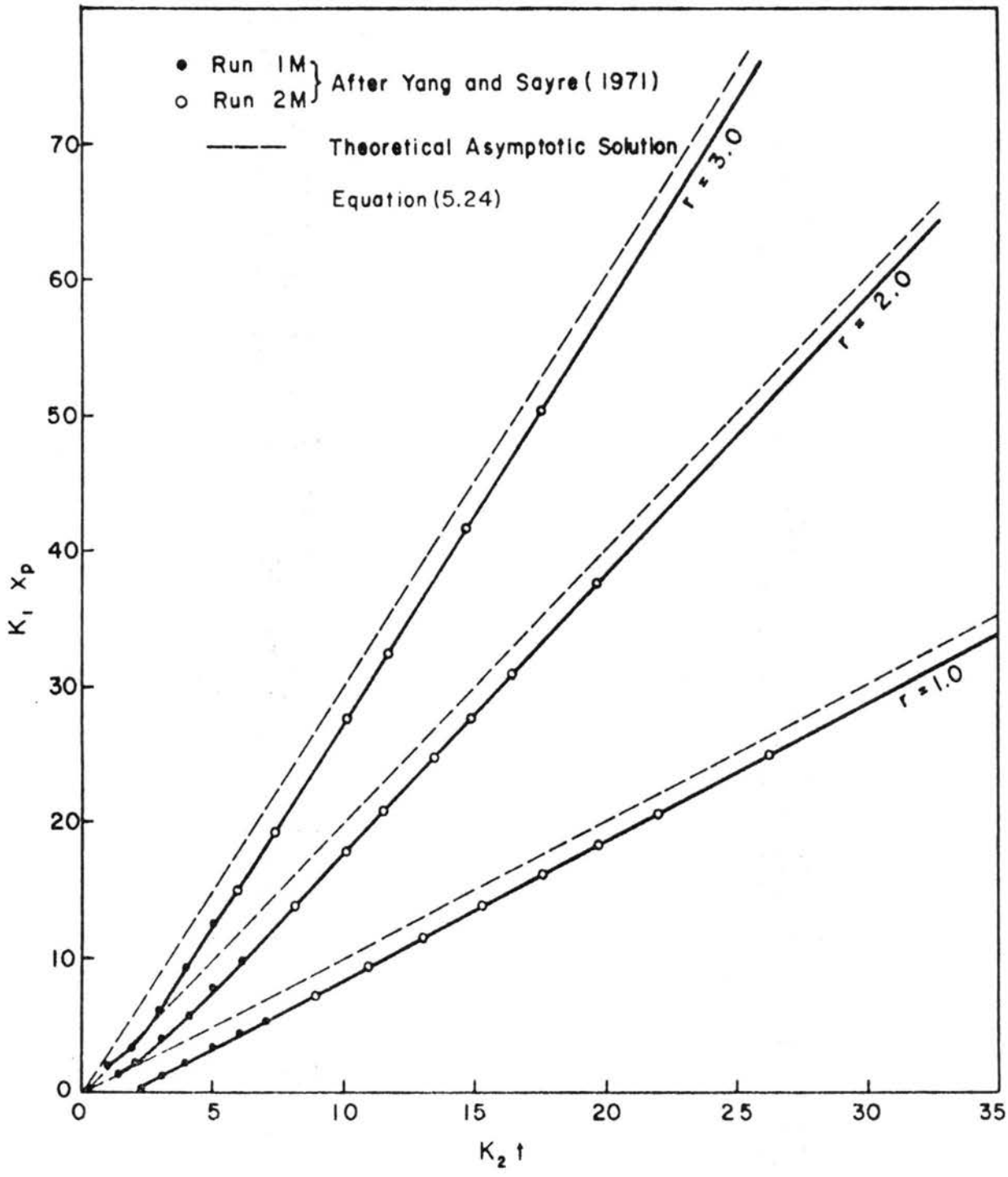

Fig.5.4 Location of Peak X_p
(After Shen and Cheong (1971))

Table 5.2. Hydraulic Data for Runs 1M and 2M after Yang and Sayre (1971)

Run No.	1M	2M
Water Surface Slope x 10^2	0.088	0.212
Water Discharge (cfs)	1.140	1.690
Normal Depth (ft)	0.518	0.521
Velocity of Water (ft/sec)	1.100	1.625
Bedform	Ripples	Dunes
Total Sediment Conc. (ppm) by Weight	60.210	871.550
Total Sediment Discharge (lb/sec)	0.00429	0.0918
Size of Tracer (mm)	0.30 - 0.35	0.30 - 0.35
Velocity of Tracer (ft/hr)	0.585	4.700
Rate of Spread of Tracer (ft^2/hr)	1.724	20.200

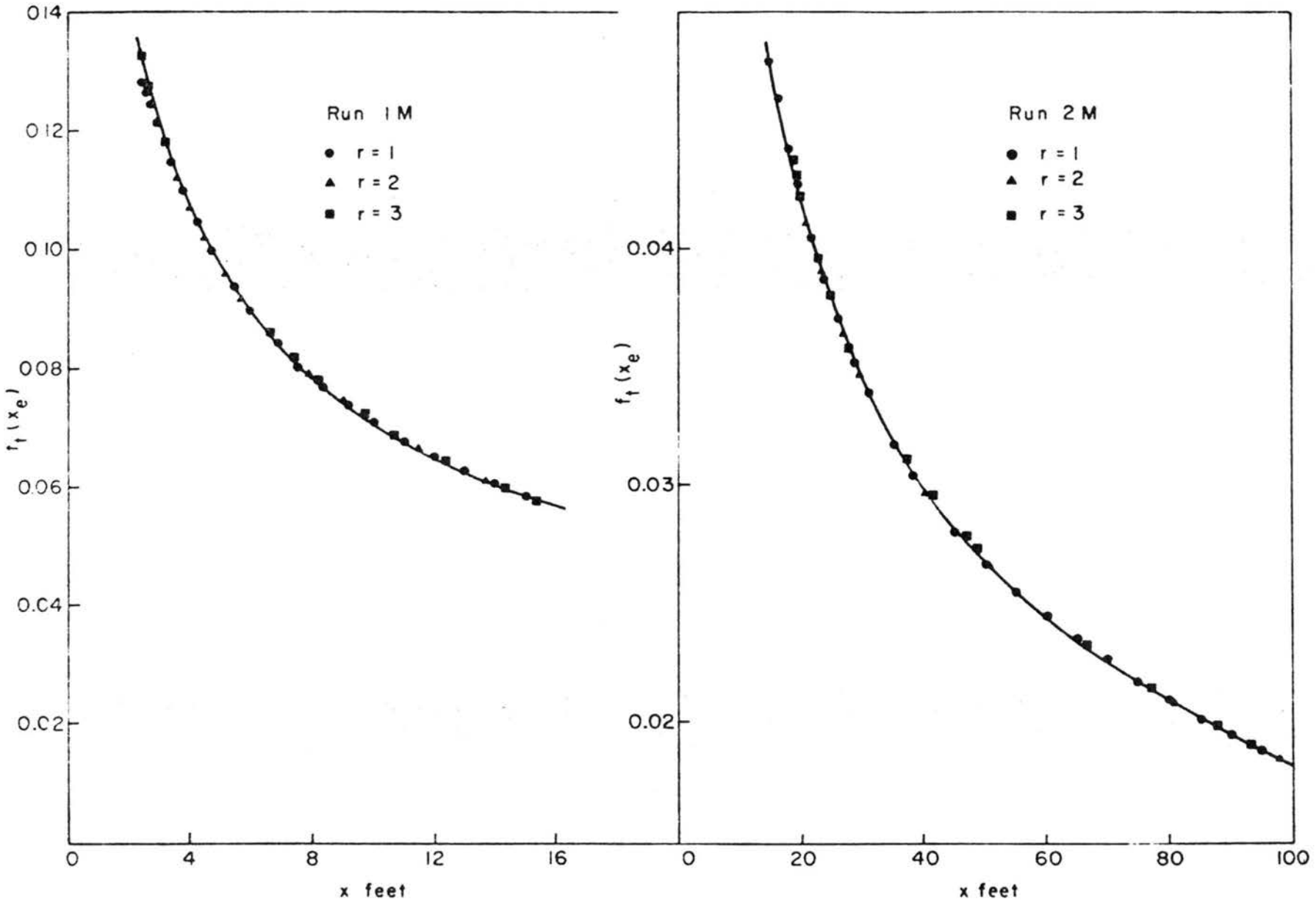

Fig. 5.5 Approximations of Envelopes for Runs 1M and 2M

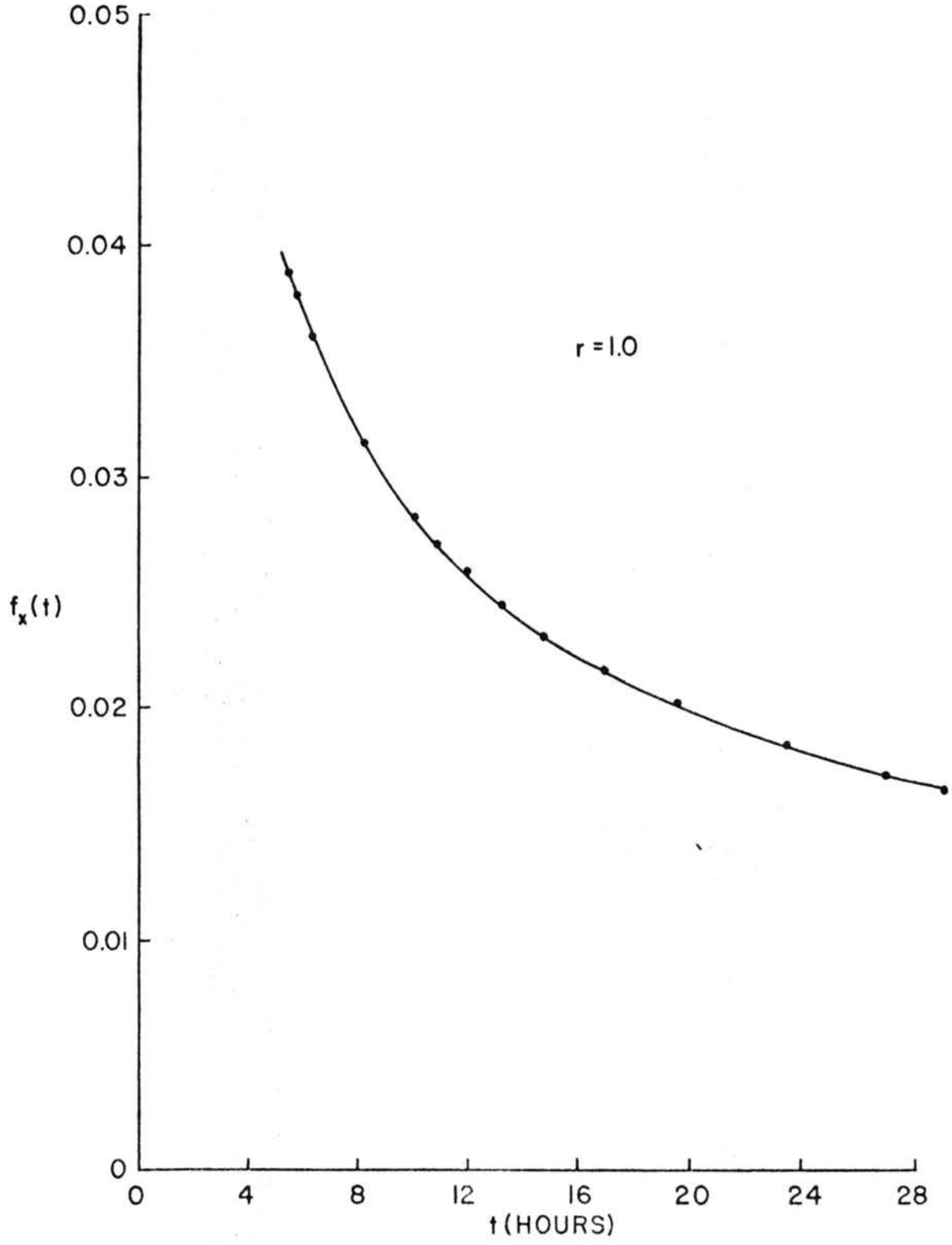

Fig. 5.6 Approximate Envelopes For Run 2M

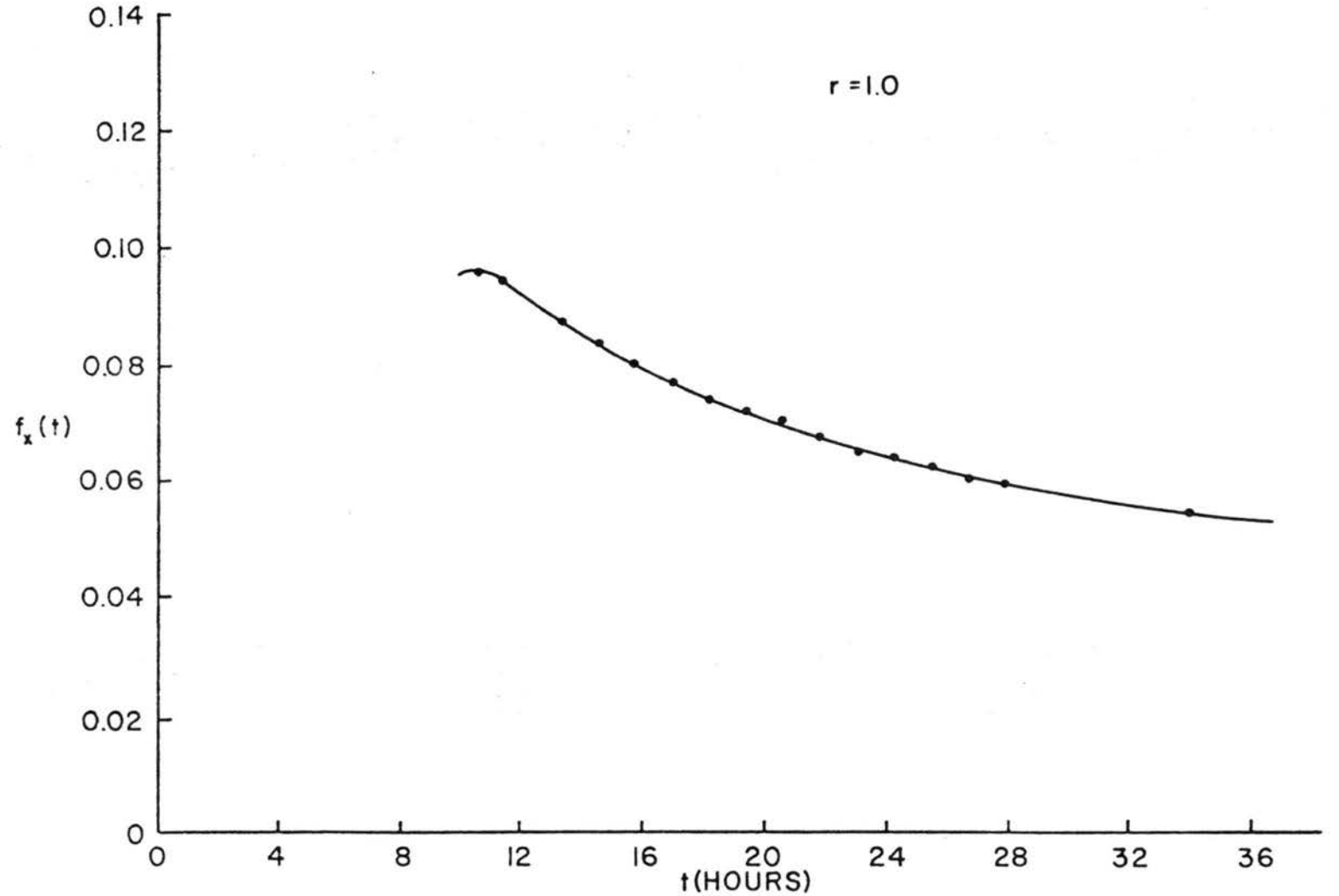

Fig. 5.6 Approximate Envelopes For Run 1M

For any $r \geq 1$ the approximate envelope is determined to be

$$f_t(x_e) = K_1 e^{-2K_1 x_e} I_1(2K_1 x_e) \tag{5.26}$$

as shown in Fig. 5.5.

Figure 5.6 gives the envelope curves for f versus t .

5. Contours of Constant Concentration as a Function of Time and Distance: Iso-concentration contours for different r values for Runs 1M and 2M are shown in Figs. 5.7 and 5.8 respectively. The intercepts of each vertical line with a specified contour indicates the two limits of the critical zone where the concentration is above that particular limit. The intercepts of each horizontal line with a contour define the limits of the critical time period when local concentrations exceed the specified level.

The movement of the mass centers for different values of r are also shown in Figs. 5.5 and 5.6. Since

$$\bar{x} = \frac{rK_2 t}{K_1} \tag{5.27}$$

then

$$\bar{x}_* = K_1 \bar{x} = rt_* \quad . \tag{5.28}$$

An iso-concentration contour for the concentration C with r=1 is given by Eq. (5.21) with $x_*=K_1 x$ and $t_*=K_2 t$.

$$\frac{C}{K_1} = e^{-x_*-t_*} \frac{\sqrt{t_*}}{\sqrt{x_*}} I_1(2\sqrt{t_* x_*}) \quad . \tag{5.29}$$

The intercept between the mass center line and the concentration contour X is, for $t_*=\bar{x}_*$, given by

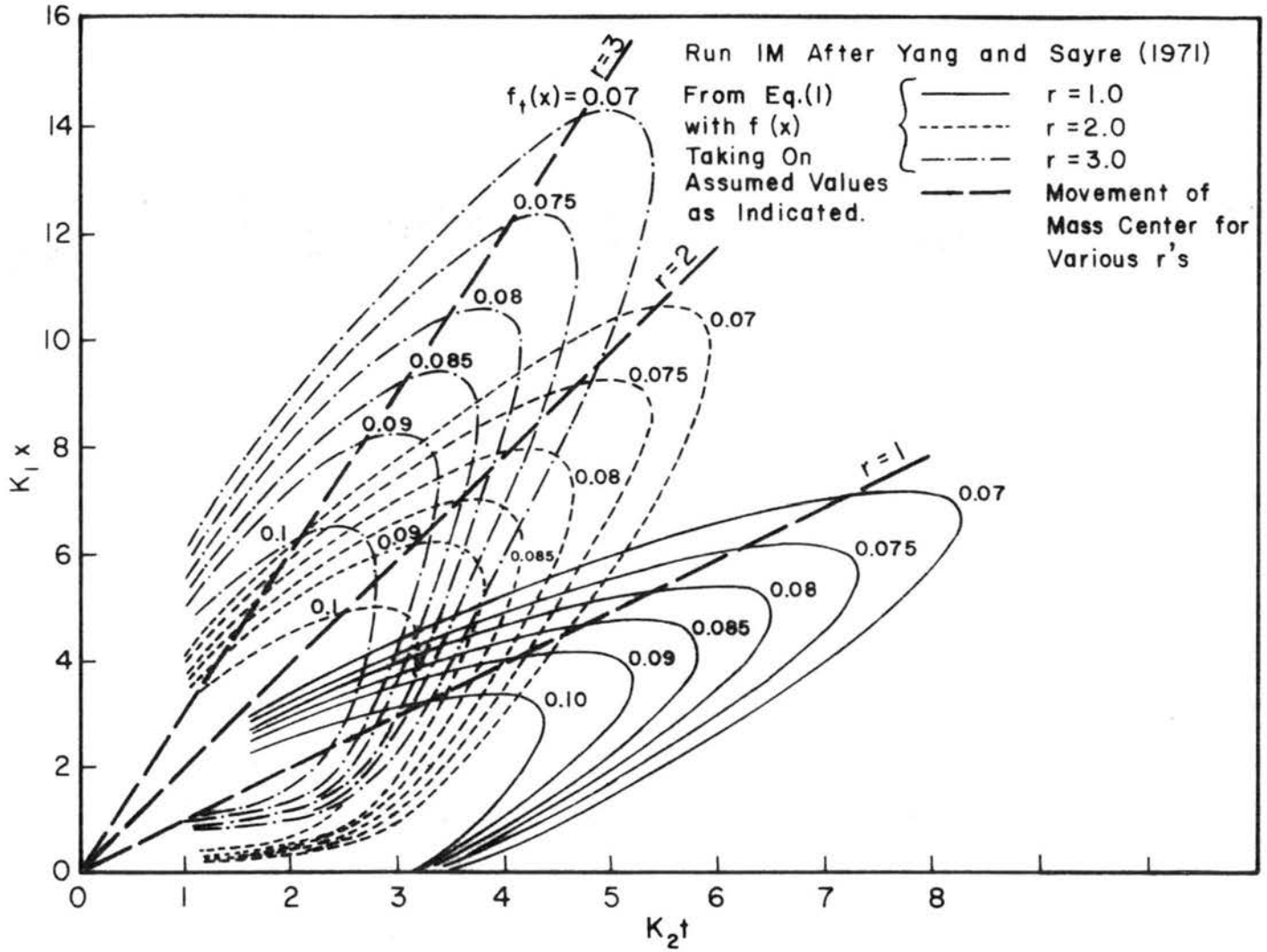

Fig. 5.7 Iso-Concentration Contours

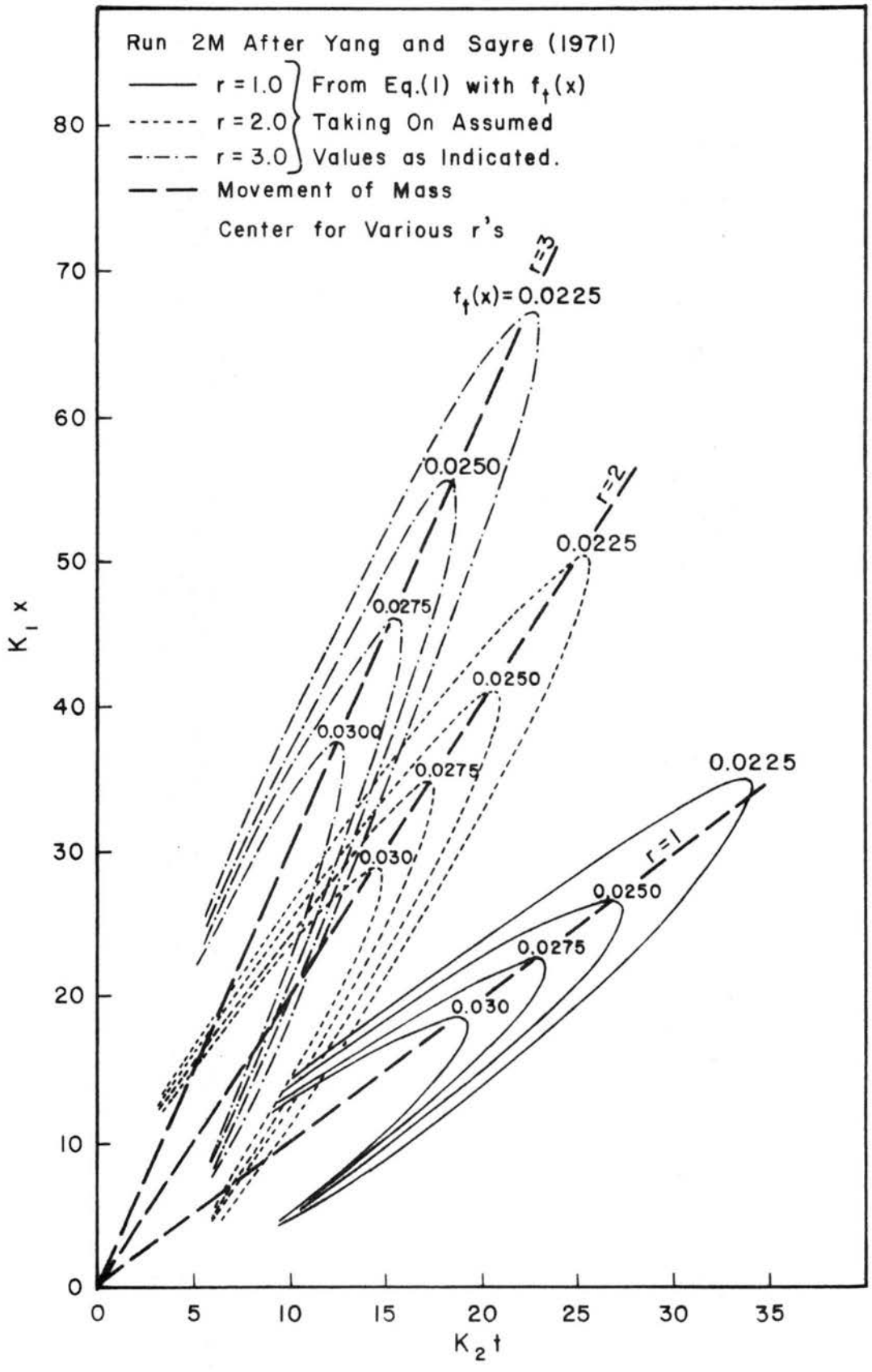

Fig. 5.8 Iso-Concentration Contours

$$\frac{C}{K_1} = e^{-2\bar{X}_*} I_1(2\bar{X}_*) \quad . \tag{5.30}$$

When the time under consideration is sufficiently large, the asymptotic solution is

$$\frac{C}{K_1} \sim e^{-2\bar{X}_*} \cdot \frac{e^{2\bar{X}_*}}{\sqrt{4\pi X_*}} \tag{5.31}$$

$$\sim \frac{1}{\sqrt{4\pi X_*}} \tag{5.32}$$

which shows that the intercept between the mass center line and the iso-concentration contour varies inversely as the square of the concentration after a long dispersion time, i.e.,

$$\bar{X}_* \propto \left(\frac{K_1}{C}\right)^2 \quad . \tag{5.33}$$

B. Continuous Injection of Contaminates at a Given Location With Uniform Rate

The study of the downstream effects of a continuous injection of contaminates is extended by Cheong and Shen (1972) from the case of the instantaneous injection by means of the convolution integral. With continuous injection at a unit rate over the time interval $[0,t_{1_*}]$, the downstream concentration at a time $t_* \geq t_{1_*}$ is

$$C(x_*,t_*) = \int_0^{t_{1_*}} f(x_*,t_*-\tau_*)d\tau_* \tag{5.34}$$

where $x_* = K_1 x$ and $t_* = K_2 t$ (see Eq. 5.29).

The envelopes for each family of curves at a specified x_* are given by the condition when the injection persists for an infinitely long time and the time under consideration is finite. The envelope

function for $r=1$ becomes (according to Cheong and Shen, 1972)

$$C(x_*,t_{*_e}) = F_{x_*}(t_{*_e}) - e^{-x_*-t_{*_e}}\sqrt{\frac{t_{*_e}}{x_*}}\ I_1(2\sqrt{t_{*_e}x_*}) \tag{5.35}$$

and is shown in Fig. 5.9 with $r=2$ and 3 .

$$C(x_*,t_{*_e}) = \sum_{n=1}^{\infty} \frac{x_*^{nr-1}\ e^{-x_*}}{(nr-1)!} \sum_{s=n+1}^{\infty} \frac{t_{*_e}^{s}\ e^{-t_{*_e}}}{s!} \tag{5.36}$$

represents the envelope functions for the time concentration function and is shown in Figs. 5.10 and 5.11. In Fig. 5.9 the envelope functions approach their asymptotic value of 1.0. This can be shown analytically by letting $t_* \to \infty$ in Eq. (5.32). In Figs. 5.10 and 5.11 the envelope functions approach different asymptotic values depending on the values of x_* and r . The asymptotes of these envelope functions are obtained by letting $t_{*_e} \to \infty$ in Eq. (5.36). We have

$$C(t_*,t_{*_e}) = \sum_{n=1}^{\infty} \frac{x_*^{nr-1}\ e^{-x_*}}{(nr-1)!} \sum_{x=n+1}^{\infty} \frac{t_{*_e}^{s}\ e^{-t_{*_e}}}{s!}$$

$$= \sum_{n=1}^{\infty} \frac{x_*^{nr-1}\ e^{-x_*}}{(nr-1)!} \int_0^{t_{*_e}} \frac{s^n e^{-s}}{n!}\, ds \tag{5.37}$$

$$\lim_{t_{*_e} \to \infty} C(t_*,t_{*_e}) = \sum_{n=1}^{\infty} \frac{x_*^{nr-1}\ e^{-x_*}}{(nr-1)!}$$

$$= \begin{cases} 1 & , r=1 \\ \frac{1}{2}\,(1-e^{-x_*}) & , r=2 \\ \frac{1}{3}\,[1-e^{-\frac{3}{2}x_*}\,(\cos\frac{\sqrt{3}\,x_*}{2}\,\sin\frac{\sqrt{3}\,x_*}{2})] & , r=3 \end{cases} \quad . \tag{5.38}$$

The asymptotes of the envelope for different values of r and different positions x_* downstream of the injection point are shown in Fig. 5.12. It is interesting to note that the asymptotes for a given r attain a limiting value of $\frac{1}{r}$ far downstream. Thus, at a position far downstream one would not expect the concentration to exceed $\frac{1}{r}$ th of the rate of injection even if the injection persists uniformly over a long time.

C. Summary for Engineering Application

The exact solution to the dispersion of contaminated bed-load particles required the knowledge of K_1, K_2 and r in the distributions of the step lengths and rest periods. Since the variations of K_1, K_2 and r with various flow conditions have still not been established, engineering solutions of this problem will be discussed in the following two cases, i.e., Case 1: if some measurements can be made under the design flow conditions, and Case 2: how to estimate the dispersion of contaminated bed-load particles when no measurements are available. In both cases, the solutions are limited to i) cohesionless sediment, ii) sediment size almost uniform, iii) contaminants must be firmly attached to sediment bed particles, iv) seepage effect is negligible, v) sediment bed material load concentration is less than 870 ppm by weight and vi) two-dimensional flows.

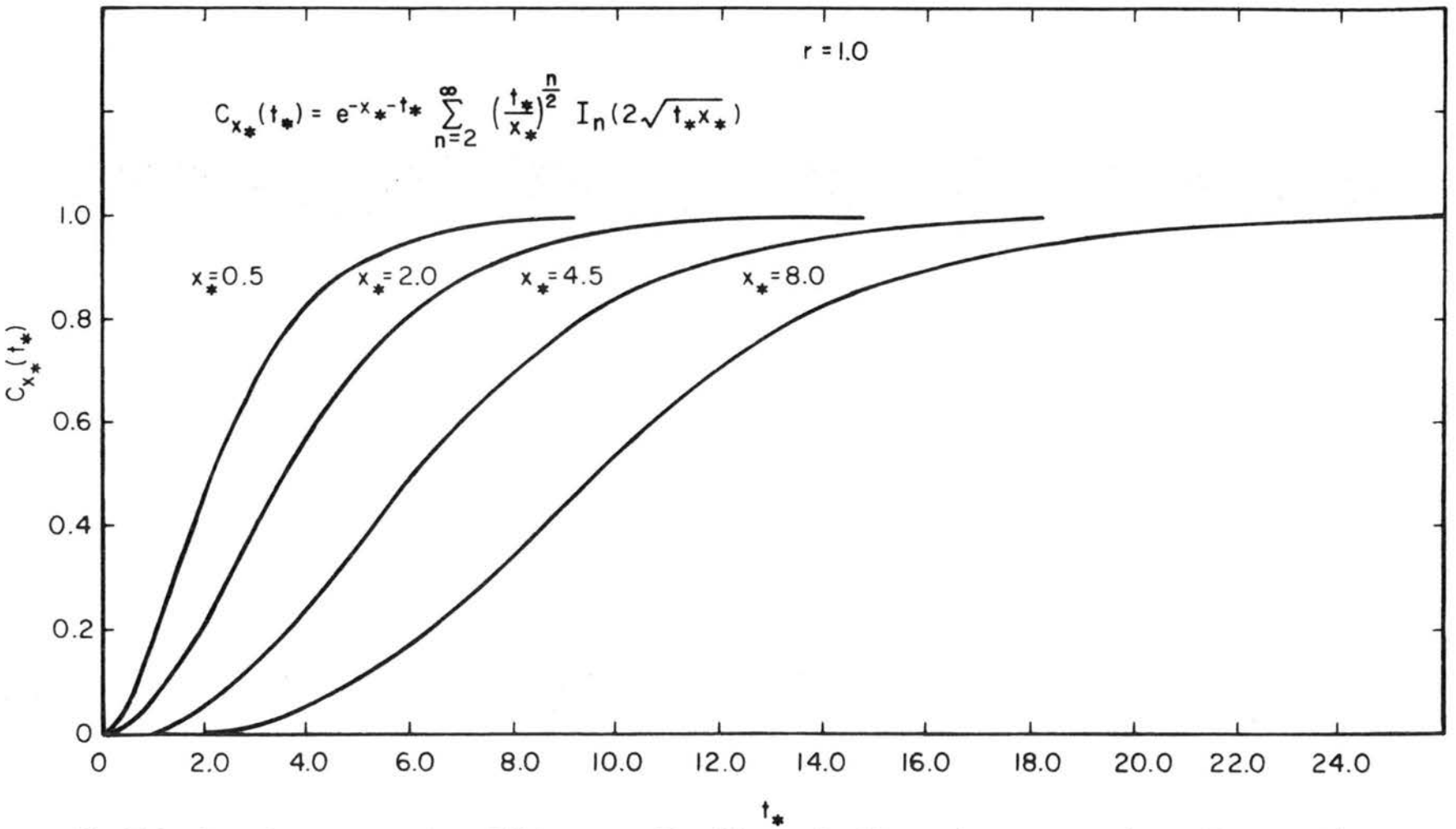

Fig.5.9 Envelopes to the Different Families of Time-Concentration Distributions for Uniform Injection Over Finite Duration, t_*.

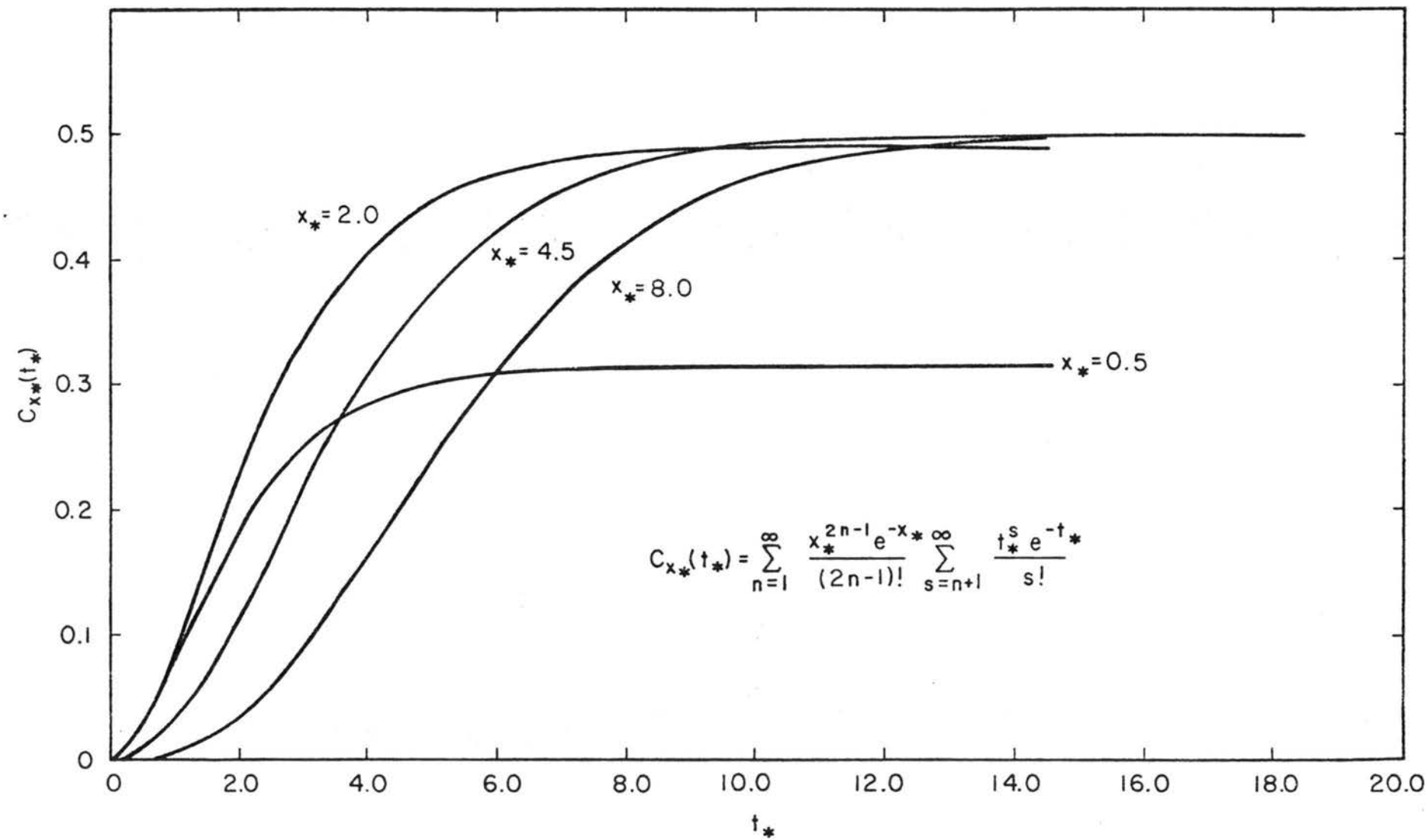

Fig.5.10 Envelopes to the Different Families of Time-Concentration Distributions for Uniform Injection Over Finite Duration, t_*. (r=2)

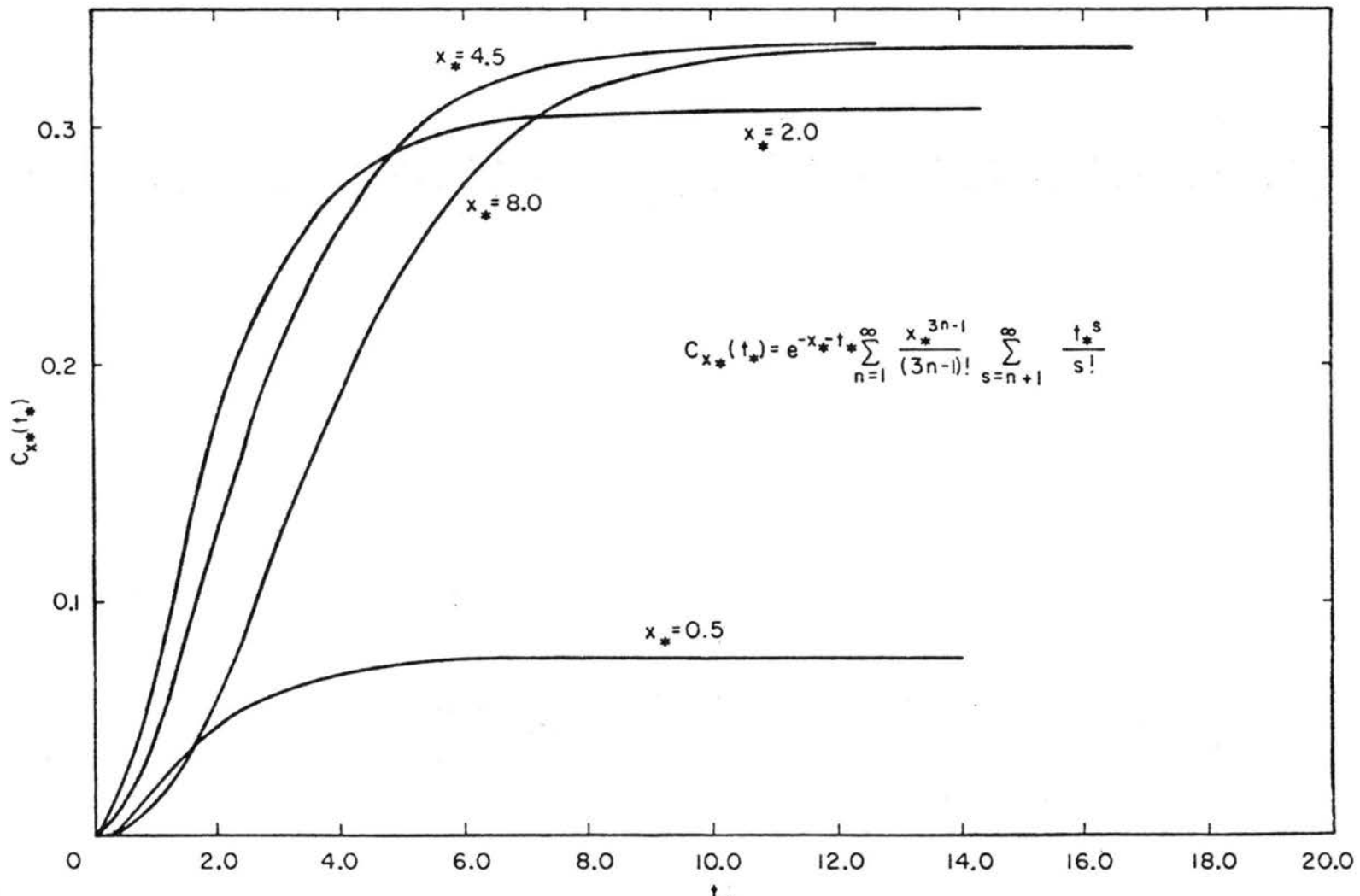

Fig. 5.11 Envelopes to the Different Families of Time-Concentration Distributions for Uniform Injection Over Finite Duration, t_*. ($r = 3.0$)

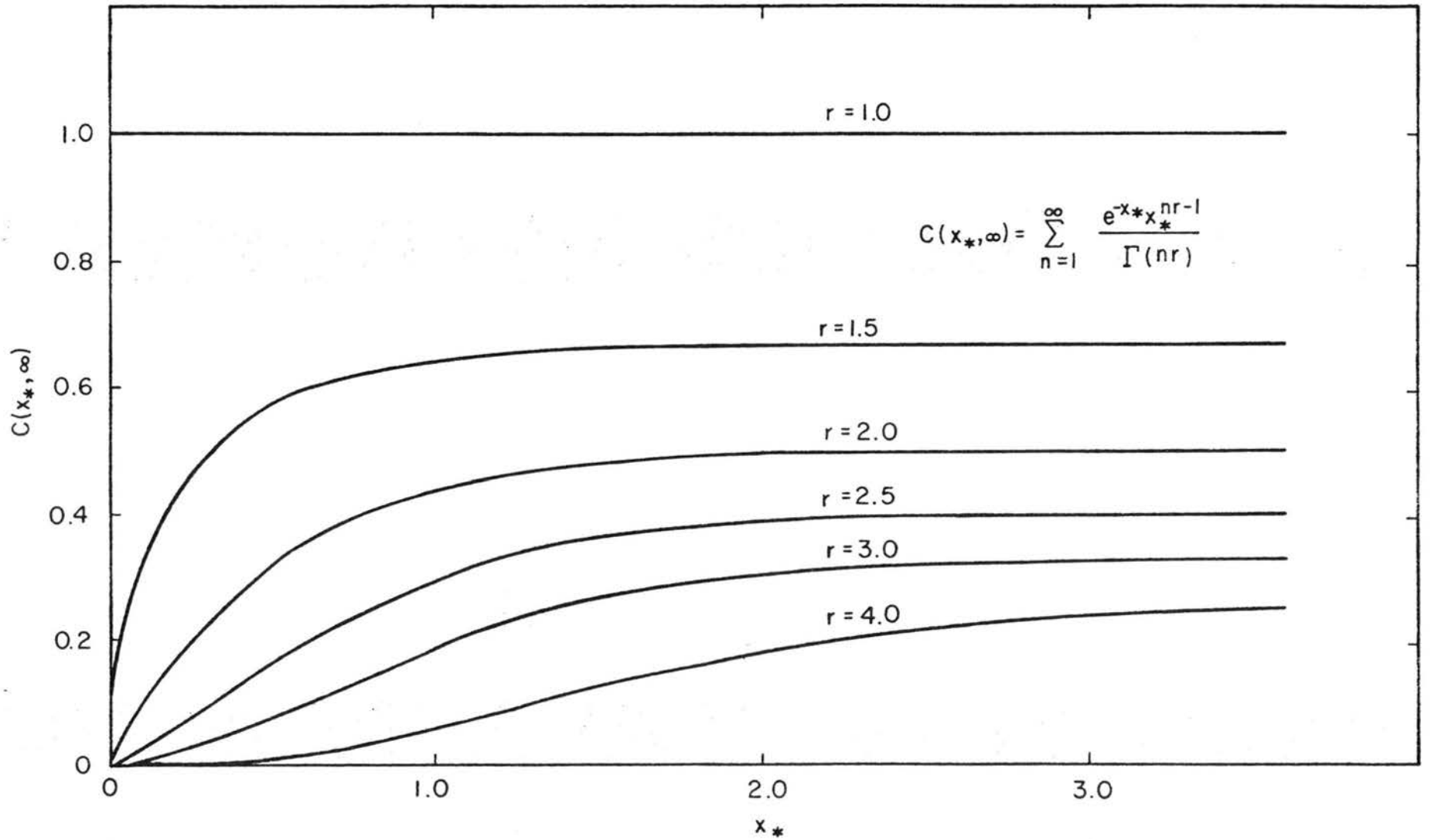

Fig. 5.12 Asymptotes of the Envelopes to the Different Families of Time-Concentration Distributions for Uniform Injection Over Finite Duration, t_* .

CASE 1 - If some measurements can be made in design flow conditions:

a) For instantaneous injections of contaminated concentrations perhaps the easiest measurements to be made are: i) $d\bar{x}/dt$ (movement of mass center), ii) $d\sigma^2/dt$ (the rate of spread), and iii) location of peak concentrations, as performed by Yang and Sayre (1971) with suitable tracers. From these three items one can calculate K_1, K_2 and r and plot curves: i) as shown in Figs. 5.2 and 5.3 for the decay of peak concentrations, ii) envelopes of concentrations as shown by Figs. 5.5 and 5.6, iii) iso-concentration contours as shown in Figs. 5.7 and 5.8. Since the envelopes of concentration (as shown by Figs. 5.5 and 5.6) are independent of the values of r, these curves can be obtained when only $d\bar{x}/dt$ and $d\sigma^2/dt$ are known. The decay of concentration at the location of contaminant injection is always exponential with time.

b) For continuous injection over finite durations of contaminated concentrations, the envelopes of the contaminated concentration at different x and t, such as given in Figs. 5.9, 5.10 and 5.11 for $r=1$, 2 and 3 respectively, can be obtained if K_1, K_2 and r are determined from the measurements of $d\bar{x}/dt$, $d\sigma^2/dt$ and a plot of asymptotic solution (over a long period of time) of concentration distribution for finite duration of continuous injection. The last plot, as shown in Fig. 5.12, gives a good determination of the value of r.

CASE 2 - If no measurement can be made in design flow conditions:

Since the variations of K_1, K_2 and r with different flow conditions are not known, it is an extremely difficult task to determine the dispersion of contaminated bed-load particles. Perhaps one can use the regression curve as shown in Fig. 5.1 to estimate the

sediment bed-material load transport rate first. One can then estimate the movement of mass center either with Eq. (5.18) as suggested by Einstein (1937) or by Eq. (5.20) as suggested by Sayre and Hubbell (1964) with an estimated h value. All of this "guessing" can only provide one set of equations and a minimum of two equations is necessary to obtain an envelope of concentration curves as shown by Figs. 5.5 and 5.6. The next avenue is to study the data and curves presented by Grigg (1970). "Hopefully" an order of magnitude estimate can be made there for K_1, K_2 and r for various flow conditions. The obvious conclusion here is that a much more comprehensive data collection program is urgently needed to study the variation of K_1, K_2 and r with flow conditions for the complete solution of the dispersion of contaminated bed-load sediment particles.

V. REFERENCES - CHAPTER 5

Shen, H. W. and Cheong, H. F., 1972, paper in progress

Einstein, H. A., 1937, "Bed Load Transport as a Probability Problem," Dr. Sc. Thesis, Federal Institute of Technology, Zurich, Switzerland.

Guy, H. P., Simons, D. B., and Richardson, E. V., 1966, "Summary of Alluvial Channel Data from Flume Experiments, 1956-61," U.S. Geological Survey, Professional Paper 462-I, 96 pp.

Hubbell, D. W., and Sayre, W. W., 1964, "Sand Transport Studies with Radioactive Tracers," Journal of the Hydraulics Division, ASCE, Vol. 90, No. HY3, pp. 39-68.

Parzen, E., 1962, "Stochastic Processes," Holden Day, San Francisco.

Sayre, W. W., and Hubbell, D. W., 1965, "Transport and Dispersion of Labelled Bed Material, North Loup River, Nebraska," U.S. Geological Survey Professional Paper 433-C.

Shen, H. W., and Cheong, H. F., 1971, "Dispersion of Contaminated Bed-Load Particles," presented at the International Association for Statistics in Physical Science (IASPS) Symposium of Hydrology, Tucson, Arizona, August 29 - September 2, 1971. To be published as a U.S.D.A. Misc. Publication.

Shen, H. W., and Todorovic, P., 1971, "A General Stochastic Sediment Transport Model," paper presented at the International Symposium on Stochastic Hydraulics held at Pittsburg, Pennsylvania, May 31 - June 2, 1971.

Shen, H. W., and Hung, C. S., 1971, "An Engineering Approach to Total Bed-Material Loan by Regression Analysis," chapter 14 of Sedimentation, edited by H. W. Shen, published by Litho Crafters, Ann Arbor, Michigan.

Yang, C. T., and Sayre, W. W., 1971, "Stochastic Model of Sand Dispersion," Journal of the Hydraulics Division, ASCE, Vol. 97, No. HY2, February.

VI. LIST OF SYMBOLS - CHAPTER 5

Symbol	Description
$a_o, a_1, \ldots a_7$	Regression coefficients
C	Sediment bed material load concentration by weight
D	Depth of flow
E	An event a particle begins and terminates astep
$E_\nu^{t,t+\Delta t}$	Event that ν steps are executed over the time interval between t and $t + \Delta t$
e	2.71828
$f_t(x)$	Concentration distribution function parameterized by time t
$f_x(t)$	Time concentration function parameterized by downstream location x .
$f_x(t)$	Mode of time concentration function for location x
h	Depth of the zone of particle movement
$I_{(o,\infty)}(\cdot)$	Indicator function defined by $I_{(o,\infty)}(\cdot) = \begin{cases} 1 & 0 \leq \cdot < \infty \\ 0 & \text{otherwise} \end{cases}$
$I_m(\cdot)$	Modified Bessel function of the first kind of order m
$K_1(x), K_2(x)$	Functions of x
K_1	Reciprocal of the mean step length of a particle
K_2	Reciprocal of the mean rest period of a particle
log	Logarithm to base 10
$N(t)$	Number of steps taken by the particle during the interval (o,t)
n	An integer notation

Symbol	Description
$P[\cdot]$	Probability of event
$P_n(x)$	Probability that event E has occured n times over the distance between (o,x)
q_s	Sediment transport rate per unit width
$q_n(x)$	Probability that event E has occured n times during the time (o,t)
r	Shape parameter in the two parameter Gamma distribution for step lengths of particle
S	Energy slope
t	Time
t_*	Dimensionless time scale defined by $t_* = K_2 t$
V	Average flow velocity
W	Fall velocity of median size sediment of the bed sample
x	Downstream coordinate
X_t	Position of particle at time t
X_n	Position of particle after n steps
$\bar{x}$	Mass center of concentration distribution function
x_*	Dimensionless length scale defined by $x_* = K_1 x$
x_p	Downstream position of the mode of $f_t(x)$
α	Porosity of sand bed
Δt	Increment in time
Δx	Increment in x
γ_s	Specific weight of sediment
$\Gamma(\cdot)$	Complete gamma function with real argument
σ^2	Second moment about $\bar{x}$ of the concentration Distribution function.

Chapter 6

BRIEF SUMMARY OF THIS INVESTIGATION AND ITS APPLICATIONS TO WATERSHED MANAGEMENT

I. BRIEF SUMMARY OF THIS INVESTIGATION

Detailed discussions of various investigations conducted in this study are given in Chapters 2-5 and the following is a rather brief description of them.

The effect of vegetation on flow retardation can be divided into three parts: i) tall vegetation (such as trees) on the order of flow depths, ii) short vegetation (such as grasses) on the order of normal boundary roughness and iii) vegetation in the order of 20-80% flow depths. The main part of Chapter 2 deals only with tall vegetation. A model to estimate the resistance of flow due to various combinations of tall vegetation is given there. Experiments have been performed at Colorado State University's research laboratory to verify this model. Chapter 2-A presents an empirical curve (by regression) to estimate the flow resistance with large rigid roughness on the order of normal boundary roughness. The possibility of applying this curve to flexible roughness has also been explored. Chapter 2-B presents a new theoretical approach to analyze the vibration of roughness. This approach appears to be superior to previous theoretical analyses although the practical application of it is still limited in its present form.

Chapter 3 calculates the relative effect of various tall vegetation on the reduction of sediment yields based on the reduction of flow rates. This analysis should be rather useful in determining the relative effect on sediment yields by clear cutting and other selective cuttings of forest lumber.

Chapter 4 investigates the effect of rainfall on thin sheet flows. It is shown that, within the experimental data range, the frictional coefficient, such as the Darcy-Weisbach, is directly effected by the rainfall intensity and not the channel slope. A simplified method to estimate the rainfall effect on flow resistance is also presented.

Chapter 5 deals with the dispersion of contaminated bed particles for different time and space. These contaminated bed particles are released at the source either instantaneously or continuously. The analysis is based on a one-dimensional stochastic sediment model. Graphical solutions to show the movement of contaminated bed particles are presented. An empirical curve obtained by regression analysis to estimate the sediment bed material load from various flow conditions is found.

II. APPLICATIONS TO WATERSHED MANAGEMENT

A. The Different patterns or groupings of tall vegetations have a significant effect on retardation of flow rates and sediment yields.

B. The retardation of flow rate due to tall vegetations, whose heights are in the same order of magnitude as flow depth, can be estimated from a method presented in chapter 2, if the spacing between the cylinders is at least six diameters in the downstream direction and three diameters in the transverse direction and the Pier Reynolds number is in subcritical range.

C. Tall vegetation's grouped into staggered patterns, are much more effective in reducing flow rate than any other pattern for the same number of tall vegetations. Thus if the main aim of planting tall vegetation's is for reducing flow rates and sediment yield, these tall vegetation's should be planted in staggered patterns.

D. Since it is difficult to harvest tall vegetation's to make a staggered pattern, the next best thing is to harvest tall vegetation's in rows which are perpendicular to flow direction's, shown as patterns III and IV in Chapter 3.

E. The average boundary shear stress on the bed is much more sensitive to its change of plot bottom slope and the size of vegetations than the variation of flow discharge and sediment size. The retardation of boundary shear stress in the bed will increase significantly as trees grow larger. All these effects can be estimated quantitatively by a method presented in this study.

F. Rainfall intensity increases friction resistance of a shallow open channel flow significantly if the flow Reynolds number is between 126 to 900. Rainfall has a smaller effect if the flow Reynolds number is above 2000.

G. A simplified, but reasonably accurate method is presented to estimate the amount of rainfall in the retardation of flow rate.

H. The migration of contaminants attached to sediment bed load can be estimated from a procedure presented in Chapter 5. With the graphs presented, one can either estimate this migration of contaminants for various times at a given location or the location of contaminants at various locations for a given time.

Chapter 7

A LIST OF PUBLISHED PAPERS AND PAPERS UNDER PREPARATION THAT ARE SPONSORED BY THIS GRANT

I. PUBLISHED PAPERS

1. DiSilvio, G., 1969, "Self-Controlled Vibration of Cylinder in Fluid Stream," Proc. paper 6498, Jour. of the Engineering Mechanics Division, ASCE, Vol. 95, EM2, April.

2. Petryk S., and H.W. Shen, 1971, "Direct Measurement of Shear Stress in a Flume," Tech. notes, Jour. of the Hydraulics Division, ASCE, Vol. 97, HY6, June.

3. Shen, H.W., and P. Todorovic, 1971, "A General Stochastic Model for the Transport of Sediment Bed Material," Stochastic Hydraulics, edited by C.L. Chiu, Pittsburg University Press, pp. 489-506.

4. Shen, H.W., and F.H. Cheong, 1971, "Dispersion of Contaminated Bed-Load Particles," Proc. of the Stochastic Hydrology Symposium, International Association for Statistics in Physical Science and the USDA, ARS, August 31-September 2. To be published as a USDA Misc. Publication.

5. Shen, H.W., and C.S. Hung, 1972, "An Engineering Approach to Total Bed Material Load by Regression Analysis," Chapter 14, Sedimentation (Einstein), edited by H.W. Shen, P.O. Box 606, Fort Collins, Colorado.

II. THESIS

1. Petryk, S., 1969, "Drag on Cylinders in Open Channel Flow," Ph.D., Colorado State University, major professor H.W. Shen.

2. Li, Ruh-Ming, 1972, "Sheet Flow Under Simulated Rainfall," M.S., Colorado State University, major professor H.W. Shen.

III. PAPERS UNDER PREPARATION (READY FOR REVIEW)

1. Shen, H.W., and Ruh-Ming Li, "Resistance of Open Channel Flow Over Large Staggered Roughness."

2. Shen, H.W., and Ruh-Ming Li, "The Effect of Rainfall on Sheet Flow."

3. Shen, H.W., and Hin Fatt Cheong, "Dispersion of Instantaneously Released Contaminated Bed-Load Particles."

4. Shen, H.W., and Ruh-Ming Li, "Effect of Various Tall Vegetation Groups on Flow Retardation and Sediment Yields."